Chemia Naissensis
ISSN 2620-1895
July 2019 Volume 2, Issue 1
www.pmf.ni.ac.rs/chemianaissensis

Cover Designer
Jovana Janković

Chemia Naissensis (ISSN 2620-1895)

Published only in electronic form

Volume 2, Number 1, July 2019

Publisher:

Faculty of Sciences and Mathematics, University of Niš

Editor-in-Chief:

Deputy Editor:

Editors:

Inorganic Chemistry

Dr Dragan Đorđević, Department of Chemistry, Faculty of Sciences and Mathematics, University of Niš, Republic of Serbia

Chemical Engineering

Dr Marjan Ranđelović, Department of Chemistry, Faculty of Sciences and Mathematics, University of Niš, Republic of Serbia

Chemical Education

Dr Vesna Stankov-Jovanović, Department of Chemistry, Faculty of Sciences and Mathematics, University of Niš, Republic of Serbia

Members of the Editorial Board:

Language Editors:

3. **Dr Velimir Ilić**, Department for Russian, Faculty of Philosophy, University of Niš, Republic of Serbia (Russian)
4. **Dr Nenad Blagojević,** Department for Russian, Faculty of Philosophy, University of Niš, Republic of Serbia (Russian)
5. **Nikoleta Momčilović**, Department of German, Faculty of Philosophy, University of Niš, Republic of Serbia (German)
6. **Katarina Stamenković**, Department of German, Faculty of Philosophy, University of Niš, Republic of Serbia (German)

PR Manager:

Lazar Kulašević, Department of Chemistry, Faculty of Sciences and Mathematics, University of Niš, Republic of Serbia

IT Support:

Predrag Nikolić, Team Lead
Petar Petković, Web Developer

Chemia Naissensis, Vol 2, Issue 1, RESEARCH ARTICLE, 1-43

Protein amino acids as a complete (periodic) system

Miloje M. Rakočević*

Faculty of Science and Mathematics, Department of Chemistry, Višegradska 33, 18000 Niš, Serbia (retired from 2003)

ABSTRACT

Referring to the results of previous research on the Cipher of genetic code and analogies of genetic and chemical code – two overall complete natural systems – this paper presents the results of the study on the most complete Protein Amino Acids System (PAAS). It is shown that 20 protein amino acids appear to be a complete system – ordered, coherent, and harmonic. In such a system, all chemical distinctions within the system are accompanied by specific arithmetical and algebraic regularities, including the existence of amino acid ordinal numbers from 1 to 20. The classification of amino acids into two decades (1-10 and 11-20) appears to be in a strict correspondence with the balances of the number of atoms. From the existence of harmonic structures and arrangements of AAs, regardless of whether they are or not the constituents of the genetic code follow the conclusions that the genetic code, through its main constituents – 20 AAs and 4 Py-Pu bases – was complete even in prebiotic conditions.

Keywords: *Protein amino acids, Amino acid code, Genetic code, Binary tree, Gray code, Golden mean, Fibonacci series.*

* University of Niš, Faculty of Science and Mathematics, Department of Chemistry, Višegradska 33, 18000 Niš, Serbia, e-mail: mirkovmiloje@gmail.com

Introduction

This paper is a step further in argumentation of the completeness of the system of protein amino acids (AAs),[1] in the sense that it is a Mendeleevian type of system, whose organization is based on the principles of continuity and minimum change, that is, on the principles of balancing the properties[2] of its elements (within the system). In other words, it is a coherent and harmonious system, both in biotic and prebiotic conditions. In this case, the harmonicity is understood as the correspondence with the golden mean and the Fibonacci series.[3] As such, the system is inevitably in relation to one specific periodic system of numbers (PSN) [Figure A1 in relation to Table B5 and Figures C2 & C3], correspondent (analog) with the periodic system of chemical elements (PSE).

„Regarding the application of theoretical-numerical representations, even Mendeleev considered as appropriate to look for an analytical expression for the law of periodicity, based on theory of numbers." (Trifonov, Dmitriev, 1981, p. 237).]

Previously we have shown that the completeness of PAAS is recognized when protein AAs are observed as constituents of the genetic code (GC) (Rakočević, 1998b; 2004a; 2011a, b; 2018a, b). In this paper, however, we are starting with a *working hypothesis* (Box 1) that the same holds true when the set of 20 protein AAs is observed regardless of their positions in the genetic code displays [in the standard Genetic code Table (Crick,

[1] When we say that the genetic code (GC) was complete even in prebiotic conditions, then we mean on constituents of standard GC, the 20 protein amino acids (AAs) and 4 nucleotide bases. If within this paper we give convincing arguments for the completeness of the system of 20 protein AAs (PAAS), whether they are GC constituents or are just a set of free molecules independent of the positions of the AAs in the Standard GC Table, then we provide evidence also for the completeness of the set of 4 Py-Pu bases, according to the scenario we gave in previous work (Rakočević, 2018a, Section 2, p. 32).

[2]The notions of *balancing* related to the state of the amino acid (genetic) code, as well as the conditions of the system of protein amino acids (PAAS), will be used in the sense of Definitions 1 and 2, given in our previous paper (Rakočević, 2018a, p. 33). Under these assumptions, in this paper we consider that these states are analogous to the same states found in the Periodic system of chemical elements (PSE), when Mendeleev discovered the elements and interpreted their properties by the method of interpolation (Kedrov, 1997, p. 231). [Encyclopedia Britannica: "Interpolation, in mathematics, the determination or estimation of the value of f(x), or a function of x, from certain known values of the function".]

[3] On determination of PSE by the golden mean and the Fibonacci series see in (Trifonov, Dmitriev, 1981) and (Rakočević, 1998a). On the determination of the protein amino acid system (as constituents of the genetic code), also with the golden mean and the Fibonacci series, see in: (Rakočević, 1998b; 2011b).

1966; Rumer, 1966)[4]; in Gray code model of GC (Swanson, 1984) and GC binary tree (Rakočević, 1998b)]. In the argumentation of the working hypothesis, we consider that the coexistence of GC with Boolean spaces (Swanson, 1984; Rakočević, 1994, 1997b, 1998b)[5], analogy with quantum physics (Shcherbak, 1994, 2008),[6] analogy of genetic and chemical code (Rakočević, 2018b) and the existence of "arithmetic inside the universal genetic code" (Shcherbak, 2003) are established facts.

Box 1. *The statements of the working hypothesis*

1. The protein amino acid system (PAAS) is an ordered, coherent, and harmonic system. [Ordered as in Figure 1 in this paper; coherent as in (Rakočević, 2011a, b); harmonic as in (Rakočević, 2004a); with the expectation that all three attributes are applying, while when the protein amino acids are not positioned in the genetic code then they are freely present in the world of molecules.].

2. The order of PAAS is also expressed through the existence of the order of AAs from the first to the 20th [The order according to the logic that each subsequent molecule is similar to the previous one.].

3. "The Little Gauss' algorithm" (Rakočević, 2011b, p. 833) is contained in the Periodic system of numbers (PSN) (Fig. A1)- it is a modified algorithm of "Little Gauss", in the sense that not the numbers are going from 1 to 100 but from 1 to 101. This phenomenon

[4] The sense of deviation, that is of the degree of freedom in deviation from the standard GC as in: (Rakočević, 2018a, Box 2, p. 41). Under the same "degree of freedom" we can now include the "21th" AA Selenocysteine (encoded by the UGA codon found in every domain of life on Earth), as well as the "22nd" AA Pyrrolysine (coded by UAG in Archaea), and we will not consider them within these considerations. Because they are encoding by stop codons, they do not disturb the order within the system of standard protein AAs. It is quite certain that it makes sense to investigate the possible completeness, coherence and harmony and for the system of "22" protein AAs, as well as the trend towards completeness; also makes sense to investigate the completeness of other potential biomolecular systems (Kostić et al., 1998 a,b, pp. 189-194; 195-200).

[5] Rakočević, 1998b, p. 46: "Swanson (1984) has shown that 'the genetic code is almost an example of a Gray code… an example of minimum change binary code' ... If so, then the genetic code can be represented in the form of a binary-code tree, according to the natural numbers sequence 0–63"; Rakočević, 1994, p. 36: „The basic concept from that we start is the Boolean logical square. This square exists within Gray code model of genetic code, [which] code can be *per se* developed in two types of the binary tree: (1) the binary tree which keeps the logic of the Gray code. ... (2) the binary tree with the logic of natural numbers series"; Rakočević, 1997b, p. 5: „Boolean spaces are the main determinants and invariants of the genetic code".

[6] For details about analogies of genetic code and quantum physics see in preprint form of paper (Rakočević, 2018b), OSF Preprints, DOI: 10.31219/osf.io/mxecj (created on October 07, 2017).

was the only analogy that could be found in relations to results in previous three works (Rakočević, 2006; 2011a,b); however, it can now be shown that this arrangement is "taken off" from the PSN (the right picture in Figure 1 in relation to Figure A1).

4. PAAS correspond with PSN [It refers to the correspondences mentioned in the preceding paragraph, but also to others that is first shown.].

5. The pattern 35-36-61 in the chemical code refers to the number of unstable and stable elements respectively in a set of 61 multi-isotopic elements; and in the genetic code refers to the number of codons encoding less and more complex AAs respectively in a set of 61 amino acid codons; and is also valid for the number of atoms in the PAAS [As stated, and what we found in Darwin's diagram (Rakočević, 2015), *i.e.* in his "computer program" (first two columns in Table C1 in relation to the third quadrant of Table C2].

6. PAAS corresponds to the uniqueness of the six-bit binary tree and correspondent Farey tree (both trees in: Rakočević, 1998b, Figures 1 & 2, pp. 284-285) [The uniqueness of the six-bit tree is in its horizontal and vertical mirror symmetry; it is the first and only possible binary tree with one mirror (010/101), as shown in Figure 2 and Figure A2, on the left. Notice that the mirror symmetry for the binary records on the genetic code of the binary tree (Rakočević, 1998b, Figure 1, p. 284) is a face to back, while for the *amino* or *oxo* functional groups is a face to face: *amino vs. amino* and *oxo vs. oxo* group, in reading the binary tree on the left half: from left to right, and on the right half: from the right to the left; the same logic – *amino vs. amino* and *oxo vs. oxo* is valid in reading two Rumer's octets of nucleotide doublets (Rakočević, 2018a, Table 2A, p. 34). Notice also that the comparable position („terminal position“) of the functional group must be the amino group in adenine because it does not have an oxo group.][7].

7. PAAS is (evolutionarily) generated through the unity of the mirror symmetry of the AAs and the mirror symmetry of the correspondent numbers [It is shown that the mirror symmetry 2 *vs.* 5 (010/101) mapped from the six-bit binary tree to the standard Genetic

[7] "The four [bases] are mutually distinguishable by three main characteristics: the type of base (purine, Pu, or pyrimidine, Py); the type of functional group in terminal position (position 6 in purine, position 4 in pyrimidine) – either oxo or amino; and the number of hydrogen bonds linking them in the system codon-anticodon" (Rakočević, 1988, p. 112).

code Table (GCT) has a quantitative meaning of the number of atoms (Table 3 in relation to Table 7 and Figure 2).].

8. PAAS corresponds with the uniqueness of the decimal number system [The uniqueness of the decimal number system: the 9 non-zero digits correspond to the Cantor triadic set: 123 / 456 / 789, which quantities we found as natural entities (Rakočevič, 2018a, Fig. 4 and Rakočević, 2018b, Equations 1 & 2 and Table 4). Notice that the generation of a binary tree represents *ipso facto* a permanent correspondence with the Cantor triad set.) On the other hand, the decimal number system is the only one that has a direct connection with the golden mean (Table B6, the second row where we find the original golden triangle, whose one cathetus is the square root of number 5. Thus, the first cathetus a = q/2, the second cathetus b = 2 and hypotenuse c = 3 = $\Phi^2 + \phi^2$ (Table B6 in relation to Table A1, second column).

9. PAAS corresponds with the uniqueness of the golden mean and the Fibonacci series of numbers. [This statement applies to PAAS when it is a component of the genetic code we have shown in several papers; we mention now only two (Rakočević, 1998b, 2004b). Here, however, we show that this fact applies to PAAS, regardless of the genetic code.]

The procedure for proving *the working hypothesis* will be realized by presenting the relevant facts in the two main segments of this paper: in the Preliminaries, we give new aspects and new knowledge about the previously presented arrangements of the AAs within the GC and/or outside of it, while in the Section "New insights" we provide new insights into the universal completeness of PAAS.

Preliminaries

Already the act of mapping the Gray code model from "A unifying concept for the amino acid code" (Swanson, 1984) into a binary code tree (Rakočević, 1998b, Figure 1, p. 284) was a hint of the existence of a complete – ordered, coherent and harmonious – system of protein AAs. [The Gray code model as in Figure C2, down on the left.] And when, with this act, the sequence of "golden" AAs, existing on positions ϕ^0 to ϕ^9, on the binary code tree, the sequence (G-Q-T-P-S-L-F), was transmitted in a sequence of Mendeleevian order, according to the growing masses of amino acid molecules: (G-S-T-

P-Q-L-F) (Rakočević, 2011b, Fig. 6, p. 832), then PAAS was obvious (Figure 1 in this paper) (Box 2).

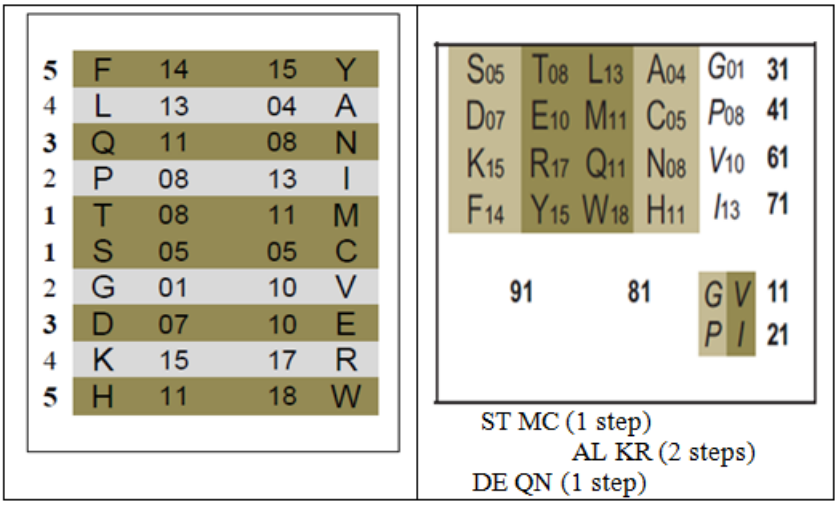

Figure 1. The left picture: Cyclic Invariant Periodic System (CIPS) of AAs (Rakočević, 2011b, Fig. 6, p. 832). The right picture from Rakočević (2011b, Fig. 9, p. 834) (Box 2).

Box 2. *The explanation of Figure 1*

In Figure 1, the left picture from Rakočević (2011b, Fig. 6, p. 832): "The Cyclic Invariant Periodic System (CIPS) of canonical AAs: 1) at the inner side – the atom number within amino acid side chains; 2) in the middle position there are chalcogen AAs (S, T & C, M); 3) follow - in next 'cycle' – the AAs of nonalanine stereochemical types (G, P & V, I); 4) then two double acidic AAs with two their amide derivatives (D, E & N, Q), 5) the two original aliphatic AAs with two amine derivatives (A, L & K, R); and, finally, 6) four aromatic AAs (F,Y & H, W) – two up and two down. The mentioned five classes belong to two superclasses: primary superclass in light areas and secondary superclass in dark areas. Notice that each amino acid position in this CIPS is strictly determined, and none can be changed".[8] New comment, for the left picture: Within "2-3-4-5" rows above plus CM from "1" there are 102 and within "2-3-4-5" down plus ST from "1" also 102 atoms.

[8] Rakočević, 1998b, p. 289: "Within seven 'golden' amino acids (within side chains) [GSTPQLF] there are 60 atoms; within their seven complements [VCMINAY] there are [60+(1×6)] and within six non-complements [DE, KR, HW] there are {[60+(1×6)]+(2×6)} of atoms. [Notice that the differences are 1×6, 2×6 and 3×6 which means realization of minimum change principle and continuity principle at the same time."]

The right picture from Rakočević (2011b, Fig. 9, p. 834): "Dark tones: Class I of amino acids handled by class I of enzymes aminoacyl-tRNA synthetases [except T]; light tones: Class II [except C]." New comment for the right picture (about exceptions C & M) is given in footnote 9.

New comment for both pictures: going from left to the right picture it is evident that chemically related groups of AAs come down for 0, 1 and 2 steps, respectively; for zero "steps" in aromatics FY-WH; for one step in chalcogen AAs ST-MC and in carboxylic DE-QN (carboxylic AAs D & E in relation with their amides N & Q); for two steps in AL-KR.

In support of the completeness of the system on the left picture goes also the splitting according to the ratio 8:12 (2:3) in molecule number: (FYLA + KRHW = 107 atoms); (QNPI + TMSC + GVDE = 97 atoms). In support of the completeness of the system on the right picture go also the relations within the set of 16 AAs of alanine stereochemical type, the balanced relations between rows and columns:

I. (STLA + KRQN = 81) (LA+MC+QN+WH = 81); LAQN = 4 x 9 = 36; STKR = MCWH = 5 x 9 = 45

II. (DEMC + FYWH = 91) (ST+DE+KR+FY = 91); DEFY = 36+10 = 46; MCWH = STKR = 5 x 9 = 45

(The cited previous papers available in www.rakocevcode.rs)

The determination of the amino acid (genetic) code with the golden mean leads to the CIPS (Cyclic Invariant Periodic System) (Figure 1, the picture on the left), in which the positions of five classes of AAs are strictly determined, two in the less complex and three in the more complex superclass: 1. (**SC-TM**), 2. (GV-PI), 3. (**DE-NQ**), 4. (AL-KR), 5. (**FY-HW**); less complex in the 2nd and 4th class and more complex in the remaining three classes (1st, 3rd and 5th), with the following distinction within the side chains of two super classes: H, C, N / N-O, O, S plus aromatic AAs.

As we can see, the CIPS is indeed a complete amino acid system, but AAs positions within the genetic code determine it, and according to our working hypothesis it must be a Mendeleevian type of system, in which AAs are ordered from the first to the last, the 20th amino acid. This condition is fulfilled in certain percentages by the arrangement of the AAs that we find on the right picture of Figure 1 as if it was mapped from one of the PSN diagonals. (In PSN, Figure A1, this diagonal is in black tones.) At the same time,

this arrangement is identical to the arrangement presented on the right picture of Table B1, if the quartets of the AAs are read in a circular direction (as in the Gray code model within Boolean spaces): STLA, DEMC, KRQN, FYWH. Both these mappings, to some extent, confirms the statements of the working hypothesis: 1, 3, and 4. We say "to some extent" because we still do not have the order of AAs from the first to the last, but we have arrangements of AAs in which their positions are independent of positions in GC (the right picture of Figure 1 in relation to the right illustration in Table B1). [The left illustration of Table B1 also shows the correspondence with the pattern 25-36-61, as it is presented in the legend of Table B1.]

It is noteworthy to mention the fact that in all presented AAs pairs, in right picture of Figure 1, the first member, as a smaller molecule, belongs to the class II of AAs, handled by class II of enzymes aminoacyl-tRNA synthetases, and the second to class I. The exceptions are only T and C.[9] [About two classes of AAs, handled by class I & II of enzymes aminoacyl-tRNA synthetases see in: (Wetzel, 1995) and (Rakočević, 1997a); also, in Box 3 in this paper.]

Box 3. *Aminoacyl-tRNA synthetases*

There are two classes of aminoacyl-tRNA synthetases. Class I consists of synthetases with two highly conserved sequence motifs, which aminoacylate at the 2'-OH of an adenosine nucleotide, and they are usually monomeric or dimeric (one or two subunits, respectively). Class II of synthetases contains three highly conserved sequence motifs, and they aminoacylate at the 3'-OH of the same adenosine, and they are usually dimeric or tetrameric (two or four subunits, respectively). Although phenylalanine-tRNA synthetase belongs to a class II, it aminoacylates at the 2'-OH. Within the standard genetic code's Table it does not follow a full distinction of AAs in relation to two classes of the aminoacyl-tRNA synthetases (Wetzel, 1995, Fig. l, p. 546), but within the ″Codon path cube″ it follows with only one exception (Rakočević, 1997a, Fig. 1, p. 646).

[9] The 18 AAs are built with four elements, one from the first (H), and three from the second period of PSE (C, N, O). The remaining two AAs have one element more (sulfur). These two sulfur AAs (C-M) have exactly two chemical analogues among the previous 18 AAs (S-T). It would be expected that in both cases, the smaller molecule belongs to Class II, and the larger to Class I; however, this is not the case: a stronger hierarchy (among periods) has the advantage: S-T, which do not reach the third period belong to Class II and C-M, which can be achieved belong to class I.

Presented classification of AAs within CIPS into classes and superclasses (left picture of Figure 1), in correspondence with two classes of aminoacyl-tRNA synthetases, can be continued further to obtain subclasses and families. Such a sophisticated classification can be useful in analyzing the structure and classification of proteins (Rakočević, 2011b, Figure 7, p. 833).

However, apart from the all above, we are now able to present new balances in CIPS. In Survey 1 it was shown that they have the meaning of the distinctions not only of the half the number of molecules *vs.* the second half, in systems and subsystems (in the ratio 1:1), but also of the distinctions with the ratio 4:6 or 6:4 which means 2:3 or 3:2 (Tables B1, B2 and B3 in relation to Table B6). The ratio 2:3/3:2 we find in the second row of Table B6, containing the system of the generalized golden mean; also 2/3 is the harmonic mean of a whole and its half, and 3/2 also represents the limit of "golden numbers" (Moore, 2004, p. 211.)[10]

Survey 1. The relationships within two systems presented in Figure 1

(FLQP 46) + (MCVERW 71) = 117 (YANI 40) + (TSGDKH 47) = 87 (FLQP 46) + (YANI MC 56) = 102 (WREV 55) + (TSGDKH 47) = 102 102 ±1	(11+91 = 102) (21+81 = 102) (31+71 = 102) (41+61 = 102) 1 ..... 51 101
[(46 + 55 = **102**-1) (56 + 47 = **102**+1)] [(56 – 55 = 1) (47 – 46 = 1)	

The left area in this Survey (Survey 1) is related to the left picture in Figure 1, and the right area to the right one. The members of AAs pairs are symmetrically distributed (F-Y, L-A, *etc.*). See details in the text.

As it is self-evident (from Table B6), in the special case of generalization, the order values of generalized golden mean are related to the series of natural numbers (0, 1), (1,

[10] Except of direct relationship of 2/3 (Tables B1 & B2) with the golden mean (Table B6, 2nd row), there is an indirect relationship in the following sense. In the cases presented here: 4 AAs *vs.* 6 AAs. But this is at the same time the 3/2 ratio as: 6 AAs *vs.* 4 AAs, and it is known that 3/2 represents "the limit of the golden numbers" (Moore, 2004, p. 211: "Our concern here is the study of the sequence $\{g_n\}$ of "golden numbers". A computer analysis of this sequence of roots indicated that the odd-indexed subsequence of $\{g_n\}$ was monotonically increasing and convergent to 3/2 from below, while the even-indexed subsequence was monotonically decreasing and convergent to 3/2 from above").

2), (2, 3) *etc.*, and to Hückel rule at the same time (the right illustration in Table B5: the first column in relation to the far right column); also to the squares of natural numbers sequence: (1, 2), (2, 3), (3, 4), ..., when they correspond to the balance "11" (Table A1).

Table 1. The order of protein amino acids based on two classes aminoacyl-tRNA synthetases

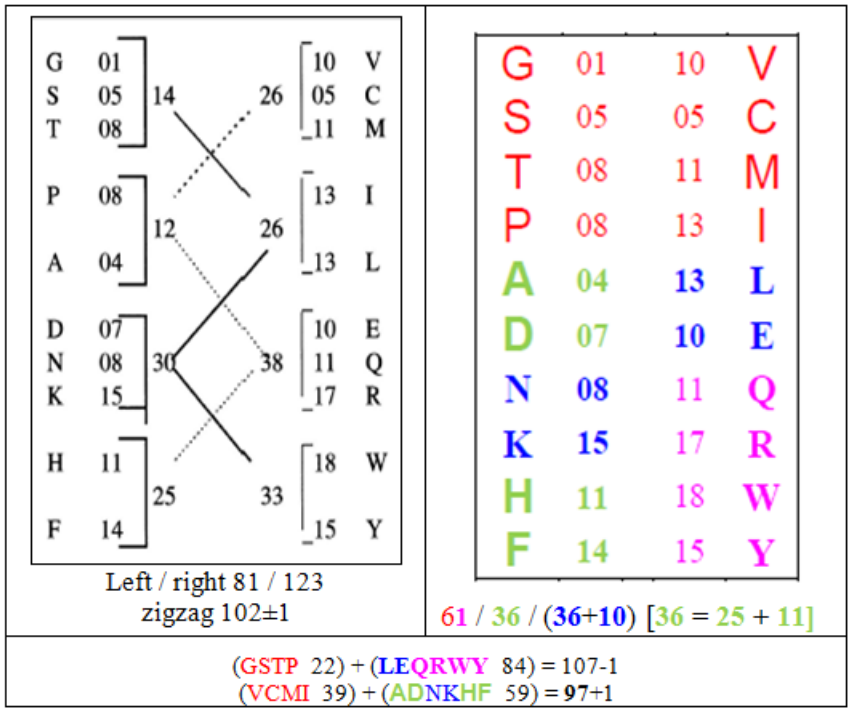

The left illustration of this Table (Table 1) follows from Rakočević (1998b, Survey 4, p. 290): „On the first (full) zigzag line, there are 102+1 atoms whereas on the second (dotted) line there are 102−1 atoms. The arithmetic means for both: 102±1. Class II handles the smaller amino acids within the pairs (on the left), whereas class I aminoacyl-tRNA synthetases handled the larger amino acids (on the right)." The right illustration is a new arrangement for this paper. See details in the text.

Now we go back to CIPS (left picture of Figure 1 in relation to Survey 1). When the first four of the AAs from the first column are added to six of the AAs from the second one, and *vice versa* (Figure 1 in relation to Survey 1), in these groups of AAs the number of atoms corresponds to the quantities indicated between the fifth and sixth row of Table

A2: 87 as (97 – 10) and 117 as (107 + 10)[11] [Notice that 87 = 86 + 01]. Here, it is particularly interesting the fact that only two sulfur AAs (C & M) appear as a tongue on balance: by moving them from one subgroup to another, the balance 87: 117 turns into a balance of 102: 102. [In the side chains of 20 standard AAs there are 117 hydrogen and 87 non-hydrogen atoms (Sukhodolets, 1985; Rakočević, 2011b, Table 7, p. 830).]. But the balancing also exists when the distinctions from the state 4 *vs.* 6 AAs, or 5 *vs.* 5 (in the shaded and non-shaded space) go on and in a different way as shown in Tables B2 & B3 and the accompanying Survey B1. In doing so, the quantization from the ratio 87: 117 goes to 97: 107.

In the left part of Figure 1, we see also that at the center of the CIPS system, there is a subsystem with high molecular diversity. Two and two AAs of non-alanine types (G-P and V-I) have "captured" the only two sulfur AAs (with sulfur existing in the third period and the sixth group of PSE: cysteine and methionine) and their two oxygen analogues (existing in the second period and a sixth group of PSE: serine and threonine). Realizing that here we have a Mendeleevian order (continuity and minimum change in atom number) with glycine in front: G-S-T-P, it makes sense to bring it in connection also with Mendeleev's based subsystem of the remaining 12 AAs of alanine type, led by alanine and presented in left picture of Table B1. [The only change in this process of connecting the two subsystems is that C and T exchange their positions.] The two subsystems thus connected give a new system, presented in Table 1.

The left illustration in Table 1 was firstly published in 1998, and then in 2004 (Rakočević, 1998b, Survey 4, p. 290; 2004a, Fig. 1, p. 222). With all provided information there, we now show distinctions from the aspect of division into 4: 6 amino acids. The illustration on the right side of Table 1 shows that the pattern 25–36–61 is really "played" here, which we already had with the genetic code and chemical code (Rakočević, 2018a and 2018b). On the right side is the first-class of amino acids, and on

[11] Relationships with quantities 97/107 we can find in all essential arrangements of AAs: Table 1 & 2, Tables B2 & B3, and Survey B1.

the left side is the second class of amino acids.[12] Each molecule from the second class is smaller than the paring member in the first class.

At the bottom of the first class, there are four amino acids in which there are exactly 61 atoms, and at the top, there is the amino acid quartet which, together, with their in the second-class partners (total of eight amino acids) together also have 61 atoms. The two quartets in the right column are separated by a doublet L-E, while in the left column the quartet A-D-H-F is splitting into doublet A-D and doublet H-F; the H-F exactly with 25 atoms, and A-D with 11 atoms; a total within the quartet of 36 atoms. In two "breakable" doublets (diagonally connected) there is 23+23 = 36+10 atoms. Altogether exactly as it is predicted by working hypothesis (statements 4 & 5), and showed in Table A2 (the fifth and sixth row).

New insights

From a chemical point of view the first step of classification of protein amino acids (AAs), must be the classification into aliphatic and aromatic AAs, where on a hierarchical scale of changes by similarity and complexity, aliphatic AAs must precede the aromatic. For the same reason of the chemical hierarchy, within the class of aliphatic AAs at the beginning must be the hydrocarbon AAs (possessing in the side chain carbon and hydrogen, or hydrogen only, in the case of glycine), and at the end two sulfur AAs, quite different from preceeded non-sulphuric AAs. It means that two sulfur AAs (as the last in the class of aliphatic amino acids) must be found in direct contact to the aromatic.

Full certainty

In the further course of the sequencing of AAs, in terms of changes by similarity, from the aspect of the AAs singlets and/or doublets, *i.e.*, pairs, the appropriate distinctions in three areas should be considered: hydrocarbon, aromatic, and those between them. In the set of aromatic AAs, Phe came the first, as the simplest, followed

[12] The class I is realized by AAs handled by class I, while class II is realized by AAs handled by class II of enzymes aminoacyl-tRNA synthetases, respectively.

by Tyr, and Trp, all three with possession of a benzene ring.[13] At the very end ultimately must be His, the only one which does not possess the aromatic benzene ring (Table 2 in relation to Survey 2).

In the set of hydrocarbon AAs, at the very beginning must be Gly as the simplest AA, followed by Ala as the first possible case of hydrocarbon series with an open carbon chain. At the same time, for chemical reasons, it seems that Gly-Ala can be considered as a pair of AAs. Then comes the par Val-Pro, both with three carbon atoms in the side chain, rather than Leu and Ile with four carbon atoms. Val with half-cyclic chain precedes Pro. [On the relations between valine and proline, such that the valine is bound by the vertices, and the proline by the side of the isopropyl "triangle" for the amino acid functional group, see in (Rakočević and Jokić, 1996).]

Order uncertainty

After the pair Val-Pro, it follows the pair Leu-Ile or Ile-Leu? One possible solution is that Ile precedes leucine (Table 2) because it has already been demonstrated that Ile chemically best suits to the proline (Rakočević and Jokić, 1996, Survey 1.2), and in addition it is a derivative and pairing-member of valine within a set of only two AAs of the valine stereochemical type (Rakočević and Jokić, 1996; Rakočević, 1998b, Survey 4, p. 290). In this solution, Ile has the status of "the first and only" possible derivative, the valine derivative, from the aspect of the change at the end of the valine side chain ("non-standard" hydrocarbon amino acid in the set of 20 AAs due to the above-mentioned "triangle" in the amino acid side chain); and the leucine has the status of "the first possible case" from the aspect of hydrocarbon chain branching.

[13] In fact, it is a toluene ring, as a condition of belonging to the alanine stereochemical type, with one CH_2 group between the "head" and "the body" of amino acid molecule (Rakočević and Jokić, 1996. [The 16 AAs of alanine stereochemical type; the 04 AAs of non-alanin stereochemical types: glycine type with only glycine, proline type with only proline and valin type with valine and isoleucine (Popov, 1989; Rakočević and Jokić, 1996).]

Table 2. The order of protein amino acids based on chemical similarity

(1)	G	01	08	N	(11)
(2)	A	04	07	D	(12)
(3)	V	10	05	S	(13)
(4)	P	08	08	T	(14)
(5)	I	13	05	C	(15)
(6)	L	13	11	M	(16)
(7)	K	15	14	F	(17)
(8)	R	17	15	Y	(18)
(9)	Q	11	18	W	(19)
(10)	E	10	11	H	(20)
		102	102		
(97)		51±1	51±1		**(107)**
In both columns: odd 50; even 52					
(—— 102) (..... 102)					

The 20 protein AAs are arranged into two decades in accordance to ordinal amino acid number, 1-10 and 11-20; the numbers presented outer: the ordinal numbers 1-20; the numbers presented inner: the number of atoms within side chain of the responding amino acid. In red color AAs handled by class I aminoacyl-tRNA synthetases. In both columns: odd 50 and even positions 52 atoms. Within two decades there are 120 atoms in each; in both zigzag lines also 102 and 102 atoms. First four plus six last equals 97/107 respectively [(GAVP) + (CMFYWH) = 97] [(NDST) + (ILKRQE) = 107][VILRQE = CMFYWH = 74] [GAPK = NDST = CMYW = 28][(1 x 74 = 74) (3 x 28 = 84)]. See details in the text.

Another possibility is that Leu precedes the isoleucine to the following logic and chemical similarity: In the relation of Val-Pro *vs.* Leu-Ile, the Leu chemically corresponds more to valine and Ile to proline (Table B4). "Paradoxically," there is a change of status: now Leu has the status of "the first and only" possible derivative, in a set of only two AAs, in the pair of Val-Leu, where happens the splitting into the valine and alanine stereochemical types. In doing so, the derivation occurs at the beginning of the valine side chain, in contact with the amino acid "head", *i.e.*, amino acid functional

group. [This uniqueness of the two-member set also follows from the above said uniqueness of the isopropyl group "triangle".] On the other hand, Ile gets now the status of the "first possible case" from the aspect of the branching.

However, this "paradox" should not be surprising. If the analogy with quantum physics is already on the scene, then this kind of analogy with Heisenberg's uncertainty principle can be expected.

The "between" area

Finally, it remains to determine the chemical distinctions of AAs in "between" area. We have already said that sulfur amino acid pair, Cys-Met, precede aromatic amino acids. As chalcogen AAs, they must be in contact with other two chalcogen amino acids, Ser-Thr. By this, the contact has to be made *via* Cys because it possesses SH group, correspondent to OH group in Ser as well as in Thr.

It is to be understood that a pair of oxygen AAs with the hydroxyl (OH) functional group in side chain must be in contact with a pair of two also oxygen AAs, but which possesses the carboxyl (COOH) functional group: Asp-Glu. However, the problem is that both of these two AAs have their amide derivatives (Asn-Gln) and it is not easy when determining the distinctions, which here proceeds and which follows.

It turns out, however, that the problem is easier to solve when returning to the beginning, in the area of hydrocarbon AAs, to the "point" of the pair Ile-Leu. Further must follow the pair of nitrogen derivatives, Lys-Arg, and Lysine must come first with four carbon atoms in the side chain, which number is also valid for Leucine; and then, with the validity of both principles – the continuity and minimum of change – comes Arginine with three atoms (not counting carbon atom in the guanidino group). Then, chemically speaking, it is very natural that after Arginine comes Gln with its precursor, the glutamic amino acid, both (Gln-Glu) with two carbon atoms in the side chain; it is natural indeed that, in terms of chemical similarity, after 3C atoms occurs changes into 2C atoms, better than into 1C atom, like in the pair Asn-Asp. [As in the case of the guanidino-functional group in arginine, no carbon atom is counting in the carboxylic or

amide functional group.] With this, chemical sequencing of series of 20 AAs closes, starting from the first, glycine, and ending with very different histidine (Table 2).

Survey 2. The relationships in the system presented in Table 2

GAVP 23 CMFYWH 74 (**97**) ILKRQE = 79 NDST = 28 (**107**)	VILRQE 74 / CMYW 49 → 123 GAPK 28 / NDSTFH 53 → 81 74 + 53 = **127** 49 + 28 = **77**
(GAVP 23) + (NDST 28) = **51 x 1** (ILKRQE 79) + (CMFYWH 74) = **51 x 3** (23 + 79 = **51 x 2**) / (28 + 74 = **51 x 2**)	

The Survey (Survey 2) presents the relationships in Table 2. The key results appear to be in relation to the quantity 97 which follow from the pattern 25-36-61 [(25+36 = 61) (61+36 = 97)]; the adding as in Fibonacci series; cf. Table A2 rows 5 & 6); other balance quantities: 102 and 51 as the ½ and ¼ of quantity 204 as the total number of atoms within 20 amino acid side chains. [Rakočević, 2004a, a legend to Fig. 1, p. 222: "within AAs (side chains) in class II there are 81, whereas in the class I the 0123 of atoms. Notice that 81 (as 9 x 9) is the first possible (zeroth) arithmetic square in module 9, and 0-1-2-3 is the first possible (zeroth) logical square (as 00-01-10-11)."]

The main result

The main result of this pure chemical sequencing of AAs, presented in Table 2, shows that these chemical distinctions are accompanied by specific arithmetic regularities, including the existence of amino acid ordinal numbers from 1 to 20, with two decades (1-10 and 11-20); and also shows the full balance of the number of atoms in the 20 amino acid molecules: 102±0 atoms in two decades, as well as on two zigzag lines, where such a system with two zigzag lines represents the first possible *periodic system* with two periods.

There is also another result, also directly "taken up" from the Periodic system of numbers (PSN), which simultaneously corresponds to the unique situation in the PSN (Figure A1) and the number of atoms in 20 AAs: 26-42-59-77, within side chains of 4 x 5

of AAs which grouping follows from four amino acid diversity types[14] (Rakočević, 2011b, Figure 3, p. 828). Since these four results are obtained from the "center" of the PSN, it makes sense to compare them with four results obtained from the diagonal of the same system, presented in the right picture of Figure 1 (Equation 1). By this, it makes sense to assume that the quantities "2" and "5" should be understood in the same manner as in Figure 2 (as well as the quantities "1" and "6"), „taken up" from the six-bit binary tree, as shown in Equation 2 (in relation to Figure C3).

31 41 61 71
5 1 2 6 → (5 + 2 = 1 + 6 = 7) ..... (1)
26 42 59 77

5 6
101 110 (101 + 010 = 111) ..... (2)
010 001 (110 + 001 = 111)
2 1

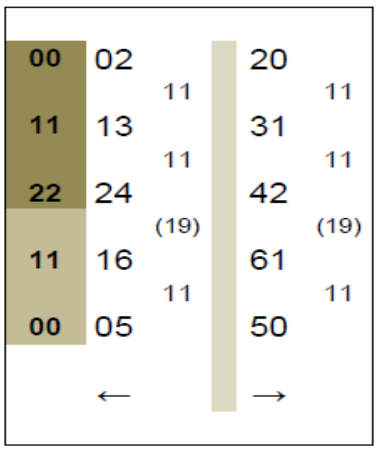

Figure 2. The arrangement is "taken off" from the Periodic Number System (PNS, Figure A1), from where the significant diagonal connects with the initial triangle in Boolean space: 0,1,2 (000, 001, 010). On the left side (shaded) there is a doubled sequence 0-1-2, connected and superposed with its mirror image. Following the logic given in statement 6 of the working hypothesis (Box 1), it makes sense to add the "2" and "5" quantities in the best balance relations. The numbers 02, 13, 24, 16, 05 are obtained, and their mirror image in the tenth step, as shown in Table A3.

[14] (G_1+A_4+C_5+N_8+P_8 = **26**); (S_5+D_7+T_8+Q_{11}+H_{11} = **42**); (Y_{15}+M_{11}+E_{10}+V_{10}+L_{13} = **59**); (W_{18}+R_{17}+F_{14}+I_{13}+K_{15} = **77**). These four sets of AAs follow from four amino acid diversity types (see explanation of Table 6 in Box 4).

Table 3. The order of five quartets of protein amino acids following from Table 2 (I)

[**72** (78 – 6)]			[**12 x 6**]		
G (01)	A (04)	N (08)	D (07)	→	**20**
V (10)	P (08)	S (05)	T (08)	→	**31**
I (13)	L (13)	C (05)	M (11)	→	**42**
K (15)	R (17)	F (14)	Y (15)	→	**61**
Q (11)	E (10)	W (18)	H (11)	→	**50**
51-1	51+1	51-1	51+1		
[**132** (2 x 66)]			[**22 x 6**]		

This Table (Table 3) follows from Table 2 and PSN (Figure A1), from a doubled starting triangle from the top of the last column; triangle switched with its mirror image and superimposed: (00-11-22 / 22-11-00 → 00-11-**22**-11-00 (Table 2 and Table A3). Now we can see that with this arrangement the distinctions and classifications of protein AAs follow another multiplication of number 6 more than was found in the golden mean determination of CIPS (see the legend of Figure 1). Together with the results: (10 x 6 = 60), (11 x 6 = 66), (13 x 6 = 78), we now have the result (12 x 6 = 72). There is still no result (14 x 6 = 84), so if it will occur, then – bingo, the only mirror logical square in the series of natural numbers is reached, also included in Darwin's "computer program". [On the only Darwin's diagram in his famous book *Origin of species*, we see that at the top of the branch "m", between the written numbers 10 and 14, the positions of unwritten numbers 11, 12 and 13 are also indicated (Figure C1).]

Table 4. The order of five quartets of protein amino acids following from Table 2 (II)

120 (2 x 60) **[20 x 6]**					
G (01)	A (04)	N (08)	D (07)	→	**20**
V (10)	P (08)	S (05)	T (08)	→	**31**
I (13)	L (13)	C (05)	M (11)	→	**42**
K (15)	R (17)	F (14)	Y (15)	→	**61**
Q (11)	E (10)	W (18)	H (11)	→	**50**
51-1	51+1	51-1	51+1		
84 (78 + 6) **[14 x 6]**					

In this Table (Table 4), all is the same as in Table 3, but with the diagonal one step lower. The colors are used to indicate the AAs that are repeated in the "84 atoms" and "120 atoms" quantities in Table 5. From that crossing a specific amino acid distinction follows: at the beginning of dark area the **8** AAs (G, A, V, P, L, N, D, S) as the first possible cases, and at the beginning of light area the **2** AAs (I, K) as "non-standard" AAs: Ile, as the only one derivative within the valine stereochemical type, and Lys as the fourth case, instead of the first as in the Ser and Cys case. In the light area follow the **4** AAs (Q, E, R, W) as the second (Gln, Glu) or different (Arg, Trp); in the dark area follow the **6** AAs (C, M, F, Y, H, T), two sulfur, three aromatic and one with hydroxide functional group. (Cf. legends of Tables 5 & 6.) [It is possible to see the "rotation" in the Ile-Leu pair, depending on which precedes, and which follows in PAAS, presented in Table 2, what is explained in the Section "Order uncertainty".]

Table 5. The order of five quartets of protein amino acids following from Table 2 (III)

[84 (78 + 6)**]** **[14 x 6]**					
G (01)	A (04)	N (08)	D (07)	→	**20**
V (10)	P (08)	S (05)	T (08)	→	**31**
I (13)	L (13)	C (05)	M (11)	→	**42**
K (15)	R (17)	F (14)	Y (15)	→	**61**
Q (11)	E (10)	W (18)	H (11)	→	**50**
51-1	51+1	51-1	51+1		
[120 (2 x 66)**]** **[22 x 6]**					

In this Table (Table 5) all is the same as in Table 3, but with the opposite diagonal in relation to diagonal in Table 3, and colors as in Table 4.

Survey 3. The balance relationships between the arrangements in Tables 4 and 5

IK QREW GV IK APLNSD GVAPLNS CF D TMYH QRE CFWTMYH	IK 28 + QREW 56 = 84 IK 28 + GVAPLNSD 56 = 84 GVAPLNSD 56 + CFTMYH 64 = 120 QREW 56 + CFTMYH 64 = 120
[(7 x 4 = 28) (7 x 8 = 56) (8 x 8 = 64)] [(6 x 14 = 84) (6 x 20 = 120)] (120 – 84 = 36 = 6 x 6)	

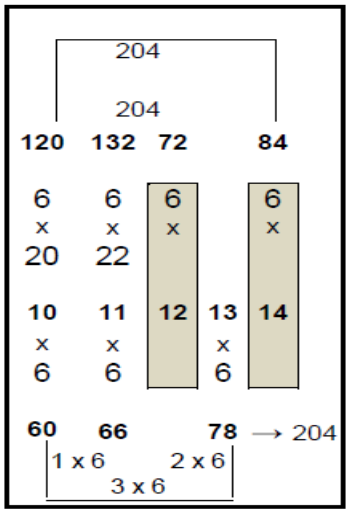

Figure 3. The multiplication of number 6 found in arrangements of AAs in Figure 1 and Tables 3, 4 and 5: the multiples of 10, 11, 12, 13, 14. (The unique sequence as in Table A4 and in top of Darwin's Diagram (Figure C1: $m^{10} – m^{14}$).

Table 6. New splitting within the arrangement presented in Table 2

(1)	G	01	08	N	(11)	G	01	11	H	12
(2)	A	04	07	D	(12)	A	04	18	W	22
(3)	V	10	05	S	(13)	V	10	15	Y	25
(4)	P	08	08	T	(14)	P	08	14	F	22
(5)	I	13	05	C	(15)	L	13	11	M	24
(6)	L	13	11	M	(16)	I	13	05	C	18
(7)	K	15	14	F	(17)	K	15	08	T	23
(8)	R	17	15	Y	(18)	R	17	05	S	22
(9)	Q	11	18	W	(19)	Q	11	07	D	18
(10)	E	10	11	H	20)	E	10	08	N	18
AAs: [(2_{28}), (4_{56}), (6_{64}), (8_{56})]						Atoms: 12–18–22 – (24 x 3)					

Box 4. *The explanation of Table 6*

The left illustration in Table 6 follows from Survey 3 and Table 4, while the right illustration follows from Table 2 by rotating the second decade by 180 degrees. [This rotation process is a kind of cyclization; thus, the amino acid arrangement in Table 2 we can call CIPS II versus CIPS I in left picture of Figure 1.] The left illustration contains the result of the crossing of Table 4 with Table 5. Four "new types" of amino acid diversity, comparable to those previously found (Rakočević, 2011b), were obtained. The new types: [(G, A, V, P, L, N, D, S); (C, M, F, Y, H, T); (Q, E, R, W); (I, K)]: the 8 AAs as the first possible cases; the 2 AAs as "non-standard" (as it is explained in the legend of Table 4); the 4 AAs as the second (Gln, Glu) or different (Arg, Trp); the 6 AAs, all the same as the 6 AAs in the "old types" of diversity (Rakočević, 2011b), all but one, Thr instead of Trp. [Thr is the only "black sheep" in the set of 16 AAs of the alanine stereochemical type, given that one of its hydrogen atoms in the CH_2 group, between the head and the body, is replaced by one CH_3 group; on the other hand, Trp is the only "black sheep" in the set of aromatic AAs, having two rings.] "Old type": [(G, P); (A, L, V, I); (C, M, F, Y, W, H); (R, K, Q, N, E, D, T, S)]: the 4 hydrocarbon AAs; the 2 as different, "non-standard" hydrocarbon; the 8 AAs that within the side chain ("body") have a functional group mapped from the "head"; the 6 AAs in which there is no mapping of functional groups from head to body.

Table 7. The generalized Table of standard Genetic code

UUN	F L	UCN	S	UAN	Y CT	UGN	C CT
CUN	L	CCN	P				W
				CAN	H	CGN	R
(0)		(1)		(4)	Q	(5)	
AUN	I M	ACN	T	AAN	N K	AGN	S R
		GCN	A				
GUN	V			GAN	D	GGN	G
(2)		(3)		(6)	E	(7)	

Table 7 presents the codon families and their positions on the six-bit binary tree (Rakočević, 1998b, Figure 1). By comparing the positions of codons and AAs on this binary tree, we find that the arrangement is determined by cross-mirror symmetry, in contrast to 000 FLL/111 SRG on the left diagonal and 010 IMV/101 CWR on the right one. In doing so, the key contrasts are: on the least change path Phe UUU 000 000 *vs.* 111 111 GGG Gly crossed with Val GUC 010 101 *vs.* 101 010 UGA "stop" on the path of the maximal changes, when each zero number follows the number one and vice versa. [Notice that "The path of the maximal changes" (101 010 etc., on the correspondent Farey tree is "The golden ruth" as it is presented in Figure 2 in (Rakočević, 1998b).]

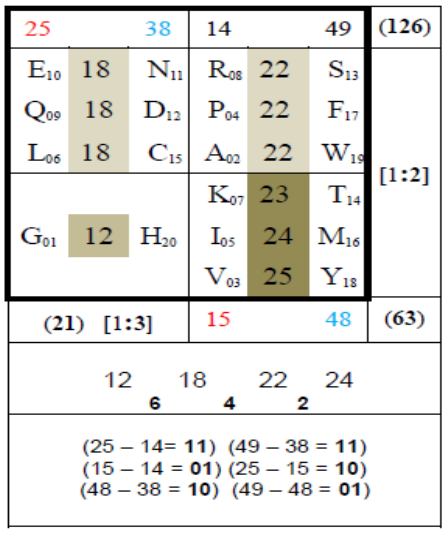

Figure 4. This arrangement of PAAS follows from the right illustration in Table 6 (from CIPS II). The expression of the principle of balancing, through the interconnection of the chemical properties of AAs, the number of atoms and the ordinal number of AAs in CIPS II, is self-evident. Confirmation of V. Shcherbak's hypothesis (1994) on the analogy of the amino acid (genetic) code with quantum physics also.

However, the result of the most surprising is the result shown in Table 3 (in relations with Tables 4 & 5). It is indeed a mirror image of our hypothetical result, which we gave with a working hypothesis (the statement 6 in relations to the statements 2, 4, 7 and 8): 20 -31-42-61-50 *vs.* 02-13-24-16-05 (Figure 2 in relation to Table A3). In the system presented in Table A3, the result is found in the 10th step, with sum 204, as well as the number of atoms in 20 AAs, in their side chains. As a curiosity or something more than that, the right neighbor is the number 220 (the first friendly number), the lower vertical

neighbor is the number 284 (the second friendly number) and the top 124 the fourth of the third perfect number (124 x 4 = 496).][15]

Altogether these are systematic natural arrangements, whose organization and determination correspond with the principle of self-similarity.[16] The already well-known facts that genetic code represents an analogy with natural (verbal) language[17] are joined now to the facts about analogies between genetic code arrangements and specific arrangements within the set of natural numbers.[18]

Conclusion

The facts and arguments presented in this paper fully confirm all nine statements of the working hypothesis (Box 1) about the existence of a complete system of protein amino acids (PAAS), both in biotic as well as in prebiotic conditions, *i.e.* within the amino acid (genetic) code, and independently from it. The existence of such facts also supports our hypothesis that the genetic code, viewed through its chemical constituents, was still prebiotic complete (Rakočević, 2004a). Also, everything that is discussed in this paper is in favor of our attitude that both genetic and chemical code corresponds to one specific spontaneous, intelligent design (SPID) (Rakočević, 2018a, Box 4).[19]

---

[15] A hypothesis on the determination of the genetic code with the perfect and friendly numbers we have presented in the book (Rakočević, 1997b). (www.rakocevcode.rs) [Perfect numbers: 6, 28, 496, 8128, *etc.*; the pairs of the friendly numbers: (220-284), (1184-1210), (17296-18416) *etc.*]

[16] "In correspondence with this, Complete Genetic Code must be based on several key principles. We are going to list only those considered to be the most important: 1. The principle of systemic self-related and self-similar organization. …" (Rakočević, 2004a, p. 231).

[17] "Rumer (1966) suggests that encoding by dinucleotide aggregations is mediated by 'grammatical' formalism (the relation between words and the root of the word), semantics (one-meaning and multy-meaning codon families) and by semiology, *i.e.* semiotics (the classification of nucleotide doublets after the number of their hydrogen bonds which appear here as 'significant' and 'signifié'" [(Rakočević, 2018a, pp. 31-32 in relation to (De Saussure, 1985, p. 99) (Cf. De Saussure's logical square of natural language in relation with the genetic code language in Figure C2)].

[18] "In determination of the genetic code, except two inherent alphabets – twenty amino acids and four amino bases (two pyrimidines & two purines – is involved still one 'hidden alphabet', the series of natural numbers, with all its regularities and laws" (Rakočević, 2011a, p. 4). An "unfaithless Tomas" may consider this to be numerology, but the facts are the facts. For any theory of probability, it is not possible to prove that all these "downloads" of chemical facts from the Periodic system of numbers (PSN) are mere coincidence.

[19] In further research, it may be possible to get a better term (and notion) by analogy with Carl Jung's term "Synchronizität" ("Synchronicity": Jung, 1993), but with the opposite meaning. This new term could be

Acknowledgment

I am very grateful to the Editorial Board of the Journal *Chemia Naissensis* for the kind invitation to write this paper. This invitation refreshed my beautiful memories on the 15 final years of my professional work at the Department of Chemistry, Faculty of Science and Mathematics, University of Niš. Especially I thank to Vesna Stankov Jovanović, Editor-in-Chief and to Biljana Arsić, Deputy Editor-in-Chief, for the great help in the editing of the paper. Also, I am very grateful to Dejan Raković for helpful and stimulating discussions in the preparation of the paper for publishing.

References

Crick, C. H. F. (1966). The genetic code yesterday, today and tomorrow, Cold Spring Harbor symposia on quantitative biology, 31, 3-9; Published also in: The chemical basis of life – an introduction to molecular and cell biology. Scientific American, 1973, 192–198.

Crick, C. H. F. (1968). The origin of the genetic code. Journal of Molecular Biology, 38, 367–379.

Darwin, Ch. (1859). On the Origin of Species. London: John Murray.

De Saussure, F. (1985). Cours de linguistique générale. Paris: Payot.

Jung, C. G. (1993) [1952]. Synchronicity: An acausal connecting principle. Bollingen, Switzerland: Bollingen Foundation. ISBN 978-0-691-01794-5. Since included in his Collected Works volume 8.

Kedrov, B. M. (1977). Predictions of Mendeleev in Atomism – Unknown Elements.

"Harmonizität" ("Harmonicity"), but while Synchronicity refers to acausal "meaningful coincidences", the Harmonycity refers to indirect-causal meaningful correspondences. These correspondences follow from interpolation relationships within PSE, with the validity of two Mendeleevian principles (continuity and minimum change), both for chemical elements and for compounds that build complete and consistent molecular systems.

Kostić, A. D., Miletić, S. S., & Rakočević, M. M. (1998a). Natural categorization of flavonoids, V Symposium on flora of Southeast Serbia, Zaječar, 1997, Proceedings, University of Niš, Faculty of Technology in Leskovac, pp. 189-194. [V Simpozijum o flori Jugoistočne Srbije, Zaječar, 1997, Zbornik radova, Univerzitet u Nišu, Tehnološki fakultet u Leskovcu, pp. 189-194.]

Kostić, A. D., Rakočević, M. M., Miletić, S. & S. (1998b). The evolution development of flavonoids characteristics, V Symposium on flora of Southeast Serbia, Zaječar, 1997, Proceedings, University of Niš, Faculty of Technology in Leskovac, pp. 195-200. [V Simpozijum o flori Jugoistočne Srbije, Zaječar, 1997, Zbornik radova, Univerzitet u Nišu, Tehnološki fakultet u Leskovcu, pp. 195-200.]

Moore, G. A. (1994). The limit of the golden numbers is 3/2. The Fibonacci Quarterly, June-July, 211-217.

Popov, E. M. (1989). Strukturnaya organizaciya belkov. Moscow: Nauka, in Russian.

Rakočević, M. M. (1988). Three-dimensional model of the genetic code. Acta Biologiae et Medicinae Experimentalis (Prishtina), 13, 109–116; excerpt in: www.rakocevcode.rs.

Rakočević, M. M. (1994). Logic of the Genetic Code. Belgrade: Naučna Knjiga.

Rakočević, M. M. (1997a). Two classes of the amino acyl-tRNA synthetases in correspondence with the Codon path cube. Bull. of the Mathematical Biology, 59, 645–648.

Rakočević, M. M. (1997b). The Genetic Code as a Unique System. Niš: Studentski Kulturni Centar, www.rakocevcode.rs.

Rakočević, M. M. (1998a). The Harmony of the Periodic System of Chemical Elements, Flogiston, 7, 169-183, Belgrade (in Serbian, with a broader summary in English).

Rakočević, M. M. (1998b). The genetic code as a Golden mean determined system. Biosystems, 46, 283–291.

Rakočević, M. M. (2004a). A harmonic structure of the genetic code. Journal of Theoretical Biology, 229, 221–234.

Rakočević, M. M. (2004b). Further generalization of Golden mean in relation to Euler's „divine" equation. FME Transactions (Faculty of Mechanical Engineering, Belgrade, Serbia), 32, 95-98.

Rakočević, M. M. (2006). Genetic Code as a Harmonic System. arXiv:q-bio/0610044 [q-bio.OT]

Rakočević, M. M. (2011a). Genetic Code: Four Diversity Types of Protein Amino Acids.

Rakočević, M. M. (2011b). Genetic code as a coherent system. NeuroQuantology, 9 (4), 821-841.

Rakočević, M.M., 2015. Enigma of Darwin Diagram. http://dx.doi.org/10.17605/OSF. IO/QZG69. stored on 2015-01-06. Also stored in: OSF Preprints, 2017-11-29 (UTC). www.rakocevcode.rs.

Rakočević, M. M. (2017a). Analogies of Genetic and Chemical Code. http://dx.doi.org/10.17605/OSF.IO/MXECJ. (stored also in: OSF Preprints 2017-08-09)

Rakočević, M. M. (2018a). The Cipher of the Genetic Code. BioSystems, 171, 31–47.

Rakočević, M. M. (2018b). Analogies of Genetic and Chemical Code. Polyhedron, 153, 292–298.

Rakočević, M. M., & Jokić, A. (1996). Four stereochemical types of protein amino acids: synchronic determination with chemical characteristics, atom and nucleon number. Journal of Theoretical Biology, 183, 345–349.

Rumer, Y. B. (1966). O sistematizacii kodonov v geneticheskom kode, Doklady Akademii Nauk SSSR, 167, 1393–1394.

Shcherbak, V. I. (1994). Sixty-four triplets and 20 canonical amino acids of the genetic code: the arithmetical regularities. Part II. Journal of Theoretical Biology, 166, 475-477.

Shcherbak, V. I. (2003). Arithmetic inside the universal genetic code. BioSystems, 70, 187–209.

Shcherbak, V. I. (2008). The arithmetical origin of the genetic code. In: Barbieri, M. (Ed.), The Codes of Life: the Rules of Macroevolution. Berlin: Springer, pp. 153–181.

Sukhodolec, V. V. (1985). The meaning of the genetic code: the reconstruction of the stages of prebiological evolution (in Russian). Генетика XXI (10), 1589–1599.

Swanson, R. (1984). A unifying concept for the amino acid code. Bulletin of Mathematical Biology, 46, 187–207.

Taylor, R. J. F., & Coates, D. (1989). The code within codons. Biosystems, 22, 177–187.

Verkhovod, A. B. (1994). Alphanumerical divisions of the universal genetic code: new divisions reveal new balances. Journal of Theoretical Biology, 170, 327–330.

Trifonov, N.D. & Dmitriev, S.I. (1981). On the quantitative interpretation of the periodical system, in the book: The Doctrine of Periodicity, edited by D. N. Trifonov, Moscow: Nauka Publishing House (in Russian)

Wade, Jr., L. G. (2013). Organic Chemistry, 8th international edition. New York.

Weaver, R. F. (2012). Molecular Biology, 4th international edition. New York: McGraw-Hill.

Wetzel, R. (1995). Evolution of the aminoacyl-tRNA synthetases and the origin of the genetic code. Journal of Molecular Evolution, 40, 545-550.

Woese, C.R., et al. (1966). On the fundamental nature and evolution of the genetic code. Cold Spring Harbor Simposia on Quantitative Biology, 31, 723-736.

APPENDIX A

Periodic system of the numbers

The periodic number system (PSN) was originally given in: (Rakočević, 2011a, Table 4, p. 12 and 2011b, Table 4, p. 826), and here is only a different shading and one relevant diagonal with its own source in the double starting "triangle": (00-11-22). [We say "triangle" thinking that this number series corresponds with the first possible "triangle" in Boolean space (0-1-2, i.e. 000-001-010). However, this is a special topic that remains outside of the scope of this paper, for some other occasion.] In both previous presentations, in order to avoid misunderstanding in the scientific public as "pure numerology," I only labeled it "Table of minimal adding". Now I can no longer run back, and here I am presenting it as a PSN, as a reality.

	...										
(-2)	...									...	-22
(-1)	-21	-20	-19	-18	-17	-16	-15	-14	-13	-12	-11
(0)	-10	-09	-08	-07	-06	-05	-04	-03	-02	-01	00
(1)	01	02	03	04	05	06	07	08	09	10	**11**
(2)	12	13	14	15	**16**	**17**	**18**	19	20	**21**	22
(3)	23	24	25	**26**	27	28	29	30	**31**	32	33
(4)	34	35	36	37	38	39	40	**41**	42	43	44
(5)	45	46	47	48	49	50	**51**	52	53	54	55
(6)	56	57	58	59	60	**61**	62	63	64	65	66
(7)	67	68	69	70	**71**	72	73	74	75	76	77
(8)	78	79	80	**81**	82	83	84	85	86	87	88
(9)	89	90	**91**	92	93	94	95	96	97	98	99
(A)	A0	A1	A2	A3	A4	A5	A6	A7	A8	A9	AA
(B)	B1	B2	B3	B4	B5	B6	B7	B8	B9	BA	BB

Figure A1. The first three non-negative numbers in the far right column correspond with the zeroth triangle (0,1,2) in Boolean spaces, and the first four (0,1,2,3) with the logical square (as in Figures C2 & C3). The end right column can also be read as (0,1), (1,2), (2,3), (3,4) and so on, as in the last column of Table B5.

Table A1. Possible periodic systems of numbers

q	*q*/2	squares	addends	diff.
2	1	$1^2 + 2^2$	$(01 + 100)_2$	$(11)_2$
4	2	$2^2 + 3^2$	$(10 + 21)_4$	$(11)_4$
6	3	$3^2 + 4^2$	$(13 + 24)_6$	$(11)_6$
8	4	$4^2 + 5^2$	$(20 + 31)_8$	$(11)_8$
10	5	$5^2 + 6^2$	$(25 + 36)_{10}$	$(11)_{10}$
12	6	$6^2 + 7^2$	$(30 + 41)_{12}$	$(11)_{12}$
14	7	$7^2 + 8^2$	$(37 + 48)_{14}$	$(11)_{14}$
16	8	$8^2 + 9^2$	$(40 + 51)_{16}$	$(11)_{16}$
...				

The row "10" in this Table follows from PSN presented in Table A1; all other rows follow from analog number systems. From the fact that pattern 25-36-61, valid both in genetic and chemical codes, follows the conclusion that in the case of the existence of biomolecules, only decimal number system has "passed" through Darwin's selective sieve. What is surprising, however, is the fact that Darwin's sieve is matched with the "pulse" of Bing Bang.

Table A2. A double Fibonaccian step

1	1						
		3	5	6	9		
2	4					13	
		5	13	17	22		6
3	9					19	
		7	25	34	41		6
4	16					25	
		9	41	57	66		6
5	**25**					31	
		11	**61**	**86**	**97**		6
6	**36**					37	
		13	85	121	134		6
7	49					43	
		15	113	162	177		6
8	64					49	
		17	145	209	226		
9	81						

The Table presents – in the red area – a double Fibonaccian step. From the fact that pattern 25-36-61 is valid both in genetic and chemical codes, and patterns 25-36-61-86 & 25-36-61-86-97 are valid in genetic code, follows the conclusion that in Nature realy exists such a double Fibonaccian step. [These are not Fibonacci numbers, but it is the Fibonacci rule.]

Table A3. The source of PAAS mirror symmetry

00	02	04	06	08	10	12
11	13	15	17	19	21	23
22	24	26	28	30	32	34
11	16	21	26	31	36	41
00	05	10	15	20	25	30
44	**60**	**76**	**92**	**108**	**124**	**140**
	12	14	16	18	***20***	22
	23	25	27	29	***31***	33
	34	36	38	40	***42***	44
	41	46	51	56	***61***	66
	30	35	40	45	***50***	55
	140	**156**	**172**	**188**	**204**	**220**
	22	24	26	28	*30*	*32*
	33	35	37	39	*41*	*43*
	44	46	48	50	*52*	*54*
	66	71	76	81	*86*	*91*
	55	60	65	70	*75*	*80*
	220	**236**	**252**	**268**	**284**	**300**
	32	34	36	38	40	42
	43	45	47	49	51	53
	54	56	58	60	62	64
	91	96	101	106	111	116
	80	85	90	95	100	105
	300	**316**	**332**	**348**	**364**	**380**
	...					

The arrangement represents the Table of distinct 2-5 adding (TDA) with starting column 00-11-22-11-00 which follows from PSN (Periodic system of numbers: Figure A1) in decimal number system by overlapping the real sequence of doubled the first possible triangle in Boolean space (0-1-2) with its mirror image through compression and superposition at the point "22"). In the 10th step we have a realization of the sequence (20-31-42-61-50), the same with the number of atoms in five AAs classes (20, 31, 42, 61, 50) as it is here presented: all five results in the 10th step are mirror image of the first step. (Cf. Figure 2 and see details in the text.)

Table A4. Mirror symmetry within the sequence 11-12-13-14 in the decimal number system (Rakočević, 1994, p. 235)

0	$11 \times 1 = 11$ $11 \times 2 = 22$ $11 \times 3 = 33$	$11 \times 1 = 11$ $11 \times 2 = 22$ $11 \times 3 = 33$	$11^2 = 121$
1	$12 \times 1 = 12$ $12 \times 2 = 24$ $12 \times 3 = 36$	$21 \times 1 = 21$ $21 \times 2 = 42$ $21 \times 3 = 63$	$12^2 = 144$ $21^2 = 441$
2	$13 \times 1 = 13$ $13 \times 2 = 26$ $13 \times 3 = 39$	$31 \times 1 = 31$ $31 \times 2 = 62$ $31 \times 3 = 93$	$13^2 = 169$ $31^2 = \overline{961}$
3	$14 \times 1 = 14$ $14 \times 2 = 28$ $14 \times 3 = ?$	$41 \times 1 = 41$ $41 \times 2 = 82$ $41 \times 3 = ?$	$14^2 = 196$

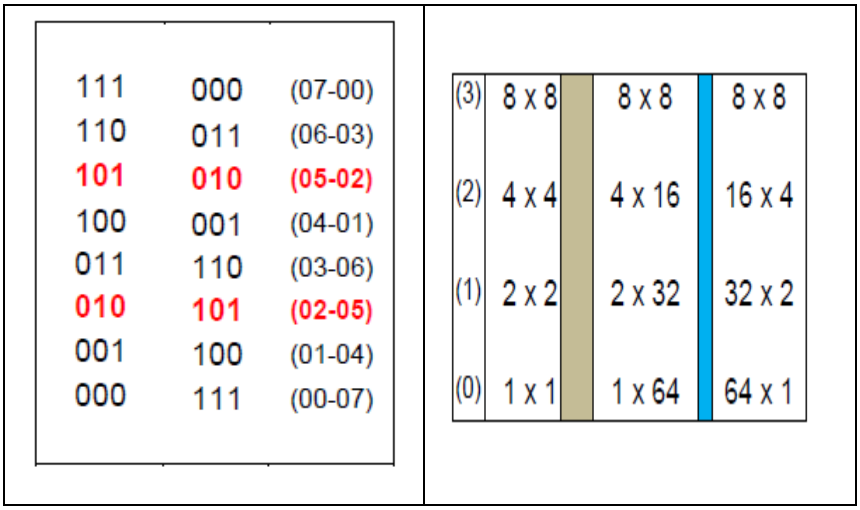

Figure A2. Mirror symmetry within the binary number record on the Boolean cube (on the left). Mirror symmetry within the codon distribution to a six-bit binary tree; an example: two branches, each with 32 codons *vs.* 32 codon pairs (on the right).

APPENDIX B

Harmonic amino acid structures

Table B1. The distinctions of 16 AAs of alanine stereochemical type

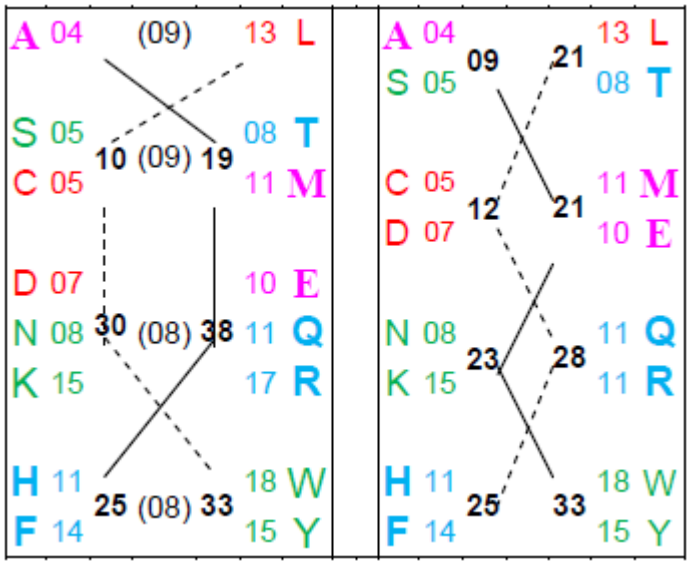

In the Table it is given a classification of 16 AAs of alanine stereochemical type into 8 chemically adequate pairs. In both crossing lines there are 86±0 atoms. [86 + GV 11 = 97 and 86 + PI 21 = 107 (cf. Table A2, 5th and 6th row)]. The differences 8 and 9 (9 - 8 = 1) express the minimum change relation among the amino acids [as in Gray code model of GC (Swanson, 1984, p. 191)]. The order (ordinal number) follows from the atom number hierarchy. Notice that within outer class (2:4 = 1:2 AAs or amino acid pairs) there is a balance of the number of atoms: [(4 + 33 = **37**) + (13 + 25 = **38**) = 75 (86 – 11)]; and within inner class (4:6 = 2:3) [(10 + 38 = **37** + 11) + (19 + 30 = **38** + 11) = 97 (86 + 11)] (All examples as Shcherbak's analogies with quantum physics.) Notice also the realization of 25-36-61 pattern: AME = LCD = 25. [This 25 + (GV 11) from non-alanine types equals 36.]; on the other hand, AAs in green as well as AAs in blue equals 61 atoms. The right illustration contains the algorithm for the generation of a variant ("wobble" variant!) of CIPS as it is the right picture in Figure 1, by reading as from a logical square in the Gray code model: STLA, DEMC, KRQN, FYWH. (Left illustration from: Rakočević and Jokić, 1996, Survey 1, p. 346; right illustration from: Rakočević, 2011b, Table 2.1, p. 823.)

Table B2. The significant distinctions in CIPS (I)

5	F	**14**	15	Y	5	F	14	15	Y
4	L	**13**	04	A	4	L	13	04	A
3	Q	**11**	08	N	3	Q	11	08	N
2	P	**08**	13	I	2	P	08	13	I
1	T	**08**	1	M	1	T	08	11	M
1	S	**05**	05	C	1	S	05	05	C
2	G	**01**	10	V	2	G	01	10	V
3	D	07	10	E	3	D	07	10	E
4	K	15	17	R	4	K	15	17	R
5	H	11	18	W	5	H	11	18	W
		97 /107					107 / 97		

The distinctions of AAs after the ratio 4: 6 = 2:3 on the left and 5:5 = 1:1 on the right. The resulting relationships are analyzed in Table B3 and Survey B1.

Table B3. The significant distinctions in CIPS (II)

(97) Y A Q P M C G D R W	Y Q M G R	55
(97) F A N P T C V D K W	F N T V K	55
(107) F L N I T S V E K H	A P C D W	42
(107) Y L Q I M S G E R H	L I S E H	52
107 / 97 ←	**46** 40 29 28 **61**	
Members of AAs pairs, symmetrically distributed in the same quantities of the number of atoms		

The analysis of relationships in Table B2 after crossing of quantities 97 and 107. New order in relation to left picture in Figure 1: [(YF AL) → aliphatic and carboaromatic]; [(QN PI) → the first three nitrogens, the fourth one links P with valine, *i.e. via* isopropyl group "triangle"] [GV DE → *vs.* PI QN]; [RK WH → all are nitrogens]; [On the left (AL FY) → initial aliphatic and initial aromatic; On the right (RK WH) → right end: all are nitrogenous]. In the middle of the system are chalcogenes. All four columns correspond to CIPS on the left picture in Figure 1: two and two rows from top to bottom.

Table B4. The number of conformations (total: 202 + 203 = 405)

(1)	G	04	16	N	(11)
(2)	A	03	10	D	(12)
(3)	V	08	09	S	(13)
(4)	P	02	08	T	(14)
(5)	L	22	21	C	(15)
(6)	I	20	20	M	(16)
(7)	K	66	12	F	(17)
(8)	R	66	12	Y	(18)
(9)	Q	38	24	W	(19)
(10)	E	20	24	H	(20)
(3 x 83)		249	(1 x 93) 156		(4 x 39)
(82 + 56) 56 = 028+028		138	82		(220)
		111	74		(185)
		(111 = 3 x 37)	(74 = 2 x 37)		

(a) (39 + 210 = 249) (64 + 92 = 156)

[(b) (39 + 64 =103) (210 + 92 = 302)]

(c) 103 = 203 – 100; 302 = 202 + 100

(d) 203 + 001; 202 – 001

(e) 82 + 111 = 203 – 10

(f) 138 + 74 = 202 + 10

[(b) (39 + 64 =103) (210 + 92 = 302)]

(g) 39 + 92 = 202 – 71 (¼ 284)

(h) 64 + 210 = 203 + 71 (¼ 284)

(i) 203 + 71 = 274 (496 – 222)

(k) 202 – 71 = 131 (333 – 202)

This Table is the same as Table 2, except that Leu proceeds Isoleucine, and instead of the number of atoms in AAs, is given the number of conformations, as in Popov (1989, Table 8, p. 88). The balancing of conformation as follows: From (a) to (c) the difference in the number of conformations in two columns (decades) in relation to the middle pair 202-203, with a change for ± 100; (d) from: (Rakočević, 2004a, Table 8, p. 228) and (Rakočević, 2018a, Table 8, p. 44) where is shown the change in the number of conformations for ± 001 in the GC Table, if the order of AAs follows the order of their coding codons, in the hierarchy of the number of hydrogen bonds; from (e) to (f) the number of conformations in odd positions in relation to multiples of Shcherbak's "Prime quantum 37" with a change for ± 10; from (g) to (h) the number of conformations in relation to the second friendly number; (i) the number of conformations in relation to the second friendly and the third perfect number; (k) the number of conformations in relation to the second friendly number and to the significant determinant of GC, as is the number 333 (Rakočević, 2018a, p. 37: the sixth column in Survey 2).

Survey B1. The relationships within two arrangements presented in Table B2

[(FLTSKH 66) (NIVE 41)] = 107 [(QPGD 27) (YAMCRW 70)] = 97	[(FPTDK 52) (ANCVW 45)] = 97 [(LQSGH 41) (YIMER 66)] = 107
(66 + 70 = **68** x 2 = 136) + (27 + 41 = **68** x 1) = 204 (136 = 118 + 018) [**68** / **86**] 52 + 66 = 118) + (41 + 45 = **86** x 1) = 204	

Survey B2. The determinations on the six-bit binary tree

/00 - 07/08 - 15/16 - 23/24 - 31//32 - 39/40 - 47/48 - 55/56 - 63/
28 92 156 220 284 348 412 476
64 64 64 64 64 64 64

/00 - 07/00 - 15/00 - 23/00 - 31//00 - 39/00 - 47/00 - 55/00 - 63/
28 120 276 496 780 1128 1540 2016
92 156 220 284 348 412 476

The Survey follows from (Rakočević, 1997b, Figure 7, p. 60): "The determination of the series of the numbers 0-63. When we look closely into the structure of the sequence 0-63 of the series of the natural numbers we come to the obvious and self-evident explanation of the reason why the genetic code must be six-bit code, no matter if it is the manifestation in the form of the Gray Code model (Swanson, 1984, p 188), or it is in the form of the Binary tree (Rakočević, 1994, p 38). There must be 8 codons, *i.e.* amino acid classes. The structure of the sequence 0-63 is strictly determined by third perfect number (496) and the sum consisted of the first pair of the friendly numbers (220+284). Along with this, the specific Boolean square is being made and it is the restrictive factor, in a sense that it is not possible to 'go on' any further - not ahead, not back: (0) 220+284=504; (1) 156+348=504; (2) 92+412=504; (3) 28+476=504. The key distinctions within the genetic code are obviously self-evident: entity 64 as a series of continuity (correspondent with 64 codons); entity 20 from 496 (III PN)-476=20 (correspondent with 20 amino acids) *etc.*"

Table B5. Some number systms: the unique arrangements and situations

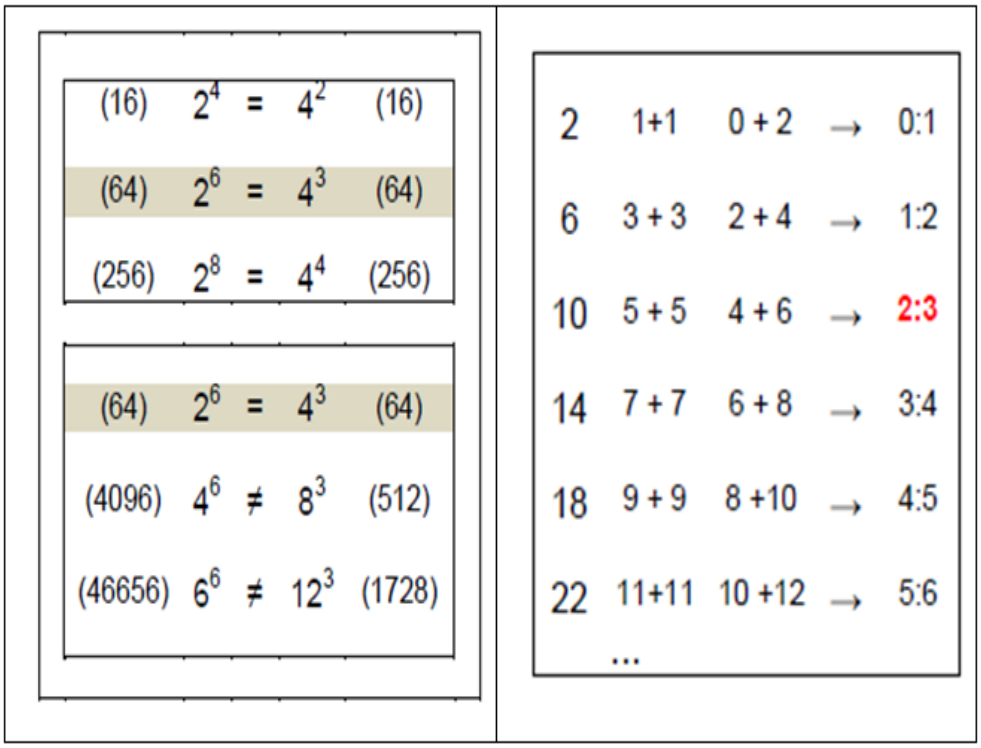

The Table corresponds with PSN (Figure A1) through the ratio 1:2 on the left above and 2:3 on the right, the third row. The left illustration shows unique arrangements and situations corresponding to 16 doublets and 64 triplets of nucleotides in the genetic code. The right illustration shows the changes by ± 1 in relation to *q*/2 of number systems whose numerical basis (*q*) corresponds to the values that follow from Hükel's rule (the first column). It can be seen that only in the case of the decimal number system we have a direct correspondance with the golden mean (footnote 10).

Table B6. The relationships within Generalized Golden mean (Rakočević, 2004b)

N	x_1	x_2	h	m	r	N	x_1	x_2	h	m	r
0.	$0^2 + 1^2 = \underline{1}$ $(0 + 1)^2 = 1$			0	$\sqrt{1}$	0.	$0^2 + 1^2 = \underline{1}$ $(0 + 1)^2 = 1$			0	$\sqrt{1}$
1.	$1^2 + 2^2 = \underline{5}$ $(1 + 2)^2 = 9$			4	$\sqrt{9}$	1.	$(x_1)^2 + (x_2)^2 = \underline{2}$ $(x_1 + x_2)^2 = 3$			1	$\sqrt{3}$
2.	$2^2 + 3^2 = \underline{13}$ $(2 + 3)^2 = 25$			12	$\sqrt{25}$	2.	$(x_1)^2 + (x_2)^2 = \underline{3}$ $(x_1 + x_2)^2 = 5$			2	$\sqrt{5}$
3.	$3^2 + 4^2 = \underline{25}$ $(3 + 4)^2 = 49$			24	$\sqrt{49}$	3.	$(x_1)^2 + (x_2)^2 = \underline{4}$ $(x_1 + x_2)^2 = 7$			3	$\sqrt{7}$
4.	$4^2 + 5^2 = \underline{41}$ $(4 + 5)^2 = 81$			40	$\sqrt{81}$	4.	$1^2 + 2^2 = \underline{5}$ $(1 + 2)^2 = 9$			4	$\sqrt{9}$
5.	$5^2 + 6^2 = \underline{61}$ $(5 + 6)^2 = 121$			60	$\sqrt{121}$	5.	$(x_1)^2 + (x_2)^2 = \underline{6}$ $(x_1 + x_2)^2 = 11$			5	$\sqrt{11}$
	(...)						(...)				

APPENDIX C

Some additional harmonic structures

The Darwin's equation

Table C1. The key of Darwin's Diagram (I)

Primary		Secondary	
B 00	06 G	B 01	01 G
C 01	02 H	C 01	01 H
D 02	00 K	D 01	01 K
E 10	01 L	E 00	01 L
F 14		F 00	
27	09	03	04
36		**(43)**	**07**
(233 + 43 = 276) (276 + 56 = 332)			
99			
$276 = 216_{down} + 60^{up}$			

"All branches (primary + secondary) for "other nine species" for the left and the right part of the Diagram, at all 15 levels. The equation 27 + 09 = 36 appears to be a special Darwin's equation, valid to determination of the genetic code (Figure 6, 7 & 8 and Table 6.1); and the equation 03 + 04 = 07 corresponds to the first three members of Lucas number series (Figure D.1). The number 233 comes from Table 4.5 and together with this result (43) makes 276 which is the total number of branches within the Diagram. In addition: 56 = 46 nodes plus 10 branchings, and from that all "branch" entities/quantities equal 332 as a mirror pattern of the 233" (Rakočević, 2015, Table 5, p. 47).
(http://dx.doi.org/10.17605/OSF.IO/QZG69)
(www.rakocevcode.rs)

The Darwin's equation (27 + 9 = 36) is the "missing link" that allows understanding of the pattern 25-36-61, contained in two linear equations, determinants of genetic and chemical code (Rakočević, 2018b, Survey 2a, 2b, 3a and 3b, p. 296). At the same time, it is also the key of Darwin's Diagram (Rakočević, 2015, Figure 1.1, p. 19; here Figure C1).

Table C2. The key of Darwin's Diagram (II)

01	+	00	=	**01**	09	+	00	=	**09**
02	+	02	=	**04**	10	+	06	=	**16**
03	+	01	=	04	11	+	05	=	16
01	+	00	=	01	05	+	04	=	09
04	+	00	=	04	12	+	04	=	16
02	+	-01	=	01	06	+	03	=	09
…					…				
25	+	00	=	**25**	49	+	00	=	**49**
26	+	10	=	**36**	50	+	14	=	**64**
27	+	09	=	36	51	+	13	=	64
17	+	08	=	25	37	+	12	=	49
28	+	08	=	36	52	+	12	=	64
18	+	07	=	25	38	+	11	=	49
…					…				

This illustration is from Figure 6 in "Darwin Enigma" (Rakočević, 2015): „The generation of the squares of natural numbers through two linear equations. Darwin's equation is in the third quadrant, in the area of dark tones surrounded by two linear equations valid in the genetic code." Notice that the second member of the equation (the second row in all four quadrants) follows from Hückel's rule (2, 6, 10, 14); the differences between the third and fourth row also from Hückel rule: (3-1 = 2), (11-5 = 6), (**27-17** = **10**), (51-37 = 14). On the other hand, the first member of the equation (2, 10, 26, 50) increases by 8n (n = 1, 2 and 3). Notice also that with the first quadrant we have the generation of the squares of the first two natural numbers 1 and 2, in second 3 and 4, in third 5 and 6 (in relation to the pattern 25-36-61) and in the forth 7 and 8. [The next step in generating would already be in the area of double-digit numbers.]

Table C3. The key of Darwin's Diagram (III)

02 + 02 = 04 03 + 01 = 04 01 + 00 = 01 $02 + 02 = 04 = 2^2$ $01 + 00 = 01 = 1^2$ $02 - 02 = 00 = 0^2$ $01 - 00 = 01 = 1^2$ (?!)	10 + 06 = 16 11 + 05 = 16 05 + 04 = 09 $10 + 06 = 16 = 4^2$ $05 + 04 = 09 = 3^2$ $10 - 06 = 04 = 2^2$ $05 - 04 = 01 = 1^2$
1 - (- 1) = **2**	
26 + 10 = 36 27 + 09 = 36 17 + 08 = 25 $26 + 10 = 36 = 6^2$ $17 + 08 = 25 = 5^2$ $26 - 10 = 16 = 4^2$ $17 - 08 = 09 = 3^2$	50 + 14 = 64 51 + 13 = 64 37 + 12 = 49 $50 + 14 = 64 = 8^2$ $37 + 12 = 49 = 7^2$ $50 - 14 = 36 = 6^2$ $37 - 12 = 25 = 5^2$
5 - (+ 3) = **2**	

The Table as in (Rakočević, 2015, Table 5, p. 47): "This Figure follows from the previous. Three linear equations within each of the four quadrants in relation to the quadruplets of natural numbers' squares. In the third quadrant: two equations are valid in the genetic code and one (in the middle position, dark tone) is given as Darwin's equation [Notice a paradox (Darwin's paradox), valid for number 1 in the first quadrant: the negative value of number 1 cannot be – negative?!]."

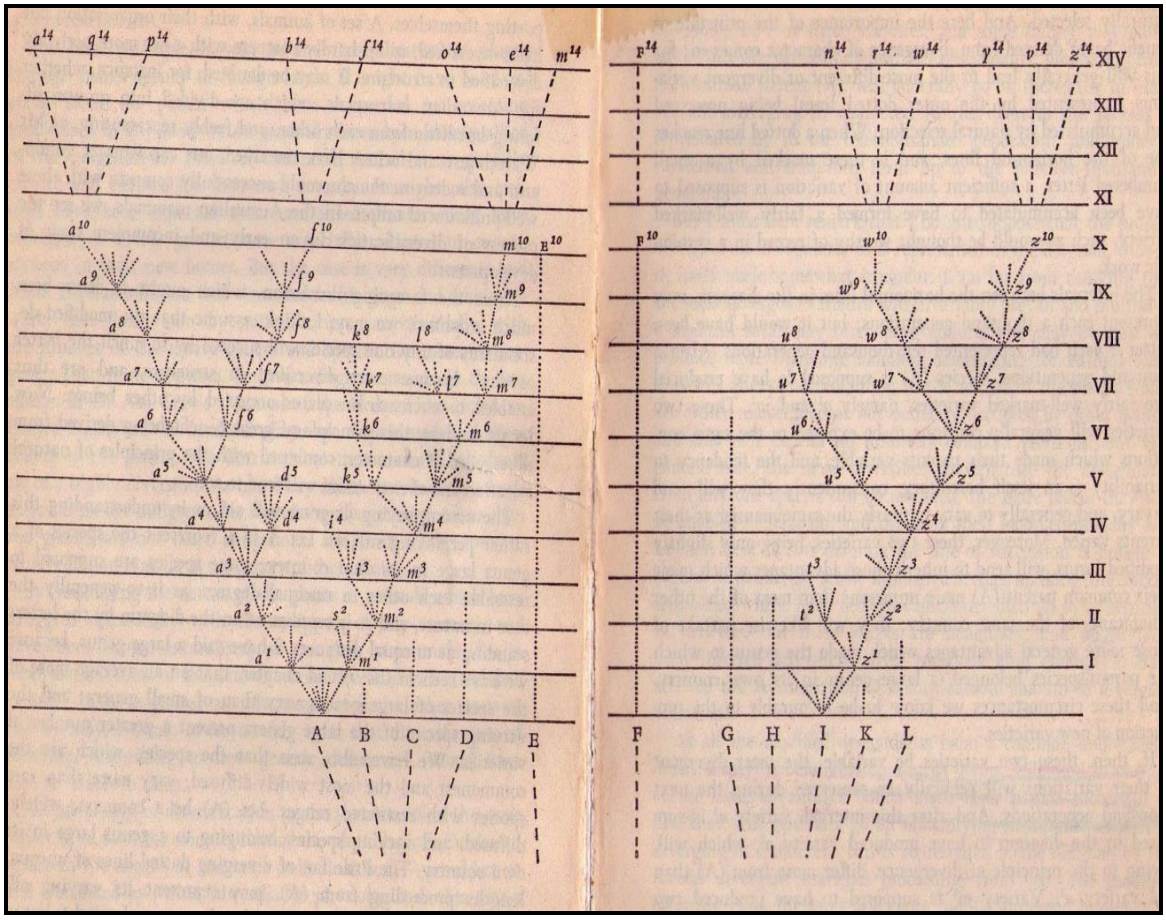

Figure C1. The "accompanying diagram" in Darwin's book "On the Origin of Species" (London, 1859)

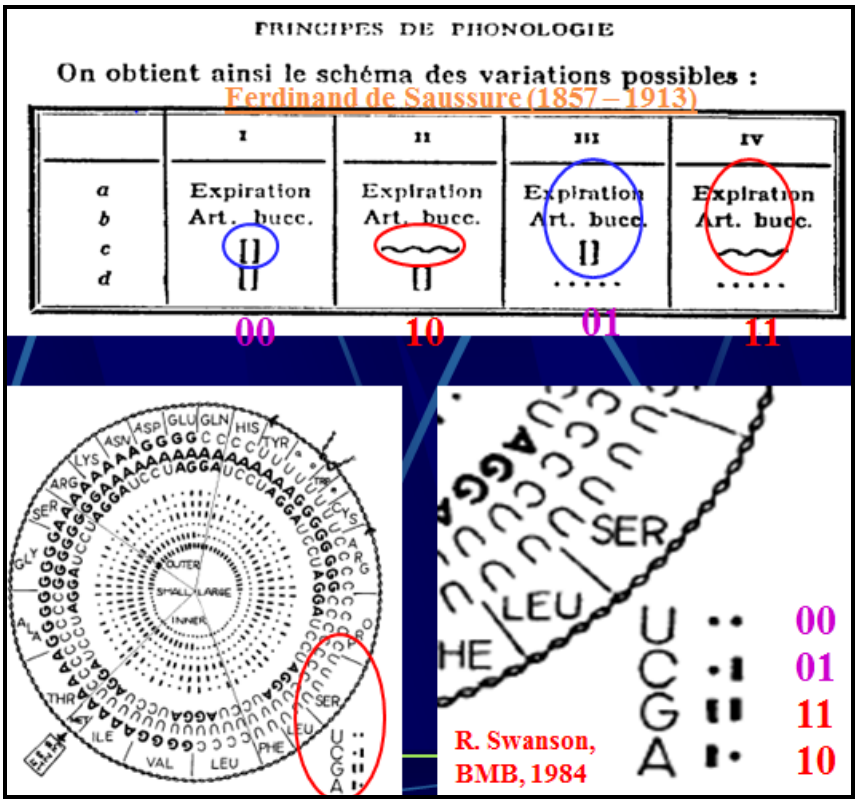

Figure C2. The correspondence with PSN (Fig. A1) through the relations between the logical square 00-01-10-11 and the first four levels in PSN: 00-11-22-33. The binary records of the logical square: up for the human language (De Saussure, 1985, p. 70); down: for the genetc language (Swanson, 1984, p. 188).

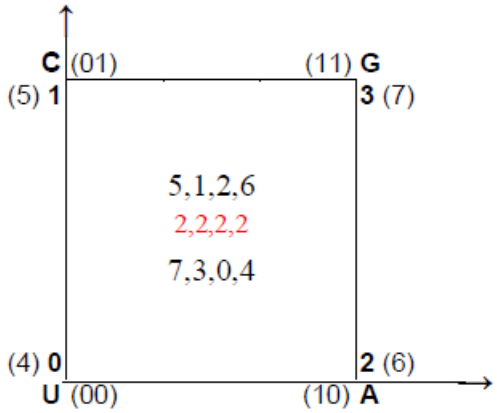

Figure C3. The correspondence with PSN (Figure A1) through the relations between the logical square 00-01-10-11 and the first four levels in PSN: 00-11-22-33. The unit Boolean logical square: **0** (00), **1** (01), **2** (01), **3** (11) in correspondence with the unit Boolean logical cube and/or with eight branches on the binary-code tree of Genetic code (Rakočević, 1998b, Figure 1, p. 284): **0** (000), **1** (001), **2** (010), **3** (011); **4** (100), **5** (101), **6** (110), **7** (111). The mirror symmetry on the binary-code tree of Genetic code: [010 / 101 → AUA / CGC etc.]; [001 / 110 → UCC / GAA etc.]. The Py-Pu logical square: U (00) → simpler ring, simpler H bond; C (01) → simpler ring, more complex H bond; A (10) → more complex ring, simpler H bond; G (11) → more complex ring, more complex H bond. From the 24 permutations of the UCAG sequence, only this, as the first, consistently follows the chemical hierarchy; the remaining 23 are in relation to it. (Cf. footnote 7; also, the sequence 5-1-2-6 with the same sequence in Equation 1.)

Preoteinske amino kiseline kao potpuni (periodni) sistem

Miloje M. Rakočević

Univerzitet u Nišu, Prirodno-matematički fakultet, Departman za hemiju, Višegradska 33, 18000 Niš, Srbija (u penziji od 2003)

SAŽETAK

Pozivajući se na rezultate prethodnog istraživanja o šifri genetskog koda i analogijama genetskog i hemijskog koda– dva u svemu kompletna prirodna sistema – ovaj rad predstavlja rezultate izučavanja najpotpunijeg Sistema proteinskih amino kiselina (engl. PAAS). Pokazano je da 20 proteinskih amino kiselina predstavljaju potpuni sistem-uređen, koherentan, i harmoničan. U takvom sistemu, sve hemijske razlike unutar Sistema su praćene specifičnim aritmetičkim i algebarskim pravilnostima, uključujući postojanje aminokiselinskih rednih brojeva od 1 do 20. Klasifikacija amino kiselina u dve dekade (1-10 i 11-20) u strogoj je korespondenciji sa balansima broja atoma. Postojanje harmonijskih struktura i rasporeda amino kiselina, bez obzira da li su ili nisu konstituenti genetskog koda, prati zaključke da je genetski kod, kroz svoje glavne konstituente-20 aminokiselina i 4 pirimidin-purinskih baza- bio kompletan čak i u prebiotskim uslovima.

Ključne reči: Proteinske amino kiseline, amino kiselinski kod, genetski kod, binarno stablo, Gray kod, Zlatna sredina, Fibonacci-jev niz.

Acides aminés protéiques en tant que système complet (périodique)

Miloje M. Rakočević

Université de Niš, Faculté des sciences naturelles et des mathématiques, Département de chimie, Višegradska 33, 18000 Niš, Serbie (à la retraite depuis 2003)

RÉSUMÉ

Se référant aux résultats des recherches antérieures sur le Chiffrage du code génétique et les analogies des codes génétique et chimique – deux systèmes presque naturels et complets – cet article présente les résultats de l'étude du Système le plus complet des acides aminés protéiques (PAAS, angl.). Il est démontré que 20 acides aminés protéiques semblent constituer un système complet, système étant ordonné, cohérent et harmonique. Dans une telle organisation, toutes les distinctions chimiques au sein du Système sont accompagnées de régularités spécifiques du type arithmétique et algébrique, y compris l'existence des nombres ordinaux d'acides aminés de 1 à 20. La classification des acides aminés en deux décades (celle de 1 à 10 et celle de 11 à 20) paraît être dans une stricte correspondance avec les équilibres du nombre d'atomes. L'existence des structures harmoniques et de la disposition des acides aminés, qu'ils soient ou non des constituants du code génétique, s'accorde avec les conclusions suivant lesquelles le code génétique, à travers ses constituants principaux – 20 acides aminés et 4 bases puriques et pyrimidiques – était complet même dans les conditions prébiotiques.

Mots-clés : acides aminés protéiques, code des acides aminés, code génétique, arbre binaire, code Gray, juste milieu, série de Fibonacci.

Белковые аминокислоты как целостная (периодическая) система

Милое М. Ракочевич

Университет в Нише, Факультет естественных наук и математики, Департамент химии, ул. Вышеградская 33, 18000 Ниш, Сербия (на пенсии с 2003 года)

АННОТАЦИЯ

Ссылаясь на результаты предыдущих исследований шифра генетического кода и аналогий генетического и химического кодов – двух общих целостных природных систем – в настоящем документе представлены результаты исследования наиболее полной белковой аминокислотной системы (PAAS). Показано, что 20 белковых аминокислот представляют собой целостную систему – упорядоченную, связную и гармоничную. В такой системе все химические различия внутри системы сопровождаются конкретными арифметическими и алгебраическими закономерностями, в том числе наличием порядковых номеров аминокислот от 1 до 20. Классификация аминокислот по двум числовым рядам (1-10 и 11-20), по-видимому, находится в строгом соответствии с балансами числа атомов. Существование гармонических структур и расположений белковых аминокислот, независимо от того, являются ли они составляющими генетического кода или нет, соответствуют выводам о том, что генетический код через его основные составляющие – 20 БА и 4 основания ПУ-ПИ, был завершен даже в пребиотических условиях.

Ключевые слова: белковые аминокислоты, аминокислотный код, генетический код, двоичное дерево, код Грея, золотое сечение, ряд Фибоначчи.

Protein-Aminosäuren als vollständiges (Perioden)System

Miloje M. Rakočević

Universität in Niš, Mathematisch-Naturwissenschaftliche Fakultät, Lehrstuhl für Chemie, Višegradska 33, 18000 Niš, Serbien (im Ruhestand seit 2003)

ABSTRAKT

In Bezug auf die bisherigen Ergebnisse früherer Forschungen über die Verschlüsselung des genetischen Codes und Analogien des genetischen und chemischen Codes – zwei fast vollständige natürliche Systeme – stellt diese Arbeit die Forschungsergebnisse des vollständigsten Systems der Protein-Aminosäuren dar (engl. PAAS). Es wird gezeigt, dass 20 Protein-Aminosäuren ein vollständiges System zu seien scheinen – geordnet, kohärent und harmonisch. In einem solchen System wird allen chemischen Unterschieden innerhalb des Systems von spezifischen, arithmetischen und algebraischen Regelmäßigkeiten gefolgt, einschließlich der Existenz von Aminosäure-Ordinalzahlen von 1 bis 20. Die Klassifikation von Aminosäuren in zwei Dekaden (1-10 und 11-20) scheint in enger Korrespondenz mit den Balancen der Anzahl der Atome zu stehen. Das Bestehen harmonischer Strukturen und Anordnungen von Aminosäuren, unabhängig davon, ob sie Bestandteile des genetischen Codes sind oder nicht, folgt den Schlussfolgerungen, dass der genetische Code durch seine Hauptbestandteile – 20 Aminosäuren und 4 Pyrimidin-Purinbasen, sogar in präbiotischen Zuständen vollständig war.

Schlüsselwörter: Protein-Aminosäuren, Aminosäure-Code, genetischer Code, Binärbaum, Goldener Schnitt, Fibonacci-Folge

Chemia Naissensis, Vol 2, Issue 1, MINI-REVIEW, 48-67

Revisiting the Arrhenius Equation in Chemical Kinetics to Analyze Kinetics Data for Photochromic Naphthoxazine-spiro-indolines

Jonathan Hobley*

OndaLabs R&D Consultancy, Deca Homes, Clark Free-Port, Barangay Margot, Angeles, 2009, the Philippines

ABSTRACT

In undergraduate courses, kinetics and thermodynamics are often taught as separate modules. It is because equilibrium data from thermodynamics do not enlighten us about the rate of attainment of equilibrium, which is kinetics. It is true that even if a chemical reaction is thermodynamically favorable, it may never happen due to kinetic considerations. However, this separation of kinetics and thermodynamics is unfortunate in some respects. In this work, the link between chemical kinetics and thermodynamics is explored based on them both being defined by a single potential energy diagram. A common misconception caused by undergraduate courses on chemical kinetics is a claim that the Arrhenius equation is deficient because it does not offer a precise meaning for the pre-exponential term ***A***. Undergraduate courses often go on to proffer more sophisticated theories in the form of collision theory CT and transition state theory TST resulting in the Eyring equation. These latter two theories are required in order to formally show that the pre-exponential term contains information on the entropy requirements of the reaction. In this work, it will be shown that by considering the link between thermodynamics and kinetics it can easily be shown that ***A*** was already implicitly linked to the product of the entropy of activation of the reaction and the natural frequency of the reaction. This work makes use of previously published and unpublished results on photochromic naphthoxazine-spiro-indolines to compare different theories.

Keywords: Arrhenius equation, transition state theory, collision theory, naphthoxazine-spiro-indoline, photochromic, chemical kinetics

---

* OndaLabs R&D Consultancy, Deca Homes, Clark Free-Port, Barangay Margot, Angeles, 2009, the Philippines, e-mail: **jonathan.hobley@gmail.com**

Introduction

Photochromic naphthoxazine-spiro-indolines (NOSI) have the general photochemical and thermal reactions shown in Figure 1. (Hobley, 1995).

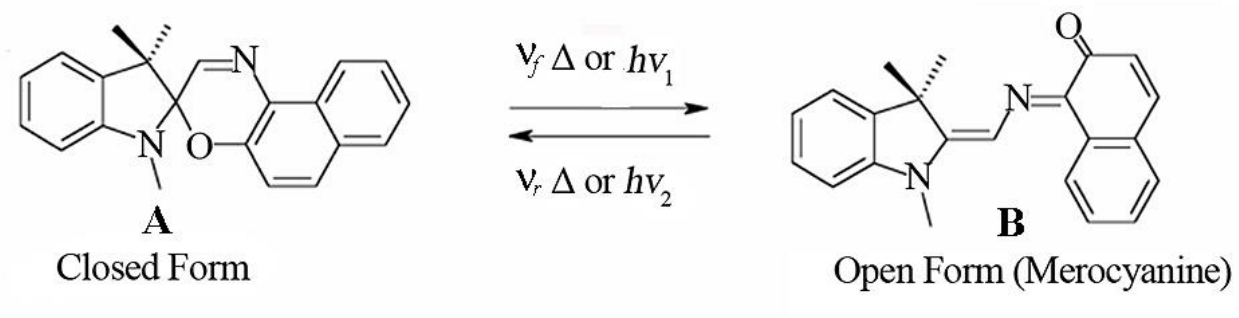

Figure 1. The NOSI photochromic reaction

where **B** is a molecular rearrangement of **A** that can be brought about photochemically or thermally in either direction of the reaction. The rate equations for the forward and reverse thermal reactions that define the thermal equilibrium are:

$$v_f = k_f[A] \text{ and } v_r = k_r[A] \quad (1)$$

where subscripts *f* and *r* denote forward and reverse reaction parameters.

Photochromic molecules of this kind are used in ophthalmic Transitions® lenses. In the case of Transitions® lenses molecule **A** is colorless and molecule **B** is coloured. In the field of ophthalmic lenses there are two very important parameters to understand. If the reaction is left alone to reach a point where the number of moles of **A** and **B** are constant (*i.e.* it has reached equilibrium), what are the constant values of the concentration of **A** and **B** relative to each other. This is important because if there is too much of colored molecule **B** in equilibrium with colorless molecule **A** at room temperature then the lens is already colored before the lens is exposed to sunlight. This parameter is covered by chemical thermodynamics. The second parameter to know is: if the reaction starts with pure **A** or pure **B** then how long does it take to convert either **A** to **B** or **B** to **A** in order to achieve equilibrium, or a quasi-equilibrium called a photostationary state (Hobley, 1995). This parameter is found from chemical kinetics.

These two fields of thermodynamics and kinetics have been studied for more than a century and are well understood based on two equations. Chemical equilibrium is described by the Van't Hoff Equation and chemical kinetics is well understood based upon the Arrhenius equation (Van't Hoff, 1887; Arrhenius, 1889). The historical background of the story of the Arrhenius equation and the Van't Hoff equation starts

with the Boltzmann distribution (Boltzmann, 1872). This distribution gives the probability of finding a component of a statistical distribution (say a molecule in the case of equilibrium of molecules) in a particular state (say state A and state B) based upon the energy gap between the two states:

$$\left(\frac{N_A}{N_B}\right) = e^{-\frac{\Delta E}{k_b T}}$$

(2)

where N_A and N_B are the number of species in state *A* or state *B*, respectively; $\Delta E = E_A - E_B$; E_A and E_B are the energies of states *A* and *B***,** respectively; k_B is Boltzmann's constant and *T* is the temperature in Kelvin (Figure 2).

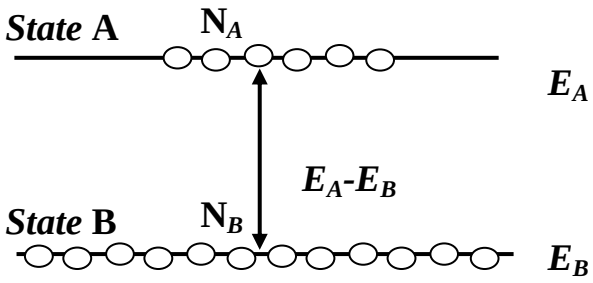

Figure 2. A Boltzmann distribution between two states with different energies

Van't Hoff took Boltzmann's distribution and applied it at the chemical equilibrium, for example where N_A and N_B are the number of molecules **A** and **B** which are linked by the chemical equilibrium.

For a simple reaction A ↔ B in dynamic equilibrium as in Figures 1 and 3, the Van't Hoff equation is:

$$K_{eq} = e^{-\frac{\Delta G^o}{RT}}$$

(3)

where $K_{eq} = \frac{[B]}{[A]}$; $\Delta G^o = (E_A - E_B)$ and R is the universal gas constant

Since, *[B]/[A]* is the same as N_B/N_A in the Boltzmann equation, so Van't Hoff and Boltzmann are the same expression, except that Van't Hoff is specific for chemical equibria. The Van't Hoff equation is often written in another form as shown below:

$$lnK_{eq} = -\frac{\Delta H^o}{RT} + \frac{\Delta S^o}{R} \text{ since } \Delta G^o = \Delta H^o - T\Delta S^o$$

(4)

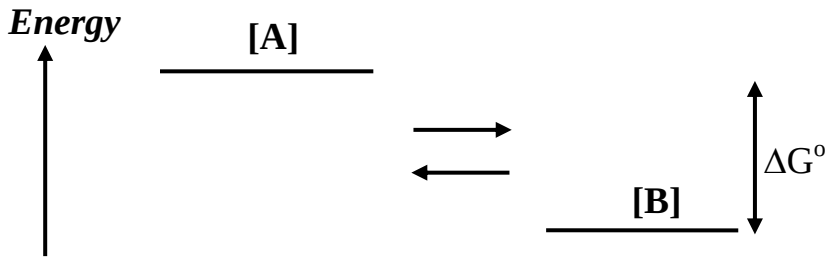

Figure 3. Energy levels for a reactant and product in chemical equilibrium.

What Arrhenius did was simply to recognise that the Van't Hoff equation assumed a dynamic chemical equilibrium. In other words, it was assumed that the chemical equilibrium is established by two competing reactions. One reaction goes one way (**A** forms from **B**) and the other reaction is the reverse of this (*i.e.* B forms from **A**). The rate of each reaction relative to the other determines the equilibrium. Arrhenius therefore simply postulated that the equation for each of these reactions was also governed by the same type of Boltzmann distribution. The addition was that in the energy diagram above (Figure 3), in which **A** and **B** are unconnected, there is an additional line that connects the *A* and *B* states (Figure 4).

The new line described a potential energy diagram in which activation energies are defined between states *A* and *B*. Let's say activation energy for A → B is E_{af} and the activation energy for B → A is E_{ar}.

From this description there is a new Boltzmann distribution between states *A* and *B* and the state that exists at the top of the "hill" that connects the two. The state at the top of the hill is a molecule with a conformation in between molecule **A** and molecule **B** (**AB***). In reality very fast reactions may not achieve a true Boltzmann distribution, but we will ignore this because it does not apply to this work.

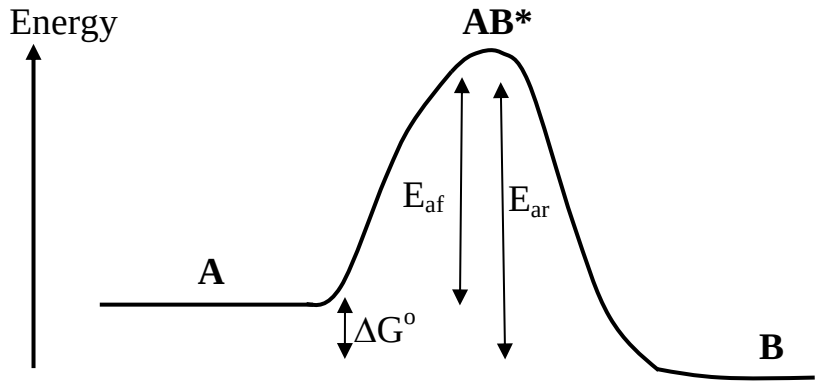

Figure 4. A potential energy diagram showing activation energies for a reversible unimolecular reaction.

Arrhenius thus proposed an empirical equation of similar form to the Van't Hoff equation. Empirical means "based on observation rather than theory or pure logic". So, it is debatable as to whether the Arrhenius equation is purely empirical, since it was perfectly logical to propose it based on the idea that equilibrium is established by a reaction that is reversible, having a different rate for the forward and reverse reaction. The equation he proposed was:

$$k = Ae^{-\frac{E_a}{RT}} \quad (5)$$

where k (s^{-1}) can either be the rate constant for either *A* going to *B* or *B* going to *A*; E_a is the activation energy (the energy gap between either state *A* or *B* and the top of the hill in between them); ***A*** is a main subject of this work and was originally known as the frequency factor (it also has units of s^{-1}), but now it is often referred to as the pre-exponential factor. This change in name is in some ways unfortunate as the title "pre-exponential factor" does not include the important point, that ***A*** is linked to the frequency at which a reaction could occur if it has enough energy.

After Arrhenius, other more sophisticated theories were proposed. The most well-known being Collision theory (CT) and Transition State Theory (TST (Trautz, 1916; Laidler and King, 1983; Atkins and De Paula, 2006)). Without fully deriving either of these theories the salient points related to this discussion will be stated.

Collision theory (CT) considered a bimolecular gas phase reaction in which molecules collide and then react if they have enough energy and if the reactive parts of the molecule are pointing the right way to react.

The rate constant is given by equation:

$$k = Z\rho e^{-\frac{E_a}{RT}} \quad (6)$$

where Z is the molar collision frequency; ρ is the steric factor; E_a is the activation energy of the reaction; T is the temperature; R is gas constant.

CT gives an equation that has the same form as the Arrhenius equation except that ***A*** is replaced by $Z\rho$, which has a steric factor ρ and a frequency factor Z. For this reason, it is generally accepted that collision theory provides a significant advance in the understanding of the pre-exponential terms compared to Arrhenius' frequency term ***A***. However, CT does have some limitations in that it only really works in some gas phase reactions, but not in dilute solutions where most of the collisions do not result in any reaction because the collisions are with solvent molecules. Additionally, it is specific for bimolecular reactions *i.e.* it cannot be applied to the simple unimolecular reaction being considered in this work.

A further level of sophistication was added by another well-known theory, Transition State Theory (TST), which again starts with a potential energy surface, but this time it is a surface specifically in ΔG^o

(Figure 5) for a reaction of the form:

$[A] \leftrightarrow [AB^*] \rightarrow [B]$

for which the following equations apply:

$$K^* = \frac{[AB^*]}{[A]} \quad (7)$$

i.e. an equilibrium is assumed between the reactant **A** and the transition sate **AB*** with an equilibrium constant K^*.

$[AB^*] = K^*[A]$

$\frac{d[B]}{dt} = k^*[AB^*]$ is the rate of formation of **B** from **AB***

$$\frac{d[B]}{dt} = K^*k^*[A]$$

where k^* is the breakdown rate constant of **AB***. and $k^* = \kappa\nu$; κ is the fractional efficiency with which the bond in **AB*** breaks to form **B** and is assumed to be 1; ν is the **AB*** breakdown frequency (assumed to be the timescale of one bond vibration or k_bT/h).

If $k = K^*k^*$ $then$ $k = K^*\frac{k_bT}{h}$

But just like in thermodynamics equations 3 and 4 it can be written:

$$lnK^* = \frac{\Delta H^*}{RT} - \frac{T\Delta S^*}{R}$$

so finally, the Eyring equation can be written:

$$k = \left(\frac{k_bT}{h}\right) e^{\frac{\Delta S^*}{R}} e^{-\frac{\Delta H}{RT}} \quad (8)$$

In TST, just like in CT, there is a frequency term (compare Z with k_bT/h) and a steric term (compare ρ with $e^{\Delta S^*/R}$) but this time the steric term is directly associated with a reaction entropy.

However, some assumptions were also made in TST and thus some flexibility on how to interpret the results obtained using this equation is lost. For example, it was assumed that 100% of **AB*** forms **B** (it was assumed the transmission coefficient κ=1). But that is not necessarily the case. It was also assumed that the breakdown frequency of **AB***, ν, is equal to a bond vibration frequency (k_bT/h) which could well be true for a bimolecular reaction or a dissociation, but in some reactions like an isomerization the timescale for a bond rotation may be more appropriate and the assumption that κ=1 is probably not valid. In summary CT and TST give a more rigorous insight as to the meaning of the pre-exponential term, but at the cost of flexibility, in terms of the general applicability of the models.

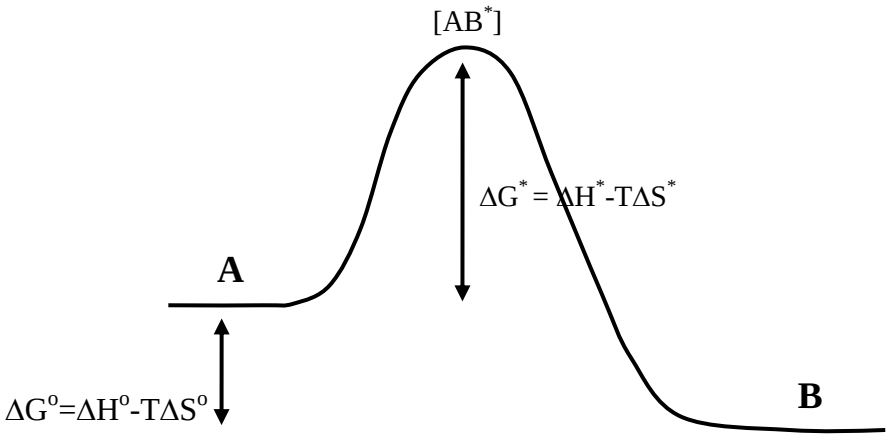

Figure 5. A potential energy surface in Gibbs free energy corresponding to the derivation of the Eyring equation in TST in which the reaction is not reversible.

Interpretation of the Arrhenius equation based upon a reversible equilibrium

From thermodynamics for a simple reaction A↔B in dynamic equilibrium, the equilibrium constant is the fractional ratio of the respective concentrations of the products over the reactants (equation 3). Furthermore, it can be shown that K_{eq} is related to the ratio of the rate constants of the forward and reverse reactions (equation 1) because at equilibrium the forward reaction rate = the reverse reaction rate *i.e.*:

$$k_f[A] = k_r[B] \quad (9)$$

$$\frac{k_f}{k_r} = \frac{[B]}{[A]} = K_{eq}$$

Previously two potential energy diagrams were presented in Figures 4 and 5. One used ΔG^* for the activation energy and the other used E_a but how does E_a relate to ΔG? Also how does ***A*** relate to any thermodynamic properties? This will be addressed next.

The Arrhenius equation (equation 5) can be written for the forward and reverse reaction:

$$k_f = A_f e^{-\frac{E_{af}}{RT}} \; and \; k_r = A_r e^{-\frac{E_{ar}}{RT}} \quad (10)$$

Inserting these into equation 8:

$$K_{eq} = \frac{k_f}{k_r} = \frac{A_f e^{-\frac{E_{af}}{RT}}}{A_r e^{-\frac{E_{ar}}{RT}}} \quad (11)$$

$$K_{eq} = \left(\frac{A_f}{A_r}\right) e^{-\frac{E_{ar}}{RT}} e^{-\frac{E_{af}}{RT}}$$

but from thermodynamics equations 3 and 4 it will be:

$$lnK_{eq} = lnA_f - lnA_r - E_{af}/RT + E_{ar}/RT = -\Delta G^o/RT = -\Delta H^o/RT + \Delta S^o/R$$

$$-lnK_{eq} = -lnA_f + lnA_r + E_{af}/RT - E_{ar}/RT = \Delta G^o/RT$$

$$\Delta G^o = \left(E_{af} - E_{ar}\right) - RTlnA_f + RTlnA_r$$

$$\Delta G^o = \left(E_{af} - E_{ar}\right) - T\left(RlnA_f - RlnA_r\right) \quad (12)$$

Comparing this with equation 4:

$$\Delta H^o = \left(E_{af} - E_{ar}\right) \quad (13)$$

$$\Delta S^o = R\left(lnA_f - lnA_r\right)$$

$$k_b = R/N_A$$

$$\Delta S^o = k_b N_A\left(lnA_f - lnA_r\right) \text{ per mole} \quad (14)$$

$$\Delta S^o = \left(k_b lnA_f - k_b lnA_r\right) \text{ per molecule}$$

Compare this equation with Boltzmann's entropy equation (Boltzmann, 1896; Boltzmann, 1898) from statistical thermodynamics:

$$S = k_b ln \quad (15)$$

where *W* is the number of microstates corresponding to a given macrostate.

Hence it is reasonable to suggest that ***A***, the pre-exponential term, is very much intrinsically an entropy term and is itself a number related to several microstates in the system that are "specific to making the reaction work". ***A*** is most likely the probability of occurrence of the exact microstates that can exist in the system that put the molecules in the reaction in exactly the right place at the right time to react. It must contain a logarithmic term as we derived, but it has units of s^{-1} so it must also contain a frequency term that is the natural frequency of the transformation taking place, just as for CT. In CT the pre-exponential term ***A*** was replaced with ρZ where ρ is a steric term, which is implicitly therefore and entropy term, and *Z* is a collision frequency. *Z* has a very specific definition based upon kinetic theory of gases and many body theories and is largely determined by gas phase diffusion. With TST and the Eyring equation ***A*** is replaced with $(k_bT/h)\, e^{\Delta S_f^*/R}$. In this case the entropy term is $e^{\Delta S_f^*/R}$ and the frequency term is k_bT/h. The Arrhenius ***A*** term frequency component would also involve a transmission probability κ, as in TST, but in the case of an isomerization like the NOSI system is likely to be ~0.5, because at the top of the hill both forward and reverse reactions would have nearly equal probability.

In summary, although by inserting the Arrhenius equation into thermodynamics, we have not derived absolute values of activated parameters, it has been shown that ***A*** is associated the reaction

activation entropy and E_a is associated with the activation enthalpy, *i.e.* $\Delta H^o = \left(E_{af} - E_{ar}\right)$ and $\Delta S^o = R\left(lnA_f - lnA_r\right)$.

Moreover $\Delta S^o = \left(k_b lnA_f - k_b lnA_r\right)$ which can be compared with Boltzmann's entropy $S = k_b lnW$.

It suggests that the ratio of A_f/A_r and W_f/W_r for forward and reverse reactions are equivalent, noting that any non-entropy related frequency terms must have cancelled out. Admittedly Arrhenius published his equation in 1889 whereas Bolzmann's entropy from statistical thermodynamics was published ~10 years later, in 1898. Note in this timeline that Trautz published his collision theory 1916 and TST was published in the 1930. So, Arrhenius may not have recognized the link between $\boldsymbol{A}$ and Boltzmann's entropy. However, since Arrhenius was one of Boltzmann's students that is highly unlikely.

What does each part of the Arrhenius equation say and how are they useful for understanding of kinetics? The units of a first order *k* are s^{-1} and the units of $\boldsymbol{A}$ also s^{-1} so both are frequencies, but they are not the same frequency of course. *k* is smaller by a factor $e^{-E_a RT}$, so in order to make them equal, $\boldsymbol{A}$ is multiplied by $e^{-E_a RT}$ and this is the first important thing. It is obvious mathematics, but it is important to note, because *k* is the frequency at which molecules react in a given reaction. That is what a first order rate constant is, just a reaction frequency. So, what does the other side of the equation say? $\boldsymbol{A}$ is a lot bigger than *k*, and it is the probability of molecules in our unimolecular reaction presenting themselves in the correct place and in the correct shape and orientation to react, combined with the limiting rate (frequency) at which they can rotate, break or otherwise modify their chemical bonds.

Now if all molecules bumping into each other (making sure they are the right kind and pointing the right way) reacted then $\boldsymbol{A} = k$, but it is not that easy for molecules to react. Normally for a reaction to occur a molecule must be pulled apart, a bond must break, or a few electrons must move *etc.* and although it may be assumed that it is going to get more stable eventually, it must be realized that there is a bit pain before the gain and it is necessary to give a little energy to get the reaction started. That energy is E_a on the potential energy diagram. The reactant molecules must have energy equal to E_a in order to get over the hill on the potential energy diagram in order to get to the other side and become a product. But where do they take it from? Well, they can only take it from the thermal reservoir which is k_bT. A single molecule gets E_a from k_bT and a mole of molecules gets E_a from RT because RT has 6.02×10^{23} times more energy.

At room temperature $k_bT = 4.11 \times 10^{-21}$ J and $RT = 2479$ J mol^{-1}. That amount of energy does not seem to be very much, because E_a is normally many times bigger, usually ~several kJ mol^{-1}. So, it may seem that it is difficult to get the molecule up the activation hill. However, k_bT is an average energy, so sometimes there is more energy and sometimes less. In fact, the molecule just waits for more energy to arrive. Boltzmann's distribution dictates how many molecules have enough energy at a given time, or, in

other words, how often a molecule possess E_a at a given temperature.

But how often it will happen that a molecule possesses E_a? Well, on average the molecules don't have enough energy, but they do $e^{\frac{-E_a}{RT}}$ of the time. Let's put numbers in. E_a could reasonably be 50000 J mol^{-1} so $e^{-(50000)/(2479)}$ of the time the molecules have sufficient energy and the reaction happens if they satisfy the entropy requirements from ***A***. That's $1.7x10^{-9\ th}$ of the time. So, this reaction could take some time! But, don't give up yet because ***A*** can easily be $>10^{11}$ s^{-1}. That's why ***A*** must be a lot bigger than *k*, for a reaction to occur in reasonable time, because Boltzmann's distribution only gives us energy equivalent to E_a for a tiny fraction of the time, and the rest of the time the energy is too low. So, the meaning of the equation can be broken down into its component parts. *k* is the number of times the reaction happens per second. ***A*** is the total number of times the molecule is positioned in the right way to react, coupled with the frequency at which the process naturally occurs, *e.g.* bond breaking, rotating, forming, *etc.* $e^{\frac{-E_a}{RT}}$ is the fraction of the time that the Boltzmann distribution gives the molecule enough energy to make the reaction happen. Next, the Arrhenius equation will be used with some published and unpublished data from previous works, assuming that the pre-exponential term is a composite of a frequency term and an entropy term (Hobley, 1995; Hobley and Wilkinson, 1996; Hobley et all., 2003; Wilkinson and Hobley, 1992; Wilkinson et all., 1996).

Experimental

All experimental procedures are already published and freely available on-line (Hobley, 1995). In the interests of brevity, they will not be repeated here.

Results and Discussion

Naphthoxazine-spiro-indolines (NOSI) are compounds from the general class of spiro-oxazine. They are best known for their use in Transitions$^{(TM)}$ ophthalmic photochromic lenses. The photochemical reaction occurs in a few picoseconds. The thermal fade reaction occurs in seconds to minutes (Hobley, 1995; Hobley and Wilkinson, 1996; Hobley et al., 2003; Wilkinson and Hobley, 1992; Wilkinson et al., 1996). These are compounds that can switch from a colorless form to a coloured form in chemical reactions induced by heat or light. The generic reaction scheme is shown in Figures 1 and 6.

A homologous series of such molecules (Figure 7) that are identical except length of an alkyl chain on the indoline nitrogen, was studied for this work. The alkyl chain modification was done with the

intention of hindering thermally induced ring closure. As can be seen from the first order rate constants for the thermal fade reaction from the colored **B** merocyanine to the colorless **A** spiro-form, shown in Table 1, this strategy worked.

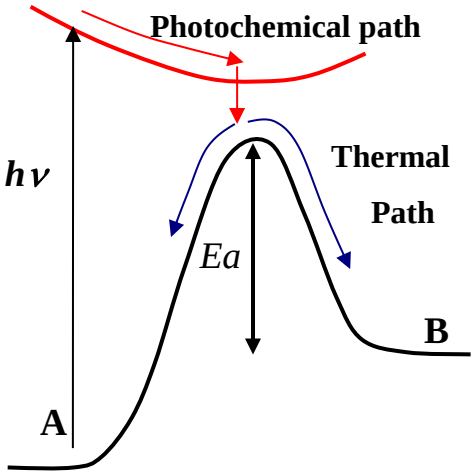

Figure 6. The ground state and excited state potential energy surface for a NOSI compound.

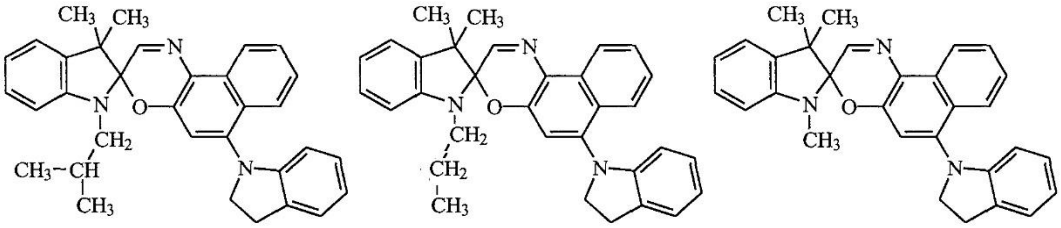

Figure 7. The homologous series of NOSI molecules studied

The first order rate constants for this thermal ring closure reaction of these three compounds were determined as a function of temperature and typical plots using the Eyring equation and the Arrhenius equations were made (Figure 8). The typical Eyring equation plot is *ln(k/T)* against *1/T* to obtain a straight line with a slope of $\Delta H^*/R$ and an intercept of $\ln(k/h) + \Delta S^*/R$. The Arrhenius plot of *lnk* against *1/T* yields a straight line with a slope of E_a and an intercept of ***A***. The extracted data is summarized in Table 1. As can be seen in Table 1, there is no significant difference in ΔH^* derived from the Eyring equation or from the Arrhenius plots for the different compounds studied. These values can be considered to be reliable, because they are not affected by assumptions in either treatment. Thus, it can be concluded that the effect of the alkyl chain length does not affect the value of ΔH^* and the source of the slowing of the thermal ring closure reaction with increasing chain length must be due to something else.

Not surprisingly since both Eyring and Arrhenius treatments yield three parallel straight lines and it

is the intercepts that are the big difference in each case. In other words, the differences are in the entropy terms, if there are no changes in the frequency components. This assumption is reasonable since the same kind of intramolecular rearrangement occurs in all three cases. This assumption is always made for Eyring as $\kappa\nu$ is assumed to be k_bT/h, and the three intercepts therefore contain the same lnk_b/h term.

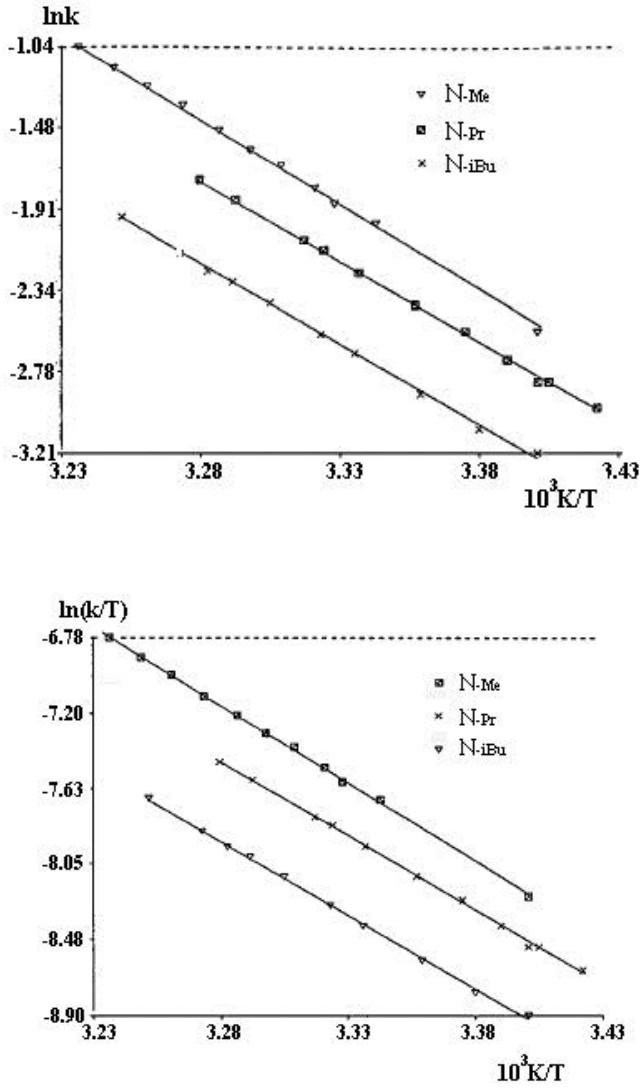

Figure 8. Arrhenius and Eyring plots for the thermal ring closure reaction of the homologous series of NOSI compounds (Hobley, 1995)

In the case of Arrhenius, the same assumption can be made based on reasoned arguments as to why it is valid or why it is invalid. In this case it is probably invalid to use the Eyring assumption. The Eyring equation gives "comforting" values of ΔS^*, however, this is because a value for $\kappa\nu$ was assumed, which

may not be valid for the following reasons. The ring closure reaction is not the same as the description of the transition state of TST in which the activated transition state dissociates within one vibration. In the ring closure reaction, nothing is dissociating. The molecule is twisting around a central single bond on the methine bridge. Arguably the use of the breakdown frequency k_bT/h for ν is incorrect because no bonds need to break at all in this twisting isomerisation. Furthermore, the transmission efficiency factor, κ, is not likely to be 1, because once the twisting molecule gets halfway through its motion, it could easily either reform the starting ring open form or continue to the ring closed form.

Table 1. Kinetic parameters for the homologous series of naphthoxazine-spiro-indolines in toluene

N_{alkyl}	$E^1_{a(B\rightarrow A)}$ $kJ\ mol^{-1}$	$\Delta H^{*}_{(B\rightarrow A)}{}^{2}$ $kJ\ mol^{-1}$	$Intercept^1$	A^1 s^{-1}	$(\Delta S^*)^2$ $J\ K^{-1}\ mol^{-1}$	$e^{-\Delta H^*/RT}$ 298 K	$k_{294\ K}$ s^{-1}
N_{-Me}	73.2	70.6	27.87	$1.3x10^{12}$	-16.6	$6.3x10^{-14}$	0.077
N_{-Pr}	71.8	69.6	25.69	$1.8x10^{11}$	-32.8	$4.3x10^{-13}$	0.059
N_{-iBu}	71.6	69.0	25.90	$1.5x10^{11}$	-37.6	$2.2x10^{-13}$	0.040

[1]from Arrhenius equation; [2] from Eyring equation

The Eyring derived values of ΔS^* can safely be taken as relative values. However, less credence should be given to the actual values.

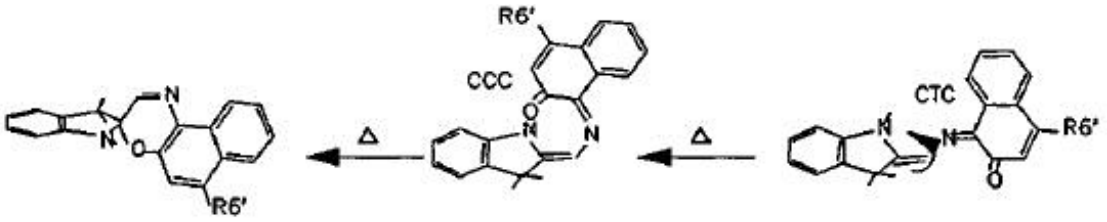

Figure 9. The proposed mechanism for the thermal ring closure reaction.

What we can say is that the ring closure reaction should go through the conformation which is *cis-cis-cis* CCC about the central methine bridge (Figure 9), because it is apparent that the N_{-alkyl} groups are hindering the reaction. The naphthalene moiety will collide with larger N_{-alkyl} chains only if it passes through the CCC form. Furthermore we can state that it is probably the activation entropy of the reaction, ΔS^*, that is slowing down the reaction for larger N_{-alkyl} groups, since the larger N_{-alkyl} groups have to move out of the way, meaning that the molecule must adopt a specific conformation before the ring closure can be completed. However, we clearly cannot trust the absolute entropy values.

In comparison, the diminishing values of ***A*** with increasing $N_{\text{-alkyl}}$ bulkiness also allows us to infer that entropy is the key factor here because we have already argued that ***A*** is a combined frequency and activation entropy term. From ***A*** we can determine the frequency of the reaction if the process was occurring in the absence of an activation energy. In changing from $N_{\text{-Me}}$ to $N_{\text{-Pr}}$ to $N_{\text{-iBu}}$ the reaction frequency changes from $1.3\text{x}10^{12}$ s^{-1} (0.8 ps) to $1.8\text{x}10^{-11}$ s^{-1} (5.6 ps) to $1.5\text{x}10^{-11}$ s^{-1} (6.7 ps). For reference the frequency factor in TST (k_bT/h) has a room temperature value of $6.3\text{x}10^{12}$ s^{-1} meaning that the reaction is expected to occur in 150 fs in the absence of other hindering factors. The ring closure reactions of NOSI compounds are between 5 to 40 times slower than that. Since this is a simple reaction in which nothing dissociates, no bonds need to break and only a simple torsion around the central single bond on the methine bridge is required. It could justifiably be suggested that the reaction activation entropy for the $N_{\text{-Me}}$ compound is close to zero, because the $N_{\text{-Me}}$ group cannot hinder the reaction and it cannot change its conformation relative to the naphthalene moiety during the reaction. Thus, it can be suggested that a realistic natural frequency for this type of reaction is equal to the value of ***A*** obtained from the Arrhenius plot intercept for the $N_{\text{-Me}}$ compound ($1.3\text{x}10^{12}$ s^{-1}) and that the reaction should proceed on the sub-picosecond timescale (0.8 ps) if a molecule possess E_a. In other words, by assuming nothing until the end. We could extract a candidate number for the frequency component of ***A*** by reasonably assuming that the activation entropy is negligible (an assumption stated is one that can later be refuted).

Using this information it can further be suggested that a reasonable candidate values of actual activation entropies for the $N_{\text{-Pr}}$ and $N_{\text{-iBu}}$ compounds by assuming there is low to no entropy term for the $N_{\text{-Me}}$ compound and assuming very reasonably that the entropy term in ***A*** is of the form $Fe^{\Delta S^*/R}$. It can just be assumed that a good value for the natural reaction frequency (F) is the same as for the $N_{\text{-Me}}$ molecule ($1.3\text{x}10^{12}$).

In the case of the $N_{\text{-Pr}}$ compound $\boldsymbol{A}$ = $1.8\text{x}10^{11}$=$1.3\text{x}10^{12}$ $e^{\Delta S^*/R}$ from which ΔS^*_{N-Pr} = -16.4 J K^{-1} mol^{-1} can be calculated. Similarly, ΔS^*_{N-iBu} = -17.9 J $K^{-1}mol^{-1}$ can be determined.

It can be seen from the first order rate constants for the thermal fade reaction from the colored **B** merocyanine to the colorless **A** spiro-form, shown in Table 1, were successfully slowed down by a bulkier $N_{\text{-alkyl}}$ group. But moreover, we can quantify this in terms of the activation entropy of the reaction. To achieve this, it has simply been proposed, based on equation (13) CT and TST, that the Arrhenius ***A*** – term has a form $(F_{\Delta}^{B\rightarrow A})\, e^{\Delta S^*/R}$ where $(F_{\Delta}^{B\rightarrow A})$ is the frequency component of the ***A*** term. However, unlike for CT and TST it was not necessary to fix a value for the frequency component or assume any breakdown efficiency that is not based on a knowledge of the system under investigation.

Comparison with NOSI photochemistry

As can be seen in Figure 6, in photochemistry it is possible to jump the molecule into an excited state using a photon's energy. In this excited state, the molecule may react with zero activation energy to form products. Thus, it is possible to compare the derived thermal-reaction frequencies with real values measured in the absence of any E_a. These photochemical reactions happen very fast. It is known from data from picosecond pump-probe experiments that in non-polar cyclohexane the $N_{\text{-iBu}}$ compound photo-isomerizes with a rise-time τ_{rise} ~ 5ps (Table 2) (Hobley, 1995; Hobley and Wilkinson, 1996; Hobley et al., 2003; Wilkinson and Hobley, 1992; Wilkinson et al., 1996). This means $\boldsymbol{A}$ in the direction A→B is $2x10^{11}$ s^{-1} (5 ps) because in photochemistry light is used to jump straight to the top of the hill and there is no activation enthalpy term (no E_a). It compares rather well with the $(F_{\Delta}^{B\rightarrow A})\, e^{\Delta S^*/R}$ ~$1.5x10^{11}$ s^{-1} (6.7 ps) for the same compound in toluene in the thermally activated reaction. The rate of the reaction is just a little slower in the ground state. However, in the case of photochemistry, for compounds with $N_{\text{-Me}}$ and $N_{\text{-iBu}}$ groups in non-polar solvents the quantum efficiency (number of molecules reacted/number of photons absorbed) $\phi_{A\rightarrow B}$ is high and it is not altered by the $N_{\text{-alkyl}}$ chain length (Table 2). Furthermore, between cyclohexane and toluene there is no significant difference in the quantum efficiencies of the ring-opening reaction. In other words, the trend observed for the thermal fade reaction in which the methine bridge rotation is hindered in the order $N_{\text{-iBu}}$>$N_{\text{-Pr}}$>$N_{\text{-Me}}$; it is not seen when comparing photochemical quantum efficiencies, for which there is no $N_{\text{-alkyl}}$ effect. It is thus proposed that the photochemical reaction does not go through the same CCC intermediate as in the thermal reaction, because in that conformation steric factors should reduce the reaction efficiency for the compounds with longer bulky chains as in the ground state. Therefore, the proposed intermediate in the photochemically induced rotation is the *trans-cis-cis* TCC form in which the naphthalene moiety cannot bump into the $N_{\text{-alkyl}}$ chains.

Comparing the reverse Arrhenius frequencies (Table 1) with the forward photochemical frequencies in non-polar solvents (Table 2) shows that the reaction frequency of the photochemical forward reaction and the thermal reverse reaction is very similar except that the thermal reaction is a little slower. Let's assume that the photochemical reaction frequency is of the same form as the $\boldsymbol{A}$ term in Arrhenius, *i.e.* it is possible to write it as a combination of an entropy term and a frequency term, for example:

$(F_{\Delta}^{B\rightarrow A})\, e^{\Delta S^*/R}$ ~ $1.8x10^{11}$ s^{-1} (6.6 ps) $N_{\text{-iBu}}$ in toluene

$(F_{\Delta}^{A\rightarrow B})\, e^{\Delta S^*/R}$ ~ $2x10^{11}$ s^{-1} (5.0 ps) $N_{\text{-iBu}}$ in cyclohexane

The high quantum yield for $\phi_{A\rightarrow B}$ in non-polar solvents implies that, all things taken into account, the progression from the S_1 state of the spiro-form to the ground state of the mero-form is highly favored by efficient internal conversion between S_1 and S_0 and upon dropping down to the ground state surface; in

non-polar solvents the molecules favor ring-opening more than ring-closure. It means that the transmission factor κ in the frequency term is >0.5, probably because the molecule does not drop onto the top of the hill in the ground state potential energy surface, but rather drops down on the B-side of the hill.

Table 2. Photochemical parameters (Hobley, 1995; Hobley and Wilkinson, 1996; Hobley et al., 2003; Wilkinson and Hobley, 1992; Wilkinson et al., 1996)

Compound	Solvent	τ_1 / ps (k_1)	τ_2 / ps (k_2)	$\phi_{A\rightarrow B}$
$N_{\text{-Me}}$	BuOH	7.1 ($1.4\text{x}10^{11}$)	790 ($1.3\text{x}10^{9}$)	
$N_{\text{-iBu}}$	PrOH	7.1 ($1.4\text{x}10^{11}$)	560 ($1.8\text{x}10^{9}$)	0.22
$N_{\text{-iBu}}$	BuOH	7.1 ($1.4\text{x}10^{11}$)	790 ($1.3\text{x}10^{9}$)	
$N_{\text{-iBu}}$	DeOH	7.1 ($1.4\text{x}10^{11}$)	1100 ($9.1\text{x}10^{8}$)	
$N_{\text{-iBu}}$	CHX	5.0 ($2.0\text{x}10^{11}$)	Over in τ_1	0.70
$N_{\text{-Me}}$	CHX			0.72
$N_{\text{-iBu}}$	Toluene			0.67
$N_{\text{-Me}}$	Toluene			0.64

Note that on the excited state the potential energy surface the molecule undergoes charge separation in which electrons from the oxazine oxygen and the spiro carbon delocalize to the indoline nitrogen as the oxazine oxygen takes on a phenolic character (Figure 10) with the TCC conformation. This is a zwitterionic intermediate in which the central bond on the methine bridge is double bonded. This double bond character should hinder rotation. However, if the molecule drops down onto the ground state surface the phenolic oxygen should transfer its negative charge back to the positive indoline nitrogen to form a non-charge separated TCC quinoidal form in which the central methine bridge bond is a single bond. In this conformation a single rotation about the single bond would easily form a merocyanine with TTC form. The lifetime of the charge separated zwitterionic state should be shorter in non-polar solvents and could be longer in polar solvents such as alcohols, because these could help to solvate the charge separated state. Indeed, from Table 2, in polar solvents (alcohols) there is a much longer lived transient in the photochemical isomerization after the rapid (7 ps) formation of an intermediate state.

The formation of the fast transient is independent of solvent viscosity and corresponds to $(F_{\Delta}^{A\rightarrow B})\, e^{\Delta S^*/R} \sim 1.4\text{x}10^{11}\ s^{-1}$. Furthermore, it does not change with the $N_{\text{-alkyl}}$ chain length. This transient must be formed with only slight changes in the molecular shape. This timescale can be attributed to the formation of the charge separated zwitterionic cisoid TCC merocyanine isomer. The longer lived transient state absorbs broadly across the visible (Hobley et al., 2003) and has an $(F_{\Delta}^{A\rightarrow B})e^{\Delta S^*/R} = 1.8\text{x}10^{9}$ (560 ps) $1.3\text{x}10^{9}$ (790 ps) – $9.1\text{x}10^{8}$ (1100 ps) in propanol, butanol, and decanol, respectively. Its lifetime is affected by viscosity but is independent of the $N_{\text{-alkyl}}$ chain length. In other words it should involve significant molecular rotation

because it is affected by solvent viscosity, but it must rotate in a way such that the $N_{\text{-alkyl}}$ chain cannot clash with the naphthalene moiety during the transformation, *i.e.* it should go through the ground state quinoidal TCC isomer. The longer lifetime, of hundreds of picoseconds, supports the transient being charge separated, *i.e.* the molecule is in its zwitterionic form in which bond rotation is hindered. This should drop down onto the ground state surface to form the TTC quinoidal merocyanine, but the hold up on the excited state should increase the chance of internal conversion and vibrational cascade, thereby lowering the quantum efficiency of the photochemical transformation from **A** to **B** (as seen in Table 2 for the polar solvent quantum efficiency). Hence, a full mechanism for the photochemical ring opening and thermal ring closure can be proposed that fits all the kinetic and photochemical data in Tables 1 and 2. This is shown in Figure 10.

From the transient absorption spectra (Hobley at al., 2003) obtained in butanol it may also be reasonably suggested that the broad absorption across the visible for the transient assigned to a zwitterionic TCC molecule on the S_1 surface implies that this transient is indeed in its excited state for which the energy gap $S_1 \rightarrow S_2$ would be smaller than transitions from ground states and because such broad featureless spectra extending to long wavelength are typical for the lower energy $S_1 \rightarrow S_2$ transition (Tamai and Masuhara, 1992).

When suggesting that a transient on the S_1 surface is stabilized compared to the transient on the S_0 surface ($S_1\nu_0$ is far higher in energy than $S_0\nu_0$) it must be remembered how internal conversion occurs. Internal conversion does not have an activation barrier, *i.e.* E_a is zero. E_a is heavily associated with ΔH^* meaning that internal conversion must be dominated by ΔS^*. This is actually obvious when it is considered that internal conversion involves the electronically excited, yet vibrationally and rotationally "cold" $S_1\nu_\mathbf{0}$ state converting into a state equal in energy (iso-energetic) that exists on the ground state surface, which is the vibrationally "hot" $S_0\nu_n$ state (subscript *n* indicates the n^{th} vibrational level of S_1 that energetically matches $S_0\nu_n$). The parameter that holds up this conversion does not involve enthalpy so much, but it is dominated by entropy. Internal conversion obeys the Franck-Condon principle (Condon, 1926; Franck, 1926). That means that for an electronic transition to happen the Born-Oppenheimer approximation must apply (Born, 1927). Born-Oppenheimer suggests that there is a zero nuclear motion during an electronic transition. It means that for internal conversion to happen the molecule must, more-or-less inter-atomically map onto the state that it is about to become. If the excited state is polar and solvated in a polar solvent, it is less likely to map, atom-to-atom onto a non-polar ground state that is less solvated in the polar solvent. Thus, the hold-up for the photo-isomerization in the alcohols is also apparently due to the entropy term in the reaction frequency of the transformation ($(F_{\Delta}^{A\rightarrow B})\ e^{\Delta S^*/R}$). The natural frequency of the reaction should be like the natural frequency on the ground state because it is still a nearly identical rotation about a single bond. It is

then possible to produce a plausible number for the entropy term for the internal conversion in alcohols (ignoring possible differences in κ).

Previously it was proposed that $F_{\Delta}^{B\rightarrow A}$ for the $N_{\text{-Me}}$ is $1.3\text{x}10^{12}$ and this number can be used to try to separate the proposed frequency component and entropy terms. We know that $(F_{\Delta}^{A\rightarrow B})\ e^{\Delta S^*/R}$ is $1.8\text{x}10^{9}$ (560 ps), $1.3\text{x}10^{9}$ (790 ps) and $9.1\text{x}10^{8}$ (1100 ps) in propanol, butanol, and decanol, respectively. For the N_{iBu} reaction in propanol we can write

$1.8\text{x}10^{9} = 1.3\text{x}10^{12}\ e^{\Delta S^*/R}$

$e^{\Delta S^*/R} = 1.8\text{x}10^{9}/1.3\text{x}10^{12} = 1.38\text{x}10^{-3}$ if the frequency term for the $N_{\text{-Me}}$ compound applies to the $N_{\text{-iBu}}$ compound, which is reasonable, because the $N_{\text{-Me}}$ substitution has been shown to affect the reaction entropy. From this we can calculate that $\Delta S^*/R$ = -6.6. This means that ΔS^*= -55 J mol^{-1} K^{-1} in propanol. Similarly, ΔS^*= -57 J mol^{-1} K^{-1} in butanol and -60 J mol^{-1} K^{-1} in decanol can be calculated. The differences between these three solvents is no doubt due to additional entropy contributions due to solvent viscosity. In other words, the solvent molecules must move out of the way of the rotating moieties.

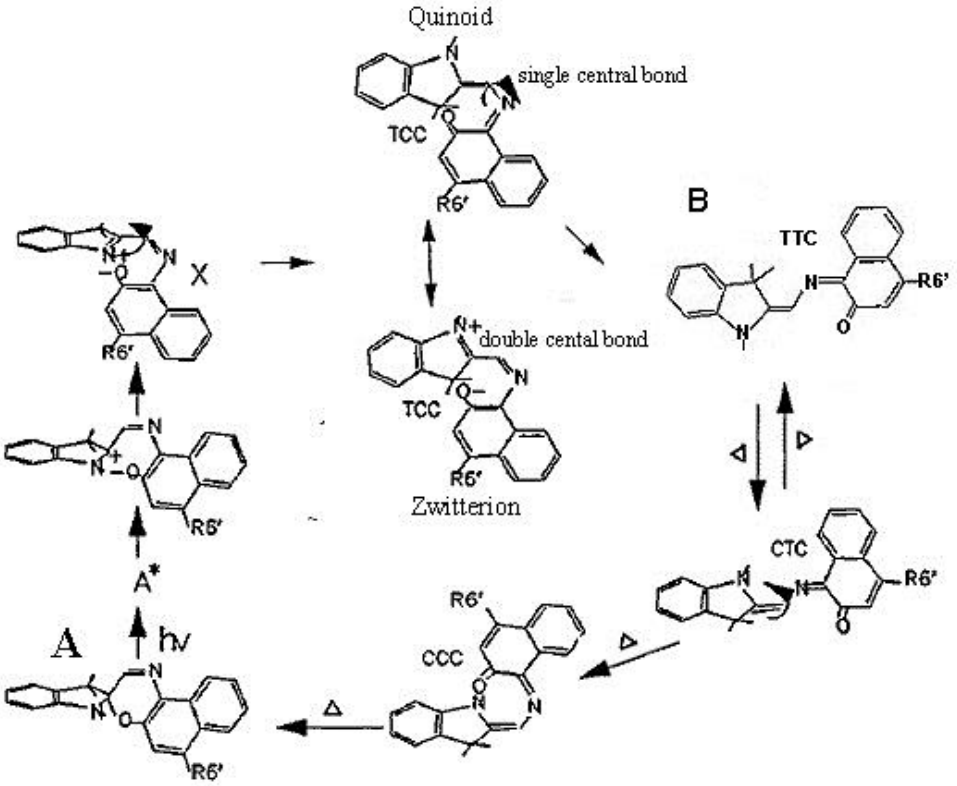

Figure 10. The proposed full photochemical and thermal reaction mechanism for a NOSI compound

Conclusion

It has been demonstrated that the simple application of the Arrhenius equation using assumptions specific to the molecular system under investigation can yield values of E_a ,and ***A***. Since ***A*** can safely be assumed to be a composite of an entropy and an enthalpy term *i.e.* A=$(F_{\Delta}^{B\rightarrow A})$ $e^{\Delta S^*/R}$, it means that in some cases the terms $(F_{\Delta}^{B\rightarrow A})$ and ΔS^*can be separated when the entropy or frequency term can be reasonably assumed to have a known probable value. Using this approach, thermal reaction and photochemical reactions of naphthoxazine-spiro-indolines have been compared. By doing so, it has been possible to propose a full reaction scheme for the entire photochromic reaction of these commercially important molecules. The Arrhenius ***A*** reaction frequency for the ground state was almost the same as the frequency of the first order rate constants for the photochemical reaction in non-polar solvents. However, the photochemical frequencies obtained in polar solvents was significantly slower than in non-polar solvents. It is suggested that this is because the molecule gets held up as a zwitterionic excited state for which the bond rotation to form the ring open merocyanine is hindered by a double central bond on the methine bridge. The molecule must drop to S_0 before it can isomerize. Hence when extracting reaction frequency terms, care must be taken to understand the type of molecular process that is being studies. Some reactions are naturally slower than others by virtue of their natural frequencies.

Acknowledgment

JH acknowledges Pilkington Glass and SERC for providing chemicals and funding.

Conflict-of-Interest Statement

There are no conflicts of interest in this research article.

References

Arrhenius, S. A. (1889). Über die Reaktionsgeschwindigkeit bei der Inversion von Rohrzucker durch Säuren. Zeitschrift für Physikalische Chemie, 4, 226-248.

Atkins, P. W., Paula, J. De. (2006). Atkins' Physical Chemistry, 8th Ed Oxford University Press, Chapter 24.

Boltzmann, L. (1872). Weitere Studien uber das Warmegleichgewicht unter Gasmolekulen. Wiener Berichte, 66, 275-370.

Boltzmann, L. (1896). Vorlesungen über Gastheorie, vol. I., J.A. Barth, Leipzig.

Boltzmann, L. (1898). Vorlesungen über Gastheorie, vol. II. J.A. Barth, Leipzig.

Born, M., Oppenheimer, R. (1927). Zur Quantentheorie der Molekeln. Annalen der Physik, 389, 20, 457-484.

Condon, E. (1926). A theory of intensity distribution in band systems. Physical Review, 28, 1182-1201.

Franck, J. (1926). Elementary processes of photochemical reactions. Transactions of the Faraday Society, 21, 536-542.

Hobley, J. (1995). PhD Thesis, Loughborough University, Available on-line https://dspace.lboro.ac.uk/dspace-jspui/bitstream/2134/33254/1/Thesis-1995-Hobley.pdf

Hobley, J., Lear, M. J., Fukumura, H. (2003). Photo-switching spiropyrans and related compounds. In: Photochemistry of organic molecules in isotropic and anisotropic media. Marcel Dekker, Inc, pp. 353-404. ISBN 9780824708832, 9780203014202.

Hobley, J., Wilkinson, F. (1996). Photochromism of naphthoxazine-spiro-indolines by direct excitation and following sensitisation by triplet-energy donors. Journal of the Chemical Society, Faraday Transactions, 92, 8, 1323-1330.

Laidler, K. J., King, M. C. (1983). Development of transition-state theory. The Journal of Physical Chemistry, 87, 2657-2664.

Tamai, N., Masuhara, H. (1992). Femtosecond transient absorption spectroscopy of a spirooxazine photochromic reaction. Chemical Physics Letters, 191, (1-2), 189-194.

Trautz, M. (1916). Das Gesetz der Reaktionsgeschwindigkeit und der Gleichgewichte in Gasen. Bestätigung der Additivität von C_v- 3/2R. Neue Bestimmung der Integrationskonstanten und der Moleküldurchmesser. Zeitschrift für anorganische und allgemeine Chemie, 96, 1-28.

Van't Hoff, J. H. (1887). Die Rolle des osmotischen Druckes in der Analogie zwischen Lösungen und Gasen. Zeitschrift für Physikalische Chemie, 1, 481-508.

Wilkinson, F., Hobley, J., M. Naftaly, M. (1992). Photochromism of spiro-naphthoxazines : molar absorption coefficients and quantum efficiencies. Journal of the Chemical Society, Faraday Transactions, 88, 1511-1517.

Wilkinson, F., Worrall, D. R., Hobley, J., Jansen, L., Williams, S. L., Langley, A. J., Matousek, P. (1996). Picosecond time-resolved spectroscopy of the photocolouration reaction of photochromic naphthoxazine-spiro-indolines. Journal of Chemical Society, Faraday Transactions, 92, 1331-1336.

Chemia Naissensis, Vol 2, Issue 1, MINI-REVIEW, 68-69

Ponovno vraćanje na Arenijusovu jednačinu u hemijskoj kinetici za analizu kinetičkih podataka za fotohromne naftoksazin-spiro-indoline

Džonatan Hobli

OndaLabs R&D Konsalting, Deca Homes, Clark Free-Port, Barangay Margot, Angeles, 2009, Filipini

SAŽETAK

U toku osnovnih studija, kinetika i termodinamika se često predaju kao zasebni predmeti. To je zato što termodinamički podaci ne govore o brzini postizanja ravnoteže-to spada u kinetiku. Čak i ako je hemijska reakcija termodinamički favorizovana, može se desiti da se ona nikada neće dogoditi iz kinetičkih razloga. Međutim, ovo odvajanje kinetike i termodinamike je manjkavo u nekim aspektima. U ovom radu, istražena je veza između hemijske kinetike i termodinamike, utemeljena u obe oblasti i definisana jednim dijagramom potencijalne energije. Uobičajena zabluda izazvana predmetima iz hemijske kinetike sa osnovih studija, je tvrdnja da je Arenijusova jednačina manjkava zato što ne pruža precizno značenje za pre-eksponencijalni član *A*. Predmeti na osnovnim studijama obično nastavljaju sa sofisticiranijim teorijama u obliku kolizione teorije CT (engl.) i teorije prelaznog stanja TST (engl.) rezultujući Ejringovom jednačinom. Ove dve poslednje teorije su potrebne da bi se formalno pokazalo, da pre-eksponencijalni član sadrži informaciju o entropijskim zahtevima reakcije. U ovom radu će biti prikazano da je razmatrajući vezu između termodinamike i kinetike, moguće pokazati da je *A* već posredno povezan sa proizvodom entropije aktivacije reakcije i prirodne frekvencije reakcije. Ovaj rad koristi prethodno publikovane i nepublikovane rezultate fotohromnih naftoksazin-spiro-indolina da bi se uporedile različite teorije.

Ključne reči: Arenijusova jednačina, teorija prelaznog stanja, koliziona teorija, naftoksazin-spiro-indolin, fotohromni, hemijska kinetika

Chemia Naissensis, Vol 2, Issue 1, MINI-REVIEW, 70-71

Révision de l'équation d'Arrhenius en cinétique chimique pour analyser les données cinétiques de naphtoxazine-spiro-indolines photochromiques

Jonathan Hobley

OndaLabs R&D Consultancy, Deca Homes, Clark Free-Port, Barangay Margot, Angeles, 2009, Philippines

RÉSUMÉ

Lors du premier cycle d'études, la cinétique et la thermodynamique sont enseignées comme les matières séparées. C'est le résultat du fait que les données thermodynamiques sur l'équilibre ne traitent pas la vitesse d'atteindre l'équilibre, ce qui représente en effet la cinétique. Il est vrai que même si une réaction chimique est thermodynamiquement favorable, elle peut ne jamais se produire pour des raisons cinétiques. Cependant, cette séparation de la cinétique et de la thermodynamique est regrettable à certains égards. Dans ce travail, est exploré le lien entre la cinétique chimique et la thermodynamique, les deux étant définies par un seul diagramme d'énergie potentielle. Une erreur habituelle provoquée par les cours du premier cycle en cinétique chimique est l'affirmation que l'équation d'Arrhenius est déficiente car elle n'offre pas de définition précise du terme pré-exponentiel *A*. Les cours du premier cycle proposent souvent des théories plus sophistiquées sous forme de théorie de la collision CT (angl.) et de théorie de l'état de transition TST (angl.), résultant en équation d'Eyring. Ces deux dernières théories sont nécessaires pour montrer formellement que le terme pré-exponentiel contient l'information sur les exigences d'entropie de la réaction. Dans cette recherche, il sera montré qu'en examinant la relation entre la thermodynamique et la cinétique, il est possible de démontrer que *A* est déjà implicitement lié au produit de l'entropie de l'activation de la réaction et de la fréquence

naturelle de la réaction. Cet article utilise des résultats précédemment publiés et non publiés des naphtoxazine-spiro-indolines photochromiques pour comparer les différentes théories.

Mots-clés : équation d'Arrhenius, théorie de l'état de transition, théorie de la collision, naphtoxazine-spiro-indoline, photochromique, cinétique chimique.

Chemia Naissensis, Vol 2, Issue 1, MINI-REVIEW, 72-73

Пересмотр уравнения Аррениуса в химической кинетике для анализа данных кинетики фотохромных нафтоксазин-спироиндолинов

Джонатан Хобли

OndaLabs R & D Consultancy, Deca Homes, Кларк Фри-Порт, Барангай Марго, Анджелес, 2009, Филиппины

АННОТАЦИЯ

В бакалавриате кинетика и термодинамика часто преподаются как отдельные модули. Это потому, что данные равновесия в области термодинамики не дают нам информацию о скорости достижения равновесия, то есть кинетики. Верно, что даже если химическая реакция термодинамически приемлема, она может никогда не произойти из-за кинетических соображений. Однако такое разделение кинетики и термодинамики в некоторых отношениях вызывает сожаление. В этой работе исследуется связь между химической кинетикой и термодинамикой, основанная на том, что оба они определены одной диаграммой потенциальной энергии. Распространенное заблуждение, вызванное курсами бакалавриата по химической кинетике, заключается в утверждении, что уравнение Аррениуса является неполноценным, поскольку оно не дает точного значения для предэкспоненциального термина A. Курсы бакалавриата часто продолжают предлагать более сложные теории в форме теории столкновения и теории переходного состояния, приводящих к уравнению Эйринга. Эти две последние теории необходимы для того, чтобы формально показать, что предэкспоненциальный член содержит информацию о требованиях реакции к энтропии. В этой работе будет показано, что, рассматривая связь между термодинамикой и кинетикой, легко можно показать, что термин A. уже неявно связан с продуктом энтропии активации реакции и собственной частотой реакции. Эта работа использует ранее опубликованные и неопубликованные результаты по

фотохромным нафтоксазин-спиро-индолинам для сравнения различных теорий.

Ключевые слова: уравнение Аррениуса, теория переходных состояний, теория столкновений, нафтоксазин-спиро-индолин, фотохромное, химическая кинетика.

Chemia Naissensis, Vol 2, Issue 1, MINI-REVIEW, 74-75

Neubetrachtung der Arrhenius-Gleichung in der chemischen Kinetik zur Analyse von Kinetikdaten für photochrome Naphthoxazin-Spiro-Indoline

Jonathan Hobley

OndaLabs R&D Beratung, Deca Homes, Clark Free-Port, Barangay Margot, Angeles, 2009, Philippinen

ABSTRAKT

In den Bachelorstudiengängen werden Kinetik und Thermodynamik oft als separate Module unterrichtet. Das liegt daran, dass die Gleichgewichtsdaten aus der Thermodynamik keinen Aufschluss über die Geschwindigkeit der Gleichgewichtserreichung geben, weil es sich um die Kinetik handelt. Es ist richtig, dass eine chemische Reaktion, selbst wenn sie thermodynamisch günstig ist, aus kinetischen Gründen niemals ablaufen kann. Jedoch ist diese Trennung von Kinetik und Thermodynamik in mancher Hinsicht bedauerlich. In dieser Arbeit wird die Verbindung zwischen der chemischen Kinetik und der Thermodynamik untersucht, basierend darauf, dass beide durch ein einziges Potential-Energie-Diagramm definiert werden. Ein geläufiger Irrtum, der in den Fächern in den Grundstudiengängen zur chemischen Kinetik verursacht wurde, ist die Behauptung, dass die Arrhenius-Gleichung mangelhaft ist, weil sie keine präzise Bedeutung für den präexponentiellen Faktor A bietet. Grundstudienfächer setzen häufig fort, komplexere Theorien zu bieten, in Form der Kollisionstheorie CT (engl.) und der Übergangszustandstheorie TST (engl.), die in der Eyring-Gleichung resultieren. Diese beiden letztgenannten Theorien sind erforderlich, um formal zu zeigen, dass der präexponentielle Faktor Informationen über die Entropieanforderungen der Reaktion enthält. In dieser Arbeit wird gezeigt, dass in Anbetracht der Verbindung zwischen der Thermodynamik und der Kinetik gezeigt werden kann, dass A bereits implizit mit dem Produkt der Aktivierung der Entropie der Reaktion und der Eigenfrequenz der Reaktion verbunden war. Diese Arbeit nutzt die zuvor

veröffentlichten und unveröffentlichten Ergebnisse zu photochromen Naphthoxazin-Spiro-Indolinen zum Vergleich verschiedener Theorien.

Schlüsselwörter: Arrhenius-Gleichung, Theorie des Übergangszustandes, Kollisionstheorie, Naphthoxazin-Spiro-Indolin, photochrome, chemische Kinetik

Chemia Naissensis, Vol 2, Issue 1, RESEARCH ARTICLE, 76-91

Kinetic and Thermodynamic Parameters for Degradation of Anthocyanins from Red Currant and Sour Cherry Juices by Hydrogen Peroxide in the Presence of Cu(II)

Jovana Lj. Pavlović*, Milan N. Mitić, Sonja M. Janković

University of Niš, Faculty of Sciences and Mathematics, Department of Chemistry, Višegradska 33, 18 000 Niš, Republic of Serbia

ABSTRACT

The kinetics of anthocyanins degradation in the red currant and sour cherry juices by hydrogen peroxide at pH 3.5 was investigated. The reaction was catalyzed by the trace of Cu (II), and it was followed spectrophotometrically at 520 nm by applying the initial-rate method. The reaction kinetic parameters are reported, and the rate equation is suggested. From the dependence of the rate constants on the temperature, the activation energy was calculated: 25.76 and 30.59 kJ mol^{-1} for the red currant and sour cherry juices, respectively. The thermodynamic functions of activation (ΔG^*, ΔH^* and ΔS^*) have been determined to understand red currant and sour cherry juice anthocyanins degradation.

Keywords: red currant, sour cherry, anthocyanins, kinetic parameters, thermodynamic functions

*Jovana Pavlović
e-mail address: jovanapavlovic@ymail.com
address: Višegradska 33, PO Box 224 Niš, 18000 Serbia

Introduction

Anthocyanins are polyphenolic pigments, responsible for the red, blue, and purple color of numerous fruits. They are reported to have antioxidant properties and thus many health benefits (Harbourne et al., 2008). There are several reports focused on the effect of anthocyanins on cancer treatments (Nichenametle et al., 2006), human nutrition (Stintzing and Carle, 2004), and biological activity (Kong et al., 2003). Red currants and sour cherries are an excellent source of anthocyanins and, therefore, very interesting because they offer potential as an ingredient in functional beverages. Anthocyanins identified in red currants are cyanidin-3-*O*-sambubioside, cyanidin-3-*O*-rutinoside, cyanidin-3-*O*-(2"-*O*-xylosyl) rutinoside (Borges et al., 2010); cyanidin-3-rutinoside, cyanidin-3-sophoroside, and cyanidin-3-glucoside (Määttä et al., 2003). Also, the most abundant sour cherry anthocyanin is cyanidin-3-glucosyl-rutinoside (Damar and Eksi, 2012). After the harvest, red currant and sour cherry fruits easily lose its red color, resulting in reduced market value (Ruenroenglin et al., 2009). Several factors influence to anthocyanin stability, including pH, light, oxygen, enzymes, ascorbic acid, sugars, metal ions, and copigments (Kechinski et al., 2010).

Thermal degradation of anthocyanins has been studied for grape juice (Hillman et al., 2011), Chinese red radish (Liu et al., 2014), the raspberry pulp (Summen and Erge, 2014), and blood orange juice (Kirca and Cemeroglu, 2013). The kinetic degradation of anthocyanins can be evaluated from a thermodynamic perspective based on activation functions such as free energy (ΔG^*), enthalpy (ΔH^*), entropy (ΔS^*) and activation energy (E_a). These functions can be estimated for reactions occurring in foods and may provide valuable information concerning thermal degradation kinetics. Additionally, hydrogen peroxide (H_2O_2) has been used in foods and food packaging materials for various purposes in many European countries for over 30 years (Nikkhah et al., 2010). Degradation of anthocyanins by H_2O_2 has also been studied for litchi fruit (Ruenroengklin et al., 2009), sour cherry, pomegranate, and strawberry juices (Özkan et al., 2002). Copper, normally occurring in fruit and vegetables, plays a vital role in these oxidation reactions. No published data have been found in the literature on the effects of H_2O_2 in the presence of Cu(II) ions on the degradation of anthocyanins from the red currant and sour cherry juices. Therefore, the objective of the presented work was to investigate the effects of Cu(II)/H_2O_2 reagent on the stability of red currant and sour cherry juices. Different temperatures

were used to predict kinetic degradation and, at a temperature of 25^{o}C, the thermodynamic functions of activation were estimated.

Experimental

Material

The samples of sour cherry and red currant fruits used in the study were obtained from the Niška Banja (Serbia). Fruits were washed in cold tap water and homogenized in a high-speed blender. The homogenate was filtered and stored at -18^{o}C until use. All the analyses were performed in three replicates.

Equipment

Spectrophotometric measurements were performed on UV-Vis spectrophotometer, model 8453 (Agilent, Germany) with a 1 cm match glass cell. For the pH measurements, Radiometer PHM 29Bb pH meter (MeterLab, USA) and a combined glass-calomel electrode, GK2311C, were used. All solutions were kept in a thermostatic water-bath, model MP-5A (Julabo, USA) at 25.0 ± 0.1 °C before the beginning of the reaction. High precision measuring for laboratory applications was performed using an analytical balance (±0.0001 g), model AB204-5 (Mettler Toledo, Switzerland). A stopwatch was used to record a reaction time.

Reagents and solutions

Analytical grade chemicals and deionized water (MicroMed high purity water system, TKA Wasseraufbereitungssysteme GmbH) were used for the preparation of all solutions. All the stock solutions were stored in polyethylene containers. All the polyethylene containers and the glassware used were cleaned in aqueous HCl (1:1) and then thoroughly rinsed with deionized water. 1.00 gL^{-1} Cu (II) (nitrate salt, Merck, KGaA, Darmstadt, Germany) was used as a stock solution. Cu (II) working solutions were made by suitable dilutions of the stock solution. A 1.0 molL^{-1} solution of hydrogen peroxide (Merck) was prepared by an appropriate dilution of 30% reagent in a volumetric flask of 50 mL with deionized water. A 0.1 molL^{-1} tartaric acid stock

solution was subsequently prepared by dissolving 1.50 g of $C_4H_6O_6$ (Merck) in water and diluting to 100 mL in a volumetric flask.

Recommended procedure

In a special four compartment vessel (Budarin's vessel), the solution of Cu (II) was placed in one compartment of a vessel, solution of H_2O_2 in the second, fruit juice in the third, and buffer solution (tartaric acid, pH = 3.5) and deionized water with the total volume 10 mL) in the fourth compartment. The vessel was thermostatted for 5 min at 25.0±0.1°C. Afterward the contents of all four separate compartments were mixed and then stirred during 60 s. The content was transferred to the spectrophotometric cell with a part length of 1 cm immediately after the stirring, and absorbance was recorded. The change in absorbance was recorded at 520 nm as a function of time every 2.5 min for the first 25 min of the reaction. The reaction rates at different concentrations of each of the reactants were obtained by measuring the slope of the linear kinetic curves to the absorbance plot (from Beer's law $A= \varepsilon \cdot l \cdot c$, $dA/dt = \varepsilon \cdot l \cdot (dc/dt)$, $dc/dt = (dA/dt)/\varepsilon \cdot l$, slope = dA/dt, rate =dc/dt).

Investigation on the effect of H_2O_2 concentration

Aliquots (0.10-0.75 mL) of H_2O_2 standard solution were pipetted into the one compartment of the four compartment vessel; 0.50 mL of the Cu (II) solution was placed in the second compartment; 0.5 mL of the red currant (0.2 mL of the sour cherry) fruit juice in the third and buffer solution (tartaric acid, pH = 3.5) and deionized water with the total volume 10 mL in the fourth compartment.

Investigation on the effect of Cu (II) concentration

Aliquots (0.12-0.50 mL) of Cu(II) standard solution were pipetted into the one compartment of the vessel; 0.5 mL (or 0.3 mL) of the H_2O_2 solution in the second; 0.5 mL of the red currant (0.2 mL of the sour cherry) fruit juice in the third and buffer solution (tartaric acid, pH = 3.5) and deionized water with the total volume 10 mL in the fourth compartment.

Investigation on the effect of anthocyanins concentration

Aliquots (0.25-0.75 mL) of the red currant juice and (0.1-0.30 mL) of the sour cherry juice were pipetted into one compartment of the four-compartment vessel; 0.50 mL for the red currant juice (0.30 mL for the sour cherry juice) of the H_2O_2 solution in the second; 0.5 mL of the standard of Cu(II) in the third, and tartaric acid (pH=3.5) and deionized water with the total volume 10 mL in the four compartment.

Analysis of kinetics and thermodynamics

Order of reaction*:* The degradation process for anthocyanins can be described by the general rate equation:

$$-\frac{dc}{dt} = kc^n \quad (1)$$

Where *-dc/dt* represents the rate of anthocyanins degradation, *k* the rate constant, *c* the anthocyanin concentration at each time, and *n* the reaction order.

For n = 1 and after integrating:

$$-\frac{dc}{dt} = kc;\ -\frac{dc}{c} = k \cdot dt$$

$$\ln(c_o/c_t) = kt \quad (2)$$

Eq. (2) is obtained where c_0 is the initial anthocyanins concentration (t = 0) and c_t the concentration of anthocyanins at each time.

Thermodynamic analysis: The temperature and degradation constant are related according to the Arrhenius equation:

$$k = A \cdot e^{-E_a/RT} \quad (3)$$

where *k* represents the rate constant for the degradation process, *A* the Arrhenius constant, E_a the apparent energy of activation, *R* the universal gas constant, and *T* the absolute temperature. Taking natural logarithms

$$\ln k = \ln A - \frac{E_a}{RT} \quad (4)$$

Eq. (4) is obtained. When the natural logarithm of the degradation constant compared with the inverse of the absolute temperature is plotted according to the Eq. (4), the E_a value from the slope and the *lnA* value from the ordinate intercept are obtained. Thus, the thermodynamic parameters, change in enthalpy (ΔH^*), entropy (ΔS^*), and free energy of activation (ΔG^*), are obtained using the following equations:

$$\Delta H^* = E_a - RT \quad (5)$$

$$\Delta S^* = 19.14[\log k - \log T - 10.3178 + \Delta H^*/19.14T] \quad (6)$$

$$\Delta G^* = \Delta H^* - T\Delta S^* \quad (7)$$

where *k*, represents degradation rate constant and *T*, absolute temperature.

Results and Discussion

Absorption spectra and kinetics of anthocyanin degradation

The juice samples were diluted with deionized water to give an absorbance reading between 0.6 and 0.8 units. These absorbance values were achieved by diluting 0.1 mL of sour cherry and 0.25 mL of red currant juice with 4.9 and 4.5 mL of deionized water, respectively. The absorption spectra were scanned from 300 to 700 nm. The absorption maximum was recorded at 520 nm (Figure 1A). All absorbance readings were made against deionized water as a blank.

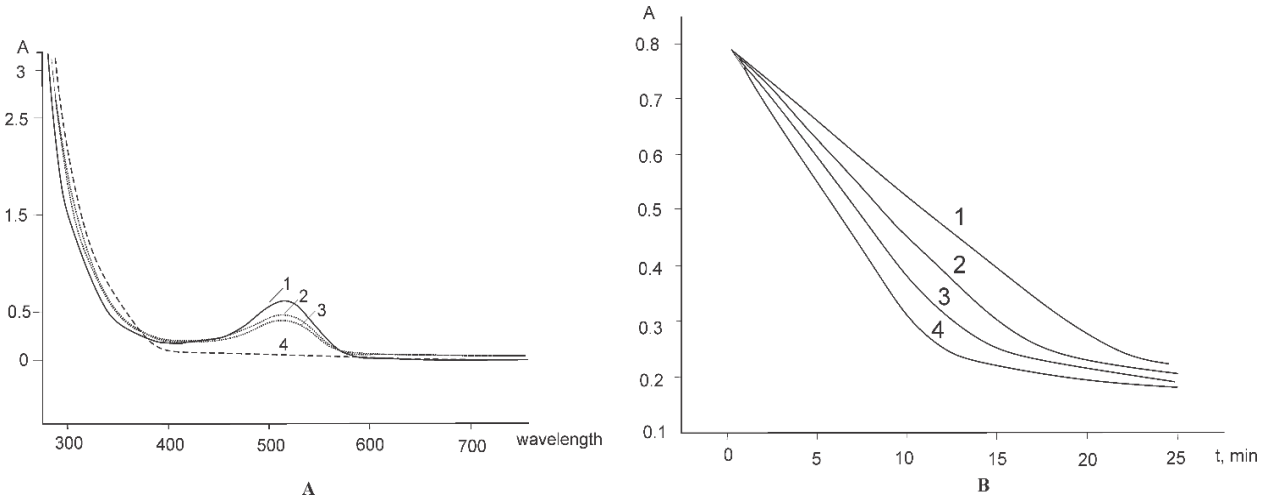

Figure 1. A) Absorption spectra of: 1) aqueous solution of sour cherry juice; 2) sour cherry juice-H_2O_2; 3) sour cherry juice- H_2O_2-Cu(II); 4) sour cherry juice- H_2O_2-Cu(II) 24 h after mixing; **B**) Relationship between the absorbance of reaction mixture and time at: 1) 25; 2) 30; 3) 35; 4) 40°C recorded at 5 min intervals, V (sour cherry juice) = 0.2 ml; c(H_2O_2) = 0.059 mol·L^{-1}, $c_{Cu(II)}$ = $1.85 \cdot 10^{-4}$ mol·L^{-1}; pH=3.5

In order to confirm that decrease of absorption at 520 nm comes from the anthocyanins' degradation, absorption spectra for different mixtures of reaction components were recorded 3 min after mixing the reagents. The spectrum of anthocyanins in aqueous solution (juice diluted with deionized water) is presented in Figure 1A, curve 1. The spectra of a mixture consisting of aqueous solution juice-H_2O_2 and mixture made of aqueous solution juice-H_2O_2-Cu (II) are presented in Figure 1A, curve 2 and 3, respectively. The reaction between anthocyanins and hydrogen peroxide occurs very slightly, but the addition of Cu (II) ions particularly accelerates this reaction as a result of the strong catalytic action of this metal ion. For mixture juice-H_2O_2-Cu (II), the absorbance band at 520 nm significantly decreased (Figure 1a, curve 4) after degradation during 24 h. Meanwhile, the baseline gradually ascended from 400 to 300 nm, similarly to the previous report (Song et al., 2011).

Figure 1B shows the relationships between the absorbance of the reaction mixture (which is directly proportional to the concentration of anthocyanins) and time at different temperatures. Anthocyanin concentration decreases with time. It is possible to follow the reaction rate spectrophotometrically as the change of the solution absorbance values with time, because of the linear dependence of absorbance on time during the first 20 min of reaction at 25^0C. The initial-rate method was used to determine partial orders (Perez-Bendito and Silva, 1988). The initial

rates of the reaction were determined by measuring the slope of the initial tangents to the absorbance-time curves, dA/dt.

The reaction rate dependence on the H_2O_2 concentration was studied in the range 0.019-0.147 $molL^{-1}$ (Figure 2). The reaction rate increased by increasing the concentration of H_2O_2. This figure shows that the degradation of anthocyanins in sour cherry and red currant juices follows the first-order reaction with respect to H_2O_2 concentrations because the curve is linear. For further work, a concentration of 0.098 and 0.059 $mol \cdot L^{-1}$ was selected for the red currant and sour cherry juices, respectively.

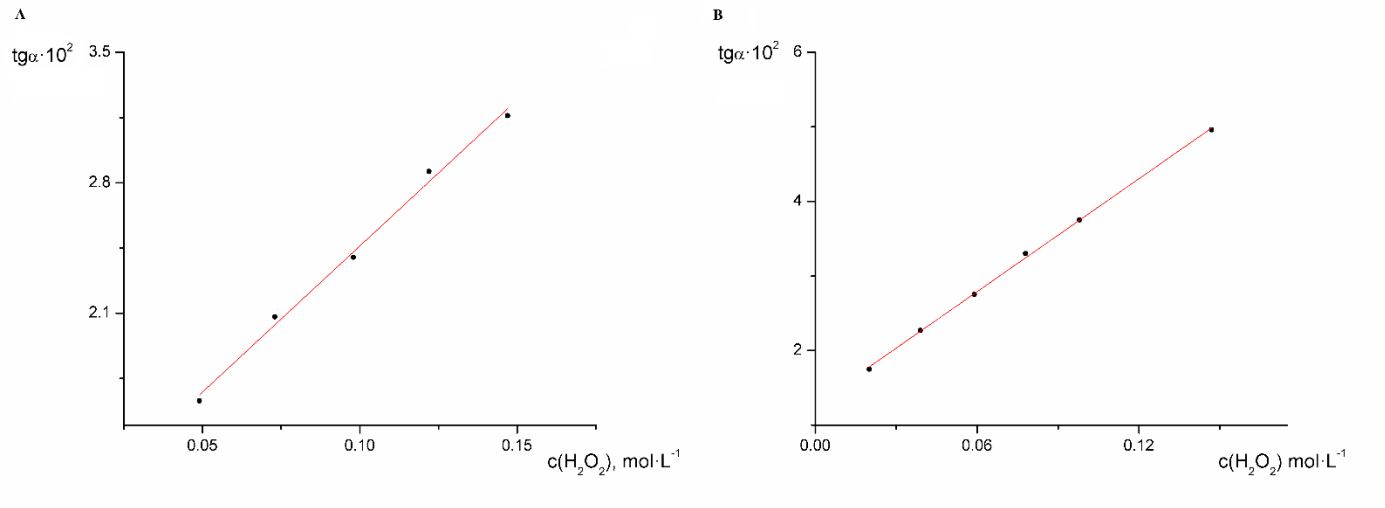

Figure 2. Dependence of the reaction rate on the H_2O_2 concentration. Concentration in measured solution: $c_{Cu(II)} = 1.23 \cdot 10^{-4}$ $mol \cdot L^{-1}$; pH=3.5; t = 25.0±0.1 ^{0}C. A) V (red currant juice) = 0.5 ml; B) V (sour cherry juice) = 0.2ml

Keeping all the other experimental parameters constant, Cu (II) dependence on the system was studied in the range $0.31 \cdot 10^{-4}$-$1.23 \cdot 10^{-4}$ $mol \cdot L^{-1}$. It was observed that Cu (II) ions had catalytic activity. The reaction is first order with respect to Cu (II) concentration (Figure 3).

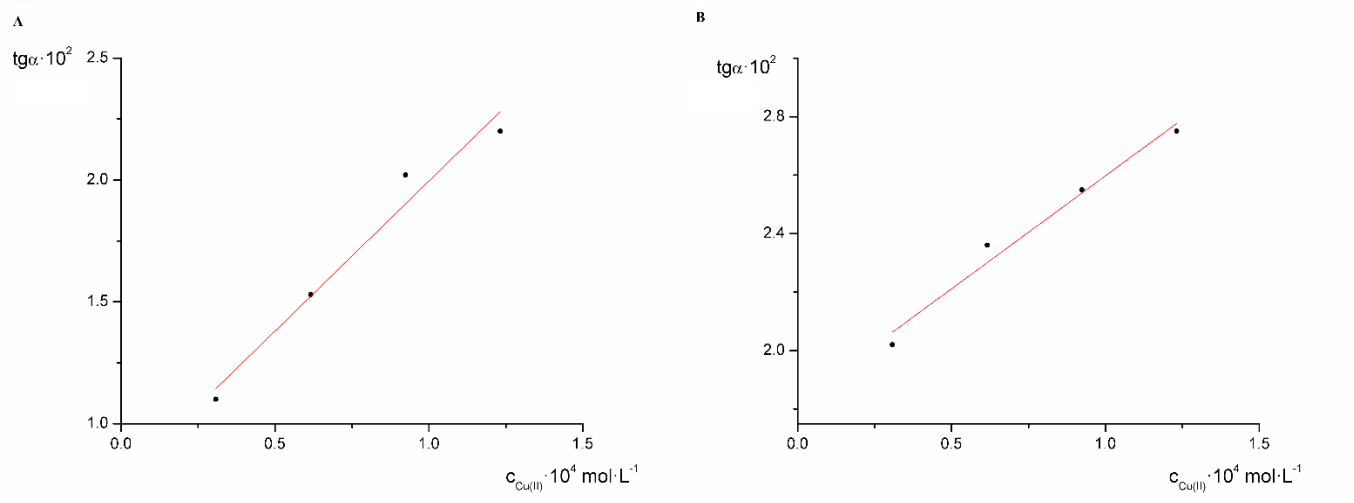

Figure 3. Dependence of the reaction rate on the Cu (II) concentration. Concentration in measured solution: pH = 3.5; t=25.0±0.1°C. A) V (red currant juice) = 0.5 ml, $c(H_2O_2)$ = 0.098 $mol \cdot L^{-1}$; B) V (sour cherry juice) = 0.2 ml, $c(H_2O_2)$ = 0.059 $mol \cdot L^{-1}$

The influence of the temperature on the reaction of the degradation of anthocyanins in sour cherry and red currant juices with H_2O_2 and Cu(II) as catalyst (at optimal conditions: pH = 3.5; $c_{Cu(II)}$ = $1.23 \cdot 10^{-4}$ $mol \cdot L^{-1}$; $c(H_2O_2)$ = 0.059 $mol \cdot L^{-1}$ and 0.098 $mol \cdot L^{-1}$, respectively) was studied.

The effect of the temperature on the reaction rate was followed in the range 298-313 K. The reaction rate was increased with increasing temperature. The degradation of anthocyanins in sour cherry and red currant juices by Cu (II)/H_2O_2 reagent followed Arrhenius equation (tartaric acid buffer, pH = 3.5; t = 25.0±0.1°C). Previous studies showed that thermal degradation of anthocyanins followed the first-order reaction (Garzon and Wrolstad, 2002; Wang and Xu, 2007; Mercali et al., 2013). The optimum reaction temperature of 298 K was selected. At the higher temperature (313 K), the reaction became too fast and not suitable for following during the 2.5-20 min after mixing. The reaction rate dependence on the anthocyanins concentration was investigated under selected and constant reaction concentrations: $c_{Cu(II)}$ = 1.23 $mol \cdot L^{-1}$, $c(H_2O_2)$ = 0.098 $mol \cdot L^{-1}$ and pH=3.5. Linear dependence confirmed that the degradation of anthocyanins in red currant and sour cherry juices followed the first-order reaction.

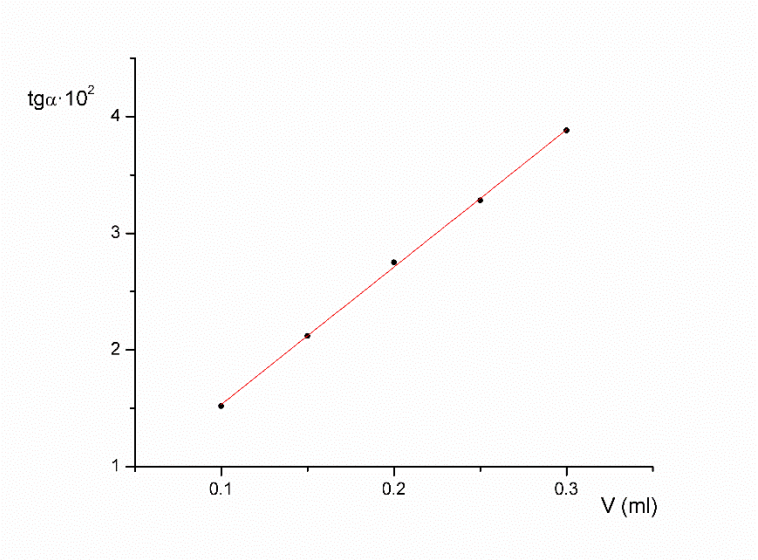

Figure 4. Reaction rate dependence on the concentration of anthocyanins. Concentration of the reactants in the solution: V (red currant juice) = 0.5 mL, c(H_2O_2) = 0.098 mol·L^{-1}, $c_{Cu(II)}$ = 1.23 mol·L^{-1}; pH = 3.5; t=25.0±0.1°C.

Based on the present kinetic investigation, the kinetic equation for degradation of anthocyanins in sour cherry and red currant juices by H_2O_2 in the presence of Cu (II) as catalyst was formulated:

$$-\frac{dc}{dt} = k \cdot c_{H_2O_2} \cdot c_{Cu(II)} \cdot c_{Anthocyanins} \quad (8)$$

where *k* is rate constant.

Mechanism of reaction

In an aqueous solution, H_2O_2 can quickly decompose to form very active products: the perhydroxyl anion (HOO^-), hydroxyl ($^{\bullet}OH$) and perhydroxyl ($^{\bullet}OOH$) radicals (De et al., 1999). These reactive oxygen species might affect anthocyanin degradation (Matta et al., 2008). The catalytic activity of Cu (II) in the decomposition of H_2O_2 has been extensively investigated due to their implication in many chemical and biological processes. The mixture Cu (II)/H_2O_2 is a Fenton-like reagent, analogues to the iron/Fenton reagent, Fe (II)/H_2O_2. The mixture Cu (II)/H_2O_2 is a strong oxidant, and it may react with various organic substances. In acidic medium, at pH 1.0 and pH 3.8 the spectra show a characteristic absorption of the cation form (AH^+) of the

flavylium structure, with a strong peak absorption at λ_{max}=520 nm. Anthocyanins are decomposed in acidic medium by H_2O_2, as shown by the following reaction scheme (Song et al., 2011; Lopes et al., 2007; Alecu et al., 2008):

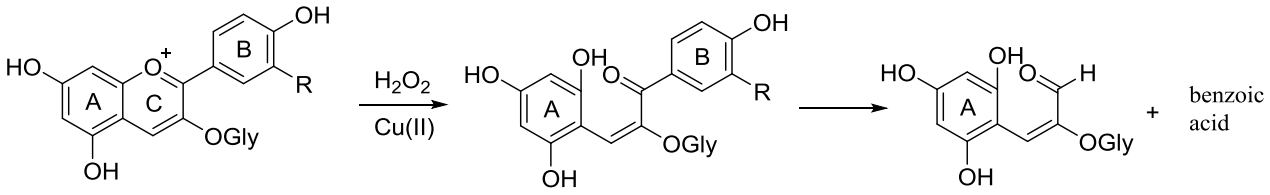

Figure 5. Hypothetical scheme for the degradation reaction of Cy-3-glycosides.

The opening of the C-ring for Cy-3-glycosides (AH^+) formed a neutral chalcone (C). This compound is further oxidized to compound D, which is in fast equilibrium with its tautomeric quinone forms (Nikkhah et al., 2010).

However, this reaction proceeds slowly without catalytic amounts of Cu(II). In the presence of the catalyst Cu(II) the process occurs at several stages:

$$Cu(II) + H_2O_2 \underset{k_2}{\overset{k_1}{\rightleftarrows}} [Cu(II)H_2O_2]$$

This is reversible formation of an intermediate product (Stewart, 1964). The second stage is the formation of an activated complex (Salem et al., 2000):

$$[Cu(II)H_2O_2] + Athocyanin \underset{k_4}{\overset{k_3}{\rightleftarrows}} [AnthocyaninCu(II)H_2O_2]$$

Finally, the activated complex decomposes into the products and the catalyst:

$$[AnthocyaninCu(II)H_2O_2] \overset{k_5}{\rightarrow} \Sigma\, Products + Cu(I)$$

The kinetics indicated that a Cu (II)-anthocyanine peroxo complex is involved in the rate-determining step. The complex $[AnthocyaninCu(II)H_2O_2]$ undergoes intramolecular electrontransfer, generating Cu(I) species that can react with hydrogen peroxide:

$$Cu(I) + H_2O_2 \rightarrow Cu(II) + HO^{\bullet} + HO^-$$

The rate of catalyzed reaction is (at constant pH):

$$v = k_5[AnthocyaninCu(II)H_2O_2] \quad (9)$$

In the stationary state the concentration of the activated complex can be determined from the relation:

$$[\text{AnthocyaninCu(II)}H_2O_2] = \frac{k_1 k_3 [\text{Cu(II)}][\text{Anthocyanin}]}{(k_4+k_5)(k_2/k_1+[H_2O_2])}$$

Substituting this into Eq. (9), an expression for the observed reaction rate is obtained:

$$v = \frac{dx}{dt} = K_I \frac{[H_2O_2][\text{Anthocyanin}]}{K_{II}+[H_2O_2]} c_{Cu} \quad (10)$$

when $[H_2O_2] << K_{II,}$

$$v = \frac{dx}{dt} = \frac{K_I}{K_{II}} C_{Cu}[H_2O_2][\text{Anthocyanin}] \quad (11)$$

where: C_{Cu}- total concentration of copper, K_I, K_{II}- new constants.

The equation (11) is in good agreement which those obtained by the experimental data (equation 8).

Thermodynamic analysis

Based on equation (8), the rate constants, as the average value of three measurements at indicated temperature, were calculated (Table 1).

Table 1. Rate constants at four temperatures

T, K	$k \cdot 10^2$, $mol^2\,dm^{-6}\,min^{-1}$	
	Red currant juice	Sour cherry juice
298	2.18	2.72
303	2.64	3.44
308	3.10	4.18
313	3.59	4.91

The temperature-dependence degradation rate constant is represented by the Arrhenius equation. Graphic dependence of the rate constant as a function of reciprocal value of absolute temperature gives a linear relationship at the studied temperature range ($r^2 > 0.9$), which allowed the calculation of the activation energy values, which was 30.59 $kJ \cdot mol^{-1}$ for sour cherry and 25.76 $kJ \cdot mol^{-1}$ for red currant juices (Table 2).

Table 2. Thermodynamic parameters for degradation of anthocyanins in red currant and sour cherry juices

Juice	E_a (kJ·mol^{-1})	ΔH^* (kJ·mol^{-1})	ΔS^* (J·K^{-1}·mol^{-1})	ΔG^* (kJ·mol^{-1})
Red currant	25.76	23.29	121.92	59.61
Sour cherry	30.59	28.12	115.48	62.53

Kirca et al. (2007) found an increase in the activation energy with increasing concentration, while research carried out by Toralles et al. (2008) indicates lack of relation dependency between the activation energy and concentration in the substance degradation. Also, different anthocyanins had different degradation kinetics in juices (Hellstrom et al., 2013). The sour cherry and red currant juices contained only cyanidin-glycosides. In any case, the effect of the sugar moiety was irrelevant compared to the effect induced by the type of core anthocyanidin in these anthocyanins. However, juice matrix had a major impact on the stability of anthocyanins. Hellstrom et al. (2013) suggested that the cyanidin 3-galactoside and cyanidin 3-arabinoside degraded 3-4 times faster in crowberry juice than in chokeberry juice. Generally, co-pigmentation of anthocyanins with other compounds is very important in the color stabilization in plants (Castaneda-Ovando et al., 2009).

Examination of thermodynamic parameters may also provide valuable information regarding degradation kinetics of anthocyanins by Cu/H_2O_2 reagent. Thermodynamic parameters (ΔG^*, ΔH^* and ΔS^*) are presented in Table 2. ΔG^* represents the difference between the activated state and reactants (Al-Zubaidi and Khalil, 2007) The positive values of ΔG^* indicate that the formation of the activated complex is a nonspontaneous reaction. ΔH^* is related to the strength of the bonds, which are broken and made in the formation of the transition state (Vikram et al., 2005). ΔH^* values evaluated in this study are 23.29 and 28.12 kJ·mol^{-1} for the red currant and sour cherry juices, respectively. The positive sign of ΔH^* represents an endothermic state between the activated complex and reactants. ΔS^* is a measure of the disorder change of molecules in the system. The negative entropy values found in this study suggest that the transition state has lower structural freedom than the reactants (Mercali et al., 2013).

Conclusion

The present study analyzed the degradation kinetics of anthocyanins in sour cherry and red currant juice by Cu (II)/H_2O_2 reagent at a temperature ranging from 25 to 40^oC. The temperature, concentration of H_2O_2, Cu (II), and anthocyanins have a significant influence on the degradation of cyanidin-3-glycosides in red currant juice. Variation of degradation rate constants with temperature obeyed the Arrhenius relationship. Compared to sour cherry juice anthocyanins, red currant juice anthocyanins were much more susceptible to Cu (II)/H_2O_2 reagent, based on the higher values of the degradation rate constants.

Conflict-of-Interest Statement

Declarations of interest: none

References

Alecu, A., Sauicier, C., & Cretescu, I. (2008). The study of catalytic degradation of malvidin-3-glucoside from red wines, using molecular absorption spectrophotometry. Revista de Chimie, 59, 314-317.

Borges, G., Degeneve, A., Mullen, W., & Crozier, A. (2010). Identification of flavonoid and phenolic antioxidants in black currants, blueberries, raspberries, red currants, and cranberries. Journal of Agricultural and Food Chemistry, 58, 3901-3909.

Castaneda-Ovando, A., Pacheco-Hernandez, M. L., Paez-Hernandez, M. E., Rodriguez, J. A., & Galan-Vidal, C. A. (2009). Chemical studies of anthocyanins: a review. Food Chemistry, 113, 859-871.

Damar, I., & Eksi, A. (2012). Antioxidant capacity and anthocyanin profile of sour cherry (*Prunus cerasus* L.) juice. Food Chemistry, 135, 2910-2914.

De, A. K., Chaudhuri, B., & Bhattacharjee, S. (1999). A kinetic study of the oxidation of phenol, o-chlorophenol, and catechol by hydrogen peroxide between 298 K and 333 K; the effect of pH, temperature, and ratio of oxidant to substrate. Journal of Chemical Technology and Biotechnology, 74, 162-168.

Garzon, G. A., & Wrolstad, R. E. (2002). Comparison of the stability of pelargonidin-based anrhocyanins in strawberry juice and concentrate. Journal of Food Science, 64, 1288-1299.

Harbourne, N., Jacquier, J. Ch., Morgan, D. J., & Lyng, J. G. (2008). Determination of the degradation kinetics of anthocyanins in the model juice system using isothermal and non-isothermal methods. Food Chemistry, 111, 2004-2008.

Hellstrom, J., Mattila, P., & Karjalainen, R. (2013). Stability of anthocyanins in berry juices strored at different temperatures. Journal of Food Composition and Analysis, 31, 12-19.

Hillmann, M. C. R., Burin, V. M., & Bordignon-Luiz, M. T. (2011). Thermal degradation kinetics of anthocyanins in grape juice and concentrate. International Journal of Food Science and Technology, 46, 1997-2000.

Kechinski, C. P., Guimaraes, P. V. R., Norena, C. P. Z., Tessaro, I. C., & Marczak, L. D. F. (2010). Degradation kinetics of anthocyanin in blueberry juice during thermal treatment. Journal of Food Science, 75, C173-C176.

Kirca, A., & Cemeroglu B. (2003). Degradation kinetics of anthocyanins in blood orange juice and concentrate. Food Chemistry, 81, 583-587.

Kirca, A., Özkan, M., & Cemoreoglu, B. (2007). Effects of temperature, solid content and pH on the stability of black carrot anthocyanins. Food Chemistry, 101, 212-218.

Kong, J.-S., Chia, L.-S., Goh, N.-K., Chia, T. F., & Brouillard, R. (2003). Analysis biological activities of anthocyanins. Phytochemistry, 64, 923-933.

Liu, J., Dong, N., Wang, Q., Li, J., Guiming, Q., Fan, H., & Zhao, G. (2014). Thermal degradation kinetics of anthocyanins from Chinese red radish (*Raphanus sativus* L.) in various juice beverages. European Food Research and Technology, 238, 177-184.

Lopes, P., Richard, T., Saucier, C., Teissedre P. L., Monti, J. P., & Glories, Y. (2007). Anthocyanine A: a quinone methide derivative resulting from malvidin 3-*O*-glucoside degradation. Journal of Agricultural and Food Chemistry, 55, 2698-2704.

Matta, R., Hanna, K., & Chiron, S. (2008). Oxidation of phenol by green rust and hydrogen peroxide at natural pH. Separation and Purification Technology, 61, 442-446.

Mercali, G. D., Jaeschke, D. P., Tessaro, I. C., Marczak, L. D. F. (2013). Degradation kinetics of anthocyanins in acerola pulp: Comparison between ohmic and conventional heat treatment. Food Chemistry, 136, 853-857.

Määttä, K., R., Kamala-Eldin, A., & Törrönen, R. (2003). High-performance liquid chromatography (HPLC) analysis of phenolic compounds in berries with diode array and electrospray ionization mass spectrometric (MS) detection: *Ribes* species. Journal of Agricultural and Food Chemistry, 51, 6736-6744.

Nichenametla, S. N., Taruscio, T. G., Barney, D. L., & Exon, J. H. (2006). A review of the effects and mechanisms of polyphenolics in cancer. Critical Reviews in Food Science and Nutrition, 46, 161-183.

Nikkhah, E., Khaiamy, M., Heidary, R., & Azar, A. S. (2010). The effect of ascorbic acid and H_2O_2 treatment on the stability of anthocyanin pigments in berries. Turkish Journal of Biology, 34, 47-53.

Ruenroengklin, N., Yang, B., Lin, H., Chen, F., & Jiang, Y. (2009). Degradation of anthocyanin from litchi fruit pericarp by H_2O_2 and hydroxyl radical. Food Chemistry, 116, 995-998.

Salem, I. A., El-Maazawi, M., & Zaki, A. B. (2000). Kinetics and mechanisms of decomposition reaction of hydrogen peroxide in presence of metal complexes. International Journal of Chemical Kinetics, 643-665.

Song, J., Li, X., Zeng, L., Liu, H., Xie, M. (2011). Determination of cyanidin-3-glucoside (red kernel food color) in beverages by high performance liquid chromatography and a study of its degradation by quadruple time-of-flight mass spectrometry. Food Additives and Contaminants, 28, 1645-1656.

Stewart, R. (1964). Oxidation Mechanisms. New York, Benjamin.

Strinzing, F. C., Carle, R. (2004). Functional properties of anthocyanins and betalains in plants, food and human nutrition. Trends in Food Science & Technology, 51, 19-38.

Summen, M. A., Erge, H. S. (2014). Thermal degradation kinetics of bioactive compounds and visual color in raspberry pulp. Journal of Food Processing and Preservation, 38, 551-557.

Toralles, R. P., Vendruscolo, J. L., Vendruscolo, C. T., del Pino, F. A. B., & Antunes, P. L. (2008). Determination of reaction rate constants for ascorbic acid degradation in peach puree: effect on temperature and concentration. Ciência e Tecnologia de Alimentos, 28, 18-23.

Wang, W. D., & Xu, S. Y. (2007). Degradation kinetics of anthocyanins in blackberry juice and concentrate. Journal of Food Engineering, 82, 271-275.

Özkan, M., Yemenicioglu, N., & Cemeroglu, B. (2002). Degradation kinetics of anthocyanins from sour cherry, pomegranate, and strawberry juices by hydrogen peroxide. Journal of Food Science, 67, 525-529.

Kinetički i termodinamički parametri degradacije antocijana iz sokova crvene ribizle i višnje vodonik peroksidom u prisustvu Cu(II)

Jovana Lj. Pavlović, Milan N. Mitić, Sonja M. Janković

Univerzitet u Nišu, Prirodno-matematički fakultet, Departman za hemiju, Višegradska 33, 18000 Niš, Srbija

SAŽETAK

Kinetika degradacije antocijana u sokovima od crvene ribizle i višnje vodonik peroksidom na pH 3.5 je istraživana. Reakcija je bila katalizovana tragovima Cu(II), i to je praćeno spektrofotometrijski na 520 nm primenom metode inicijalne brzine. Kinetički parametri reakcije su prikazani, i jednačina brzine je predložena. Iz zavisnosti konstanti brzine od temperature, aktivaciona energija je izračunata: 25.76 and 30.59 kJ mol^{-1} za sokove crvene ribizle i višnje, respektivno. Termodinamičke funkcije aktivacije (ΔG^*, ΔH^* i ΔS^*) su određene kako bi se razumela degradacija antocijana u sokovima crvene ribizle i višnje.

Ključne reči: crvena ribizla, višnja, antocijani, kinetički parametri, termodinamičke funkcije

Paramètres cinétiques et thermodynamiques de la dégradation des anthocyanines des jus de la groseille rouge et de la griotte par le peroxyde d'hydrogène en présence de Cu (II)

Jovana Lj. Pavlović, Milan N. Mitić, Sonja M. Janković

Université de Niš, Faculté des sciences naturelles et des mathématiques, Département de chimie, Visegradska 33, 18000 Niš, Serbie

RÉSUMÉ

Le présent travail se propose d'étudier la cinétique de la dégradation de l'anthocyanine dans les jus de la groseille rouge et de la griotte au moyen du peroxyde d'hydrogène à pH 3,5. La réaction a été catalysée par les traces de Cu (II) et observée par la spectrophotométrie à 520 nm en appliquant la méthode de la vitesse initiale. Ainsi, sont démontrés les paramètres cinétiques de la réaction et l'équation de la vitesse est suggérée. L'énergie d'activation a été calculée de la dépendance des constantes de vitesse de la température : 25,76 et 30,59 kJ mol^{-1}, respectivement, pour les jus de la groseille rouge et de la griotte. Les fonctions thermodynamiques d'activation (ΔG^*, ΔH^* et ΔS^*) ont été déterminées afin de comprendre la dégradation des anthocyanines dans les jus de la groseille rouge et de la griotte.

Mots-clés: groseille rouge, griotte, anthocyanines, paramètres cinétiques, fonctions thermodynamiques.

Кинетические и термодинамические параметры деградации антоцианов в соках красной смородины и кислой вишни перекисью водорода в присутствии Cu (II)

Йована Л. Павлович, Милан Н. Митич, Соня М. Янкович

Университет в Нише, Факультет естественных наук и математики, Департамент химии, Вышеградская, 33, 18000 Ниш, Сербия

АННОТАЦИЯ

В статье исследуется кинетика деградации антоцианов в соках красной смородины и вишни пероксидом водорода при pH 3,5. Реакция была катализирована следом Cu (II), и отслеживалась спектрофотометрически при 520 нм, применяя метод начальной скорости. Представлены кинетические параметры реакции и предложено уравнение скорости. Из зависимости констант скорости от температуры была рассчитана энергия активации: 25,76 и 30,59 кДж / моль для соков красной смородины и вишни соответственно. Термодинамические функции активации (ΔG *, ΔH * и ΔS *) были определены для понимания разложения антоцианинов сока красной смородины и вишни.

Ключевые слова: красная смородина, вишня, антоцианы, кинетические параметры, термодинамические функции

Kinetische und thermodynamische Parameter für den Abbau von Anthocyanen aus den Säften roter Johannisbeeren und Sauerkirschen durch Wasserstoffperoxid in Gegenwart von Cu(II)

Jovana Lj. Pavlović, Milan N. Mitić, Sonja M. Janković

Universität in Niš, Mathematisch-Naturwissenschaftliche Fakultät, Lehrstuhl für Chemie, Višegradska 33, 18000 Niš, Serbien

ABSTRAKT

Untersucht wurde die Kinetik des Anthocyaninabbaus in den Säften der roten Johannisbeeren und Sauerkirschen durch Wasserstoffperoxid bei pH 3,5. Die Reaktion wurde durch die Spuren von Cu(II) katalysiert und das wurde spektrophotometrisch bei 520 nm durch die Anwendung der Initial-Rate-Methode verfolgt. Die kinetischen Reaktionsparameter werden angegeben und die Geschwindigkeitsgleichung wird vorgeschlagen. In Abhängigkeit von der Geschwindigkeitskonstante der Temperatur wurde die Aktivierungsenergie berechnet: 25,76 und 30,59 kJ mol^{-1} für die roten Johannisbeeren- bzw. Sauerkirschsäfte. Die thermodynamischen Aktivierungsfunktionen (ΔG^*, ΔH^* und ΔS^*) wurden bestimmt, um den Anthocyaninabbau aus roten Johannisbeeren und Sauerkirschensaft zu verstehen.

Schlüsselwörter: rote Johannisbeere, Sauerkirsche, Anthocyane, kinetische Parameter, thermodynamische Funktionen

Chemia Naissensis, Vol 2, Issue 1, RESEARCH ARTICLE, 96-109

Metal content in common daisy (*Bellis perennis* L.) and correspond soils from Niš city area (Serbia)

Milan Stojković*, Marija Jevtić, Jovana Pavlović

University of Niš, Faculty of Sciences and Mathematics, Department of Chemistry, Višegradska 33, 18000 Niš, Serbia

ABSTRACT

Bellis perennis L. is a common species of daisy, of the Asteraceae family. It is usually found in grasslands, meadows, gardens, urban areas and areas near the roadsides. Emission of heavy metals from traffic activities is an important pollution source to roadside ecosystems. This study focused on ICP OES quantification of some metals of common daisy samples and their growing soils. Plant material (*B. perennis* L.) and belonging soils from 16 different locations of Niš city area (South-East Serbia) were used for the ICP OES determination of metal content. The concentrations of Al, Ba, Cd, Co, Cr, Cu, Fe, Mn, Ni, Pb, V, and Zn were calculated on a dry weight basis. The pseudo-total metal content of equivalent growing soils was also determined. The study showed that heavy metal content of plant material and growing soils was below the maximally allowed concentrations or below the limit of detection, so we can say that contamination was detected neither in *B. perrenis* plant material nor in the growing soils.

Keywords: daisy, metals, ICP OES, contamination, soil

*Corresponding author: Milan Stojković,
e-mail address: milan@chemistry.rs
address: Višegradska 33, PO Box 224 Niš, 18000 Serbia

Introduction

Bellis perennis L., also known as common daisy, is a plant species from *Bellis* genus and Asteraceae family. Asteraceae is a family of herbaceous plants, rarely bushes, lianas or low trees. They are mostly ground halophytes or epiphytes, rarely wetland and aquatic plants. The family currently has more than 30000 accepted species names, in around 1900 genera and 13 subfamilies. The *Bellis* genus consists of dicotyledonous species native in Europe, Mediterranean region and North Africa. Common daisy is perennial plant species native to western, central and northern Europe. It generally blooms from early to midsummer producing spherical blooms in a range of sizes (approx. 2–3 cm) with white ray florets (often tipped red) and yellow disc florets. The daisy blossom (rarely leaf or whole plant) is used in folk medicine for tea preparation (Kojić et al., 1998).

According to their biological function, elements can be divided into essential and non-essential. The essential elements are further classified into two categories: macro and microelements. Microelements, such as copper, iron, zinc, manganese, molybdenum, nickel, and cobalt are essential for the healthy growth and development of plants. The lack or complete absence of these metals can lead to severe disorders in the plant organism, even to death. Non-essential metals include lead, cadmium, mercury, arsenic, and chromium. They do not have any known beneficial role and only show a toxic effect on the plant organism (Alagić et al., 2013; Nagajyoti et al., 2010).

Heavy metals represent one of the contaminants in the environment. Besides natural activities, almost all human activities also have a potential contribution to produce heavy metals as side effects. Heavy metals are constituents of the Earth's crust, but concentrations of some of them, in many ecosystems, have reached toxic levels, primarily as a result of anthropogenic activity. Heavy metals directly cause harm by entering the body *via* soil and dust (Abrahams, 2002). In ecological terms, any metal, or metalloid causing a problem in the environment, or one that cannot be biologically destroyed, should be regarded as heavy metal. Metal pollution shows a negative effect on biological systems and does not undergo biodegradation. Toxic heavy metals (*e.g.*, lead, cobalt, cadmium) can be distinguished from other pollutants since they cannot be biodegraded but can be accumulated in living organisms (causing various diseases and disorders even in relatively lower concentrations) (Pelhivan et al., 2009; Tangahu et al., 2011). The typical elements cadmium, lead, zinc, and copper, which can be found in the roadside soils, can be transported through the food chain, and thus be very toxic to people. A total of 53 elements have been classified as heavy metals, which is more precisely defined as a group of elements whose density is higher than 5 $g \cdot mL^{-1}$ (Kastori et al., 1997). Their abundance in the place of work or the

environment can be a serious health and environmental risk because they are toxic, remain in the soils for a long time and accumulate in live systems through the food chain (Sarma, 2011).

The determination of some metal contents in the *B. perennis* L. samples and its growing soil, as well as the correlation between the concentration of metals in plant and soil samples, were objectives of our study. Particular interest is devoted to the potential accumulation of metals in plant tissue, due to the proximity of major roads in the urban area of Niš.

Experimental

Plant and soil material

Aerial parts of *B. perennis* and corresponding soil materials were collected in May 2017 from the 16 different location in Niš city area. The sampling locations are graphically represented in Figure 1.

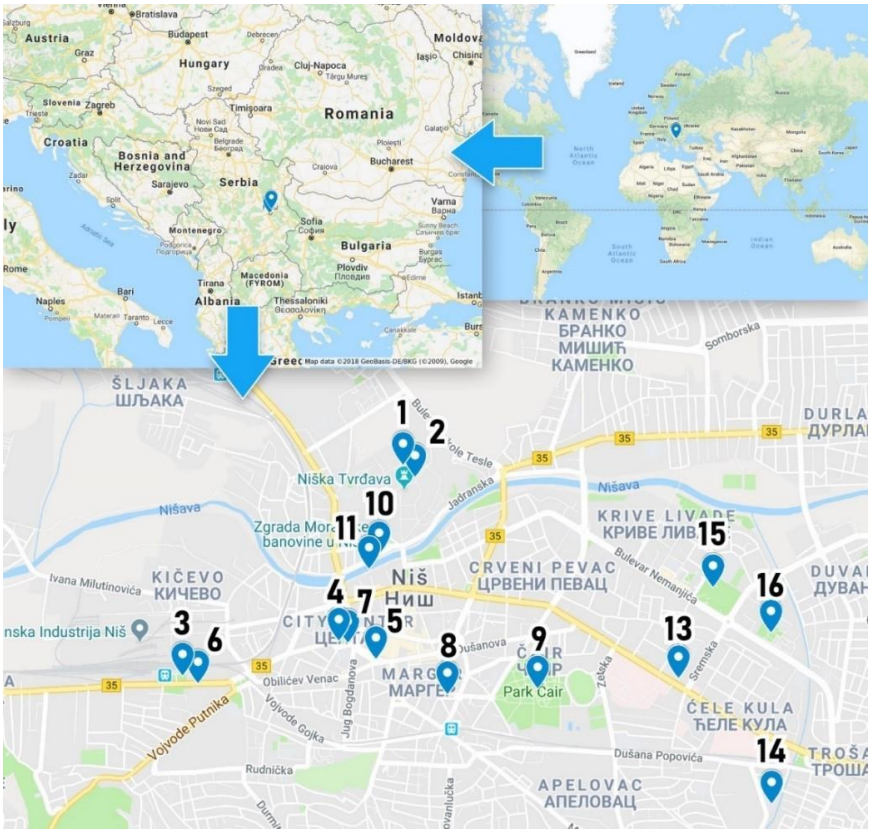

Figure 1. Graphical representation of sampling locations of common daisy from Niš city area

Reagents

Nitric acid (65%, m/m), hydrochloric acid (36%, m/m) and hydrogen peroxide (30%, m/m) were purchased from Merck (Darmstadt, Germany). Ultrascientific (USA) ICP multi-element standard solution (20.00±0.10 $\mu g \cdot mL^{-1}$) was used as a stock solution for calibration. Deionized water (0.15 $\mu S \cdot cm^{-1}$), obtained using MicroMed high purity water system (TKA Wasser auf bereitungs systeme GmbH, Germany), was used to prepare all standards and sample solutions. The plasma torch argon, with purity greater than 99.999%, was obtained from Messer (Messer Tehnogas AD, Serbia).

Instrumentation

The iCAP 6000 inductively coupled plasma optical emission spectrometer (Thermo Scientific, Cambridge, United Kingdom) with Echelle optical design and a Charge Injection Device (CID) solid state-detector was used for all mineral determinations. The analytical lines used for each element and the instrumental conditions are given in Table 2 and Table 3. Dry ashing method was carried out in the electric furnace (VIMS, Serbia) equipped with a microprocessor's program for the temperature (±1°C).

Table 1. Operating ICP OES parameters

Flush pump rate	100 rpm
Analysis pump rate	50 rpm
RF power	1150 W
Nebuliser gas flow	0.7 $L \cdot min^{-1}$
Cooling gas flow	12 $L \cdot min^{-1}$
Auxiliary gas flow	0.5 $L \cdot min^{-1}$
Plasma view	Axial

Plant samples preparation

The samples of the plant were put in the oven at 105 °C to remove the water content. The dried material was crushed with an electric mill into a fine powder. Around 5 g of the obtained powder was weighted with an analytical balance. Afterward, samples were ashed in a furnace for 20 h. The furnace was programmed to raise the temperature from starting 50 °C to 450 °C in the first 8 h, after which it was kept at constant 450 °C until the end of the process. The ash was dissolved in 4 mL of HNO_3:H_2O (1:1 v/v), filtered and diluted to 50 mL using HNO_3 (5%, v/v) (Radojevic and Bashkin, 1999).

Soil sample preparation

The soil samples were dried in thin layers in an oven at 105 °C to remove all moisture and prepared according to a method for the acid digestion of sediments, sludges, and soils (EPA method 3050B). The dried material was passed through a 1 mm sieve, eliminating stones and roots. The obtained material was measured on an analytical balance (1 g) and transferred into the round bottom boiling flask. Afterward, 10 mL of diluted HNO_3 (1:1, v/v) was added and treated in reflux at 95±5 °C for 15 min. The sample was allowed to cool, 5 mL of concentrated HNO_3 was added, and reflux was continued for 30 min. Subsequently, 10 mL of H_2O_2:H_2O (4 mL H_2O_2 and 6 mL H_2O) was added, and reflux proceeded for another 15 min. Another 10 mL of concentrated HCl was added, and reflux was continued for 15 min. After that, the solution was cooled, filtered through Whatman No. 41 filter paper and diluted to 100 mL with deionized water. Three replicates of each dried sample were analyzed.

Validation

Method for each element was created by selecting four wavelengths with the highest relative emission intensity. The calibration curve was constructed using three standard solutions. Two of them, a concentration of 2 $mg \cdot L^{-1}$ and 5 $mg \cdot L^{-1}$, were prepared diluting the reference multi-standard while the third standard was deionized water. The working wavelength was selected based on the relative emission intensity, the standard deviation of the calibration parameters, the correlation coefficient, and the interference at wavelengths left and right of the selected wavelength.

The validation of the measurements based on ICP OES technique was checked using the linearity of the calibration curve, the limit of detection (LOD) and the limit of quantification (LOQ) (Table 2), and spike recovery test. The correlation coefficients of calibration curves assessed the linearity.

Quantification wavelengths for each element, the calibration parameters (k-slope and n-intercept), LOD, LOQ, and the coefficients of determination (r^2) are represented in Table 3.

Table 2. Emission wavelengths (λ), coefficients of determination of calibration graphs (r^2), limit of detection (LOD), limit of quantification (LOQ), and calibration curve parameters (n-intercept and k-slope) for each element analyzed

Element	λ (nm)	r^2	LOD ($mg \cdot L^{-1}$)	LOQ ($mg \cdot L^{-1}$)	N	k
Al	309.271	0.99914	0.00441	0.01470	5964	2548
Ba	455.403	0.99902	0.00004	0.00013	22930	390821
Cd	226.502	0.99992	0.00021	0.00071	36	5673
Co	228.616	0.99972	0.00030	0.00100	35	4816
Cr	267.716	0.99948	0.00068	0.00228	47	6765
Cu	324.754	0.99982	0.00043	0.00142	1742	17377
Fe	259.940	0.99930	0.00042	0.00142	11389	10302
Mn	257.610	0.99926	0.00011	0.00035	15615	36963
Ni	221.647	0.99926	0.00078	0.00259	-120	2443
Pb	220.353	0.99978	0.00200	0.00667	14	585
V	309.311	0.99920	0.00080	0.00266	-3554	24141
Zn	213.856	0.99880	0.00011	0.00038	5072	9134

Statistical analysis

Pearson's correlation analysis and Agglomerative Hierarchical Cluster Analysis-(AHC) were used on original variables – metal concentration in soils and plant materials. In the case of AHC analysis, Dissimilarity matrix, and Euclidean distance as a measure of diversity were used. Complete linkage was used as the grouping criterion. Results were expressed as the mean±standard deviation.

Results and Discussion

The metal content of soil samples and *B. perennis* L. plant samples from 16 different locations was determined by the ICP OES method. The concentrations of twelve elements (Al, Ba, Cd, Co, Cr, Cu, Fe, Mn, Ni, Pb, V, and Zn) determined in the plant, and soil samples are summarized in Tables 3 and 5. The results are represented as milligram of metal per kilogram of dry weight ($mg \cdot kg^{-1}$ dry weight).

Content of metals found in soil samples from sixteen different locations is represented in Table 3. Aluminum (0.61-1.36%) and iron (0.38-0.63%) were the most abundant elements. It is known that aluminum is the third most abundant element in the Earth's crust (about 8.2%), and it is naturally expected high concentration to be found in the analyzed soil samples. Nevertheless, the content of aluminum is lower than the average values for typical soils, ranged between 0.5% and 5% (Radojević and Bashkin, 1999). This phenomenon is because aluminum is constituent of aluminosilicate rocks, which are insensitive on the treatment applied.

Micronutrients (boron, copper, iron, manganese, molybdenum, and zinc) are essential elements. These elements are used in small quantities and despite low requirements, plants functions, growth, and yields could be limited if those are unavailable for plant uptake (Wiedenhoeft, 2006). Some authors also consider Ni as micronutrient (Berker and Pilbeam, 2007). The same authors claim that Co and V are useful elements that enhance the plants' growth. Besides iron, which is the most abundant element in soil, of the other micronutrients detected, manganese was the most prevalent (80-387 $mg \cdot kg^{-1}$). Zinc was the next most abundant micronutrient (1.77-369 $mg \cdot kg^{-1}$), with the highest content in the soils from the Niš fortress 1 and Niš fortress 2 sampling locations (369 $mg \cdot kg^{-1}$ and 139 $mg \cdot kg^{-1}$, respectively).

The contamination of soils is caused by the accumulation of heavy metals from various sources (Khan et al., 2008; Zhang et al., 2010), and those most commonly found at contaminated sites are lead, chromium, arsenic, cadmium, copper, mercury and nickel (Raymond et al., 2011). The content of analyzed pollutants in this study ranged from 0.54-1.53 $mg \cdot kg^{-1}$ for cadmium, 5.2-72 $mg \cdot kg^{-1}$ for copper, 10.1-20.9 $mg \cdot kg^{-1}$ for chromium, 12.6-47.8 $mg \cdot kg^{-1}$ for lead and 17.3-35.1 $mg \cdot kg^{-1}$ for nickel. The allowed levels of toxic elements, cadmium, and lead for agricultural soils approved by the EPA Clean Water Act are 39 ppm and 300 ppm, respectively. Accordingly, toxic metals concentrations in the analyzed soil samples from this study were below the maximal allowed values. The obtained results were compared to those for the metal content of the typical soil obtained by the Radojević and Bashkin (1999) and Aloway (1995). Those results are represented in Table 4, and they are following the previous studies.

Table 3. Metal contents* in the soil samples

Sample	Al	Ba	Cd	Co	Cr	Cu	Fe	Mn	Ni	Pb	V	Zn
1	0.61±0.04	80±2	0.75±0.03	0.39±0.11	10.1±0.5	72±1	0.38±0.01	138±2	21.8±1	47.8±1.4	34±1	369±58
2	0.75±0.01	86±3	0.89±0.02	4.71±0.11	12.1±0.3	33±1	0.44±0.01	171±7	22.8±0.4	37.6±0.7	38.1±0.4	139±4
3	0.83±0.01	66±1	1.16±0.03	5.76±0.05	15.4±0.3	19.9±0.3	0.52±0.01	131±2	27.3±0.2	28.2±0.1	41.3±0.3	37.6±0.6
4	0.73±0.01	65±2	0.99±0.03	5.19±0.08	12.3±0.1	14.6±0.1	0.47±0.01	125±6.	23.9±0.3	26.8±0.5	38.6±0.4	34.0±0.9
5	0.71±0.03	65±2	0.95±0.02	4.32±0.03	11.2±0.3	49±1	0.44±0.02	106±5	20.1±0.2	45.2±0.3	34.1±0.9	42.7±0.7
6	1.07±0.02	67±2	1.08±0.03	5.56±0.13	15.9±0.4	12.6±0.3	0.51±0.01	141±3	27.1±0.6	18.1±0.4	41±1	14.8±0.1
7	1.11±0.03	61±1	1.23±0.02	6.66±0.09	19.5±0.3	10.6±0.2	0.56±0.01	159±3	32.5±0.5	14.1±0.3	46±1	20.3±0.6
8	0.92±0.02	55±1	0.92±0.02	5.03±0.04	12.9±0.2	10.6±0.3	0.46±0.01	118±2	21.7±0.2	13.1±0.1	41±1	56.7±0.8
9	1.15±0.03	68±3	1.28±0.01	5.93±0.06	17.1±0.3	10.5±0.2	0.54±0.01	131±3	27.4±0.2	13.0±0.2	43±1	18.7±0.3
10	0.86±0.03	57±2	1.05±0.02	5.73±0.11	16.3±0.4	8.8±0.3	0.50±0.01	128±3	29.7±0.6	26.3±0.5	38±18	79±2
11	1.23±0.02	61±1	1.23±0.02	6.86±0.15	20.2±0.5	7.4±0.2	0.53±0.01	145±3	35.1±0.7	15.6±0.3	44.5±0.5	18.3±0.7
12	1.36±0.05	51±2	1.07±0.03	8.93±0.34	20.2±0.6	5.2±0.2	0.58±0.03	372±19	32.2±1.2	15.1±0.1	45±2	41.8±0.5
13	1.13±0.03	62±1	1.53±0.03	9.01±0.02	20.9±0.3	9.2±0.2	0.63±0.03	3879 ±13	32.6±0.4	29.9±0.4	52±1	32±1
14	0.91±0.01	50±1	0.54±0.02	4.45±0.13	12.1±0.2	5.9±0.2	0.40±0.01	80±2	21.9±0.4	6.5±0.2	38.1±0.9	<LOD**
15	0.89±0.02	50±3	0.73±0.02	5.95±0.14	16.0±0.2	5.65±0.01	0.46±0.01	126±1	29.6±0.7	12.6±0.3	36±2	1.77±0.09
16	1.30±0.01	57±3	0.84±0.01	6.50±0.04	19.5±0.2	6.26±0.07	0.50±0.02	135±2	17.3±0.1	13.0±0.1	44.8±0.3	18.0±0.2

*The metal content, mean value ± standard deviation, is given in $mg \cdot kg^{-1}$ (dry weight), except for the Al and Fe which values are given in %;

**<LOD-below the limit of detection.

Table 4. Normal content range* of different elements in soil and plants (ppm)

Element	Typical soils[1]	Normal level in the soils[2]	Normal level in the plants[2]	Uncontaminated agricultural soils[3]
Al	5000-50000	-	-	-
Cd	<0.01-8	0.01-2.0	0.1-2.4	0.27
Co	-	0.5-65	0.02-1	-
Cr	0.9-1500	5-1500	0.03-14	-
Cu	<1-390	2-250	5-20	-
Mn	<1-18300	20-10000	20-1000	-
Ni	0.1-1520	2-750	0.02-5	-
Pb	<1-890	2-300	0.2-20	0.1-5
V	0.8-1000	3-500	0.001-1.5	-
Zn	1.5-2000	1-900	1-400	-

*[1]Radojevic i Bashkin, 1999 ; [2]Adapted from Aloway, 1995; [3]Wiersma, 1986 and Holmgren et al., 1993

Comparing the results for the content of individual metals from different locations, obtained in this study, it was noted that concentrations are of the same order of magnitude, with the exception of zinc content from the Niš fortress soil samples.

Content of metals found in *Bellis perennis* L. samples from sixteen different locations is represented in Table 5.

The most abundant elements in *B. perennis* L. samples from different locations were found to be aluminum and iron. Content of aluminum and iron ranged from 102-856 $mg \cdot kg^{-1}$ and 9.1-231 $mg \cdot kg^{-1}$, respectively. Micronutrients content in the plant samples ranged from 102-231 $mg \cdot kg^{-1}$ for iron, 0.37-18.5 $mg \cdot kg^{-1}$ for manganese, and 0.6-1.92 $mg \cdot kg^{-1}$ for copper while the zinc content in all analyzed samples was below the LOD.

The lead content in the plant samples ranged from 0.57-4.96 $mg \cdot kg^{-1}$, while the cadmium content was below the detection limit. According to the Joint Food and Agriculture Organization of the United Nations (FAO) and World Health Organization (WHO) (1999), the maximum allowed concentrations of cadmium and lead in fresh vegetables are 0.2 and 1.0 μg per gram of fresh plant, respectively. The concentrations of both elements are below the allowed concentrations. Lead content calculated on raw vegetable mass is about 0.20 $mg \cdot kg^{-1}$.

Table 5. Metal contents* in the *B. perennis* L. samples

Sample	Al	Ba	Cd	Co	Cr	Cu	Fe	Mn	Ni	Pb	V	Zn
1	542±2	6.23±0.14	<LOD**	0.187±0.003	0.88±0.01	1.02±0.01	139±1	0.37±0.07	5.16±0.02	4.84±0.11	11.4±0.2	<LOD
2	655±8	7.1±0.1	<LOD	0.04±0.01	1.20±0.05	<LOD	149±3	18.5±0.1	5.25±0.04	3.06±0.06	11.1±0.1	<LOD
3	599±19	6.06±0.03	<LOD	0.040±0.003	1.07±0.03	0.79±0.01	231±7	14.5±0.1	5.46±0.11	3.33±0.03	11.6±0.1	<LOD
4	795±18	5.5±0.1	<LOD	0.067±0.003	4.08±0.14	1.14±0.02	264±9	9.6±0.3	8.40±0.07	4.16±0.09	12.6±0.1	<LOD
5	346±17	4.2±0.1	<LOD	0.06±0.01	0.42±0.02	1.23±0.07	88±1	13.3±0.6	4.72±0.12	2.12±0.11	11.5±0.2	<LOD
6	770±1	8.74±0.06	<LOD	0.12±0.01	1.99±0.09	1.92±0.01	173±2	4.83±0.10	5.83±0.04	4.96±0.05	11.80±0.04	<LOD
7	755±14	4.9±0.1	<LOD	0.19±0.01	1.38±0.04	0.60±0.02	114±4	7.38±0.64	4.61±0.07	2.10±0.05	11.0±0.1	<LOD
8	288±15	1.6±0.3	<LOD	0.03±0.01	0.49±0.05	<LOD	54±6	<LOD	3.99±0.03	0.76±0.02	9.5±0.1	<LOD
9	289±12	1.7±0.2	<LOD	<LOD	0.62±0.05	<LOD	35.7±0.4	<LOD	3.94±0.01	0.25±0.02	10.6±0.3	<LOD
10	757±18	2.1±0.1	<LOD	0.09±0.01	0.41±0.01	<LOD	119±5	<LOD	4.98±0.11	2.47±0.07	11.43±0.03	<LOD
11	856±27	4.4±0.1	<LOD	0.057±0.003	3.35±0.03	<LOD	163±8	7.46±0.10	6.09±0.06	1.20±0.03	11.0±0.3	<LOD
12	233±2	0.34±0.02	<LOD	0.15±0.04	0.21±0.01	1.40±0.03	16.5±0.1	1.65±0.43	4.03±0.02	0.58±0.04	9.8±0.3	<LOD
13	299±8	3.26±0.01	<LOD	0.157±0.003	0.47±0.02	1.04±0.05	58.2±0.9	4.53±0.12	4.20±0.19	1.17±0.07	11.3±0.1	<LOD
14	161±6	3.7±0.1	<LOD	0.18±0.01	0.42±0.03	1.13±0.04	9.1±1.9	11.4±0.6	3.94±0.02	0.57±0.04	10.9±0.1	<LOD
15	158±6	1.52±0.04	<LOD	0.15±0.01	0.11±0.01	1.01±0.01	9.3±1.8	12.9±0.1	3.68±0.03	0.68±0.02	10.5±0.1	<LOD
16	102±5	1.91±0.03	<LOD	0.12±0.01	0.12±0.01	1.00±0.02	12.8±0.7	7.24±0.28	3.76±0.05	0.91±0.06	10.5±0.1	<LOD

*The metal content, mean value ± standard deviation, is given in $mg \cdot kg^{-1}$ (dry weight); **<LOD - below the limit of detection

Correlation analysis was performed in order to determine the correlation between the concentrations of the metals in the soil and plant tissue in analyzed samples. A statistically significant positive correlation between the concentration of barium in the soil and the concentration of barium in plant samples ($r = 0.696$; $p = 0.002$) was observed.

The Agglomerative Hierarchical Cluster Analysis (AHC) of the obtained data sets (concentration of metals in soil and plant material) was performed using the XLSTAT Excel plug-in program, version 2014.4. In the ACH analysis, the Dissimilarity matrix algorithm, and the Euclidean distance as a measure of diversity were applied, and the complete linkage was used as the grouping criterion. It enables to statistically group the analyzed samples of the plant as well as soil samples according to the concentrations of the specified metals in them. The obtained dendrograms are shown in Figures 2 and 3.

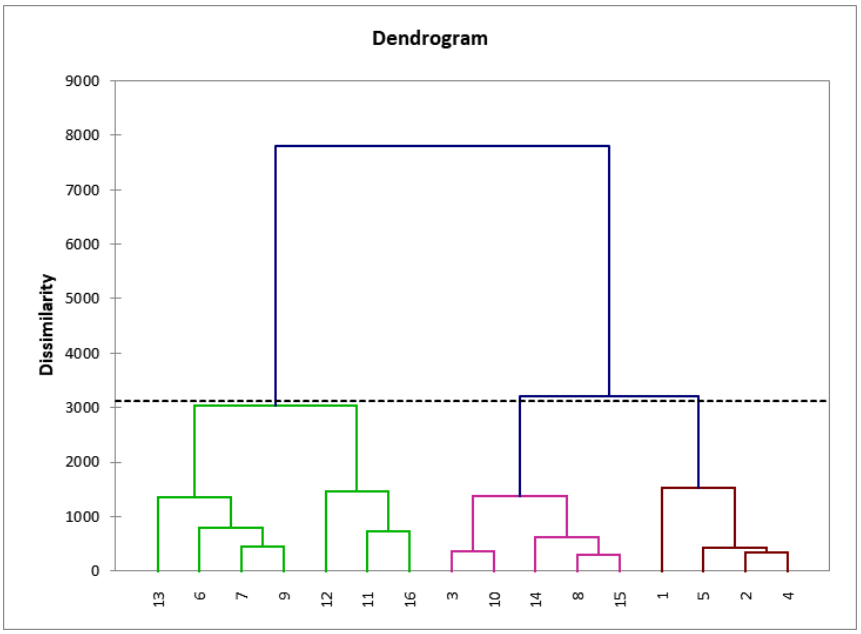

Figure 2. Cluster analysis of soil samples

The results of cluster analysis of soil samples show the existence of three different clusters. The most numerous is the C3 group (samples 6, 7, 9, 11, 12, 13, 16), where the soil samples have been distinguished by the high content of aluminum and iron.

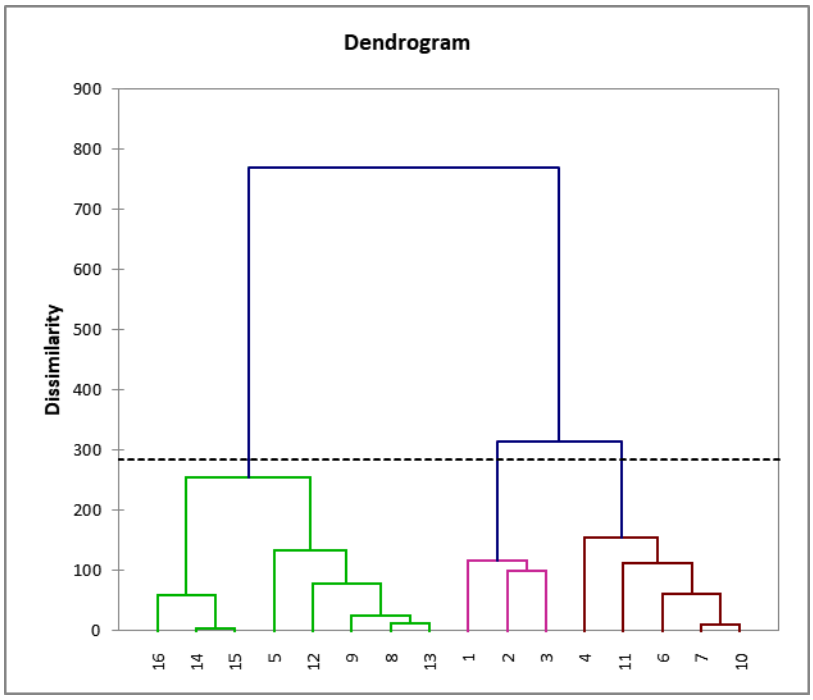

Figure 3. Cluster analysis of plant samples

Grouping the plant material samples, the three different clusters were distinguished. Cluster C3 (5, 8, 9, 12, 13, 14, 15, 16) is the most numerous and includes plant samples with 8 locations. This cluster is characterized by a low concentration of aluminum, barium, chromium, and lead.

Conclusion

The content of 12 metals (Al, Ba, Cd, Co, Cr, Cu, Fe, Mn, Ni, Pb, V, and Zn) has been determined, in soil samples as well as in the plant samples of species *Bellis perennis* L. from sixteen different locations of the urban area of Niš city. Heavy metals contamination was detected neither in soil nor plant samples analyzed. The mean concentrations of elements determined were within the range of the maximum allowed values given by authorities. No correlation between the heavy metals as the potential pollutants, either in soil or plant samples, and the proximity of the road was found.

Conflict-of-Interest Statement

Declarations of interest: none

References

Abrahams, P. W. (2002). Soils: Their implications to human health. Science of the Total Environment, 291, 1–32.

Alagić, S. Č., Šerbula, S. S., Tošić, S. B., Pavlović, A. N., Petrović, J. V. (2013). Bioaccumulation of Arsenic and Cadmium in Birch and Lime from the Bor Region. Archives of Environmental Contamination and Toxicology, 65, 671– 682.

Alloway, B. J. (1990). Heavy metals in soil. Blackie and Son Ltd, London.

COMMISSION REGULATION (EC) No 1881/2006 of 19 December 2006 setting maximum levels for certain contaminants in foodstuffs.

EPA method 3050B: Acid digestion of sediments, sludges, and soils. (2015).

FAO/WHO (1999). Joint FAO/WHO Expert Committee of Food Additives. Summary and Conclusions, In 53rd meeting, Rome, 1-10 June.

Holmgren, G. G. S., Meyer, M. W., Chaney, R. L., Daniels, R. B. (1993). Cadmium, Lead, Zinc, Copper, and Nickel in Agricultural Soils of the United States of America. Journal of Environmental Quality, 6, 335-348.

Kastori, R. (1997). Teški metali u životnoj sredini. Novi Sad.

Khan, S. Q., Zheng, Y., M., Huang, Y. Z., Zhu, Y. G. (2008). Health risks of heavy metals in contaminated soils and food crops irrigated with wastewater in Beijing, China. Environmental Pollution, 152, 686–692.

Kojić, M., Stamenković, V., Jovanović, D. (1998). Lekovite biljke jugoistočne Srbije. Zavod za udžbenike i nastavna sredstva, Beograd, Srbija.

Mirić, M., Šobajić, S. (2002). Zdravstvena ispravnost namirnica. Zavod za udžbenike i nastavna sredstava, Beograd.

Nagajyoti, P. C., Lee, K. D., Sreekanth, T. V. M. (2010). Heavy metals, occurrence and toxicity for plants: A review. Environmental Chemistry Letters, 8, 199–216.

Pehlivan, E., Özkan, A. M., Dinç, S., Parlayici, S. (2009). Adsorption of $Cu^{2+}$and Pb^{2+}ion on dolomite powder. Journal of Hazardous Materials, 167, 1044–1049.

Radojevic, M., Bashkin, V. (1999). Practical Environmental Analysis. The Royal Society of Chemistry, Cambrige, UK.

Raymond, A. W., Okieimen, F. E. (2011). Heavy Metals in Contaminated Soils: A Review of Sources, Chemistry, Risks and Best Available Strategies for Remediation. International Scholarly Research Network. 1-20.

Sarma, H. (2011). Metal Hyperaccumulation in Plants: A Review Focusing on Phytoremediation Technology. Journal of Environmental Science and Technology, 4, 118-138.

Wiersma, D., Goor, B. V., Veen, N. V. D. (1986). Cadmium, Lead, Mercury, and Arsenic Concentrations in Crops and Corresponding Soils in The Netherlands. Journal of Agricultural and Food Chemistry, 6, 1067-1074.

Zhang, M. K., Liu, Z. Y., Wang, H. (2010). Use of single extraction methods to predict bioavailability of heavy metals in polluted soils to rice. Communications in Soil Science and Plant Analysis, 41, 820–831.

Sadržaj metala u beloj radi (*Bellis perennis* L.) i odgovarajućim zemljištima iz grada Niša (Srbija)

Milan Stojković, Marija Jevtić, Jovana Pavlović

Univerzitet u Nišu, Prirodno-matematički fakultet, Departman za hemiju, Višegradska 33, 18000 Niš, Srbija

SAŽETAK

Bellis perennis L. je uobičajena vrsta bele rade iz porodice Asteraceae. Obično se nalazi na travnjacima, livadama, baštama, urbanim površinama i površinama pored puteva. Emisija teških metala u saobraćaju je glavni izvor zagađenja ekosistema pored puteva. Ovo istraživanje je bilo usmereno na ICP OES kvantifikaciju nekih metala u uzorcima bele rade i njihovim staništima. Biljni material (*B. perennis* L.) i odgovarajuća zemljišta sa 16 različitih lokacija u gradu Nišu (Jugoistočna Srbija) su korišćeni za ICP OES određivanja sadržaja metala. Koncentracije Al, Ba, Cd, Co, Cr, Cu, Fe, Mn, Ni, Pb, V, i Zn su izračunate u odnodu na suv uzorak. Takođe je određen i pseudo-ukupni sadržaj metala odgovarajućih staništa. Istraživanje je pokazalo da su sadržaji teških metala u biljnom materijalu i staništima bili ispod maksimalno dozvoljenih koncentracija ili ispod limita detekcije, tako da možemo reći da kontaminacija nije detektovana ni u biljci *B. perrenis*, ni u zemljištu.

Ključne reči: bela rada, metali, ICP OES (engl.), kontaminacija, zemljište

Teneur en métaux de la pâquerette (*Bellis perennis* L.) et des sols correspondants de la ville de Niš (Serbie)

Milan Stojković, Marija Jevtić, Jovana Pavlović

Université de Niš, Faculté des sciences naturelles et des mathématiques, Département de chimie, Višegradska 33, 18000 Niš, Serbie

RÉSUMÉ

Bellis perennis L. est une espèce commune de pâquerette, de la famille des Asteraceae. On la trouve généralement dans les pelouses, les prés, les jardins, les zones urbaines et les surfaces à côté des routes. L'émission de métaux lourds due à la circulation constitue une source principale de pollution des écosystèmes en bordure des routes. Cette étude se focalisait sur la quantification par ICP-OES de certains métaux provenant d'échantillons de pâquerette et de leurs habitats. Le matériel végétal (*B. perennis* L.) et les sols appartenant à 16 localités différentes de la ville de Niš (la Serbie du Sud-Est) ont été utilisés pour la détermination de la teneur en métaux par ICP-OES. Les concentrations en Al, Ba, Cd, Co, Cr, Cu, Fe, Mn, Ni, Pb, V et Zn ont été calculées sur la base du poids sec. La teneur en pseudo-total des métaux des habitats équivalents a également été déterminée. La recherche a montré que la teneur en métaux lourds du matériel végétal et de ses habitats a été inférieure par rapport aux concentrations maximales autorisées ou inférieure par rapport à la limite de détection. De ce fait, nous pouvons dire que la contamination n'a été détectée ni dans le matériel végétal de *Bellis perennis* ni dans le sol.

Mots-clés : pâquerette, métaux, ICP OES (angl.), contamination, sol.

Содержание металла в ромашке обыкновенной (Bellis perennis L.) и соответствующих почвах области города Ниша (Сербия)

Милан Стойкович, Мария Евтич, Йована Павлович

Университет в Нише, Факультет естественных наук и математики, Департамент химии, Вишеградская, 33, 18000 Ниш, Сербия

АННОТАЦИЯ

Bellis perennis L. – распространенный вид ромашки семейства сложноцветных. Обычно он встречается на лугах, полянах, в садах, в городских районах и областях, прилегающих к обочинам дорог. Выброс тяжелых металлов в результате дорожного движения является важным источником загрязнения придорожных экосистем. Это исследование было сосредоточено на количественной ICP OES оценке некоторых металлов из общих образцов ромашки и почвы, на которой они растут. Растительный материал (*B. perennis* L.) и относящаяся к нему почва из 16 различных районов города Ниша (Юго-Восточная Сербия) были использованы для определения содержания металлов ICP OES. Концентрации Al, Ba, Cd, Co, Cr, Cu, Fe, Mn, Ni, Pb, V и Zn были рассчитаны на основе сухого веса. Также было определено псевдо-общее содержание металла в эквивалентных почвах, пригодных для выращивания. Исследование показало, что содержание тяжелых металлов в растительном материале и пригодных для выращивания почвах было ниже максимально допустимых концентраций, или ниже предела обнаружения. Поэтому можем сказать, что загрязнение не было обнаружено ни в растительном *материале B. perrenis*, ни в почвах для выращивания.

Ключевые слова: ромашка обыкновенная, металлы, ICP OES, загрязнение, почва.

Der Metallgehalt in Gänseblümchen (*Bellis perennis L.*) und korrespondierenden Böden aus dem Stadtgebiet von Niš (Serbien)

Milan Stojković, Marija Jevtić, Jovana Pavlović

Universität in Niš, Mathematisch-Naturwissenschaftliche Fakultät, Lehrstuhl für Chemie, Višegradska 33, 18000 Niš, Serbien

ABSTRAKT

Bellis perennis L. ist eine geläufige Gänseblümchenart aus der Familie der *Asteraceae*. Üblicherweise ist es in Grasland, Wiesen, Gärten, städtischen Gebieten und Gebieten in Straßenrandnähe vorzufinden. Die Emission von Schwermetallen aus dem Verkehr ist die Hauptschadstoffquelle für die Ökosysteme am Straßenrand. Diese Studie konzentrierte sich auf die ICP OES Quantifizierung einiger Metalle in Gänseblümchenproben und Böden, auf denen sie wachsen. Das Pflanzenmaterial (*B. perennis L.)* und die zugehörigen Böden aus 16 verschiedenen Standorten der Stadt Niš (Südostserbien) wurden für die ICP OES Bestimmungen des Metallgehalts verwendet. Die Konzentrationen von Al, Ba, Cd, Co, Cr, Cu, Fe, Mn, Ni, Pb, V und Zn wurden auf Trockengewichtsbasis berechnet. Der pseudo-gesamte Metallgehalt äquivalenter Böden wurde auch bestimmt. Die Studie zeigte, dass der Schwermetallgehalt des Pflanzenmaterials und der Böden, auf denen sie wachsen, unter den maximal zulässigen Konzentrationen oder unter der Nachweisgrenze lag, so dass man sagen kann, dass eine Kontamination weder im *B. Perrenis*-Pflanzenmaterial noch in den Böden nachgewiesen wurde.

Schlüsselwörter: Gänseblümchen, Metalle, ICP OES (engl.), Kontaminierung, Boden

Chemia Naissensis, Vol 2, Issue 1,RESEARCH ARTICLE, 114-133

Mineral composition of soil from urban area of Niš – chemometric approach

Jelena S. Nikolić[1*], Violeta D. Mitić[1], Marija V. Dimitrijević[1], Marija D. Ilić[2], Slobodan A. Ćirić[1], Vesna P. Stankov Jovanović[1]

1- University of Niš, Faculty of Sciences and Mathematics, Department of Chemistry, Višegradska 33, 18000 Niš, Serbia

2- Veterinary Specialist Institute "Niš", Dimitrija Tucovića 175, Niš, Serbia

ABSTRACT

The evaluation of the macroelement and microelement content in soil samples collected in the urban area of Niš, Serbia, was the objective of the study, as well as the determination of soil chemical characteristic impact on metal availability in soil. Fourteen metals (Al, Ca, Fe, Mg, Na, Ag, As, Ba, Cd, Cu, Cr, Hg, Pb, and Sr) content and four soil chemical characteristics (pH H_2O, pH KCl, organic matter content, and conductivity) were determined in 15 soil samples collected near road in urban area of Niš. Element with the highest concentration in analyzed samples was Ca (35.8 mg g^{-1}). Among the analyzed microelements, Pb had the highest concentration (0.352 mg g^{-1}). Hierarchical cluster analysis divided samples into two statistically significant clusters. Application of PCA analysis indicated soil chemical characteristic impact on metal content and permitted separation of metal content based on soil chemical characteristics.

Keywords: metal, ICP-OES, soil chemical characteristics, cluster, PCA

[*] Corresponding author: Jelena S. Nikolić, jelena.cvetkovic7@gmail.com, University of Niš, Faculty of Sciences and Mathematics, Department of Chemistry, Višegradska 33, 18000 Niš, Serbia

Introduction

Soil as the upper layer of the Earth's crust is formed of mineral particles, organic substances, water, air, and living organisms (European Commission, 2006). Their combination determines the properties of the soil: texture, structure, porosity, color, and chemical properties. Soil is a complex and vulnerable system. Since its formation is a long-term process, it can be considered as a hard renewable source.

Soil is an important source of both nutrients and potentially toxic elements for plants. They can reach the atmosphere through evaporation, and various physical-chemical processes might lead to their release in the aquatic environment. Plants adopt them from the soil, where they can show their harmful effects on the plant organism, but more importantly, using plants in animal and/or human nutrition may impact on the function of these organisms.

Mineral matter consists of many elements, but only eight of them are present more than 1%: oxygen (46.6%), silicon (27.7%), aluminum (8.1%), iron (5.0%), calcium (3.7%), sodium (2.8%), potassium (2.6%), magnesium (2.1%). In most soils, plants, and animals there are elements in a very low concentration (order of mg kg^{-1} and less), and therefore they are called "trace elements" (Haq et al., 2005). Trace elements include essential metals, such as Zn, Cu, and Ni, but also useless and toxic metals (Cd, Pb, and Hg). In the last decades' analysis of trace elements is of high interest because through polluted air, soil, or water can reach the food chain (He et al., 2005). In addition to the elements naturally occurring in the soil, a presence of heavy metals (metals with a density higher than 5 g cm^{-3}) has been recorded recently, due to anthropogenic activity. Heavy metals represent a risk to the ecosystem. Soil is a depot of heavy metals since they are not subject to microbiological or chemical degradation (Kirpichtchikova et

al., 2006). The most common heavy metals in the soil are Pb, Cr, As, Zn, Cd, Cu, Hg, and Ni (Wuana and Okieimen, 2011).

Soil chemical characteristics, such as organic matter content, pH, and conductivity, affect the behavior of metals in soil. These parameters affect the solubility of many substances, adsorption, and desorption of ions, coagulation, and peptization of colloids, as well as the chemical reactions in the soil. Quenea et al. (2009) showed the influence of soil organic substances on the availability and behavior of certain metals. The bioavailability of metals such as Cd, Zn, Cu, and Pb has been significantly reduced in the presence of organic soil substances. Metals bind soil organic soil substance to build complexes, and in this way, their bioavailability is reduced (Impellitteri et al., 2002). A factor that also affects the behavior of metals in soil is pH (Kazlauskaitė-Jadzevičė et al., 2014). The pH value also affects the organic substances binding ability. At a pH higher than 5, the ability of the organic substance to bind heavy metals increases (Kazlauskaitė-Jadzevičė et al., 2014). The reason for this phenomenon is the ionization of functional groups of organic substances present in the soil.

This study aimed to evaluate the metal content in soil samples collected in the urban area of Niš, Serbia, and evaluate soil chemical characteristic impact on metal content. Chemometric methods, cluster and principal component analysis, were applied to classify localities according to metal content. Also, the impact of soil chemical characteristics was evaluated using chemometric techniques.

Experimental

Chemicals and reagents

HCl, HNO_3 and multi-element standard containing Al, Ca, Fe, Na, Mg, P, S, Ag, As, Ba, Cd, Co, Cr, Cu, Ga, Hg, In, Li, Mn, Ni, Sr, Pb and Zn in concentrations of 1000 mg L^{-1} were obtained from Merck (Darmstadt, Germany). KCl, $K_2Cr_2O_7$, H_2SO_4, and H_3PO_4 were obtained from Merck (Darmstadt, Germany), $FeSO_4 \times 7H_2O$ from Zdravlje (Leskovac) while diphenylamine was supplied from Sigma Aldrich (Germany). Deionized water used for analysis had a specific conductivity of 0.05 μS cm^{-1}.

Instrumentation

Digestion was performed in a microwave oven equipped with a rotor holding 10 PTFE cuvettes (Ethos 1, Advanced Microwave Digestion System, Milestone, Italy).

An inductively coupled plasma-optical emission spectrometer (ICP OES) (Thermo Scientific, United Kingdom), model 6500 Duo, equipped with a CID86 chip detector, was used for determination of metals. System was controlled with iTEVA software.

pH meter and conductometer were supplied from Hanna Instruments (USA).

Soil sample collection

Soil samples (n=15) were collected in February 2015 near the road, covering urban part of city Niš, Serbia (Figure 1). Samples were taken from corners and center of a square grid, at a depth of 5-20 cm. After that, samples were combined and homogenized. Then they were air-

dried at room temperature (25 °C) for one week, sieved through 0.154-mm mesh sieve and stored at -18 ºC up to analysis.

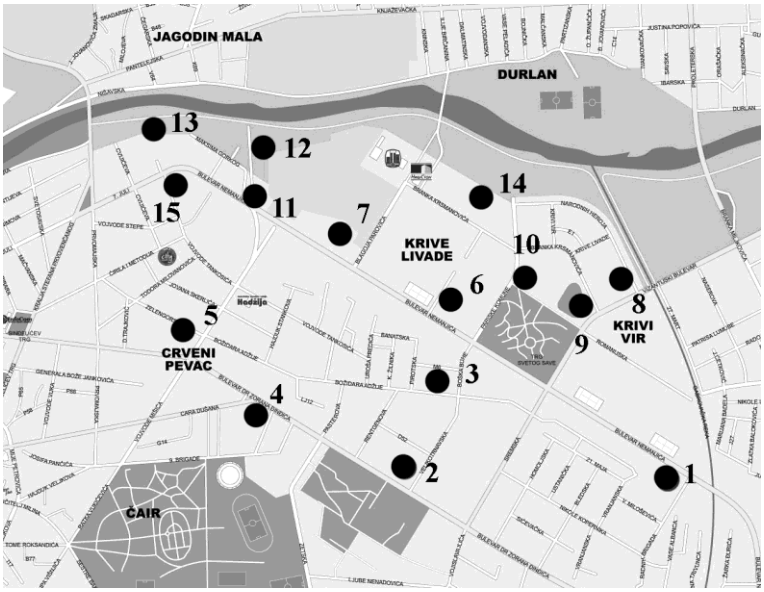

Figure 1. Map showing sampling location

Soil samples preparation for ICP-OES analysis

Collected soil samples were measured (0.5 g) and mixed with 15 mL of concentrated HCl (36%, w/w) and 5 mL of HNO_3 (65% w/w). The microwave digestion lasted for 5 h, and the samples were heated up to 80 ° C. Subsequently, samples were filtered through Whatman no. 42 filter paper and dissolved to a final volume of 100 mL.

Soil samples for ICP-OES analysis

The analysis was performed using ICP OES 6500 Duo model. Instrument conditions are shown in the Table 1.

Table 1. ICP OES conditions

Instrument conditions	
RF power	1150 W
Cooling gas flow	12 L min^{-1}
Nebuliser gas flow	0,5 L min^{-1}
Auxiliary gas flow	0,5 L min^{-1}

Quantification wavelengths for each element, the detection limits (LOD), the limits of quantification (LOQ), and the correlation coefficients (r^2) are represented in Table 2.

Table 2. Emission wavelengths, correlation coefficient of calibration curves, limit of detection (LOD) and limit of quantification (LOQ) for each element analyzed

Element	λ (nm)	r^2	LOD (μgL^{-1})	LOQ (μgL^{-1})
Al	309.2	0.9994	18	60
Ca	393.3	0.9975	2.1	7
Fe	259.8	0.9989	1.5	5
Mg	280.2	0.9968	1	1.7
Na	588.9	0.9999	30	100
Ag	338.2	0.9994	2.5	8.3
As	193.7	0.9989	25	83.3
Ba	455.4	0.9999	3.0	10
Cd	228.8	0.9988	0.21	0.7
Cr	283.5	0.9980	1.6	5.3
Cu	327.3	0.9993	3.0	10
Hg	184.9	0.9990	21	70
Pb	220.3	0.9996	7.9	26.3
Sr	407.7	0.9998	3.3	11

Soil chemical characteristics analysis

Soil pH determination: Soil samples collected in the city of Niš were mixed with water (10 g of soil and 25 mL of water) after drying and grinding, and the pH value of this suspension was measured with a pH meter. In addition to the soil pH in water, a pH value of 1 M KCl solution was also determined. The soil was mixed with 1M KCl solution, and the pH value of this suspension was measured with a pH meter.

Soil electrical conductivity determination: The electrical conductivity of soil samples was determined using conductometer. An aqueous solution of soil was prepared by mixing 25 mL of water with 10 g of soil, and after 30 min at room temperature conductivity was measured.

Soil organic matter determination: Soil organic matter was determined by the Walkley-Black titration (Schumacher, 2002). 5 g of soil was transferred to Erlenmeyer flask, and 10 mL of 0.1667 mol L^{-1} $K_2Cr_2O_7$ and 20 mL of concentrated H_2SO_4 (98%, w/w) was added. Erlenmeyer flask was allowed to stand for 30 min. After that, 200 mL of water, 10 mL of H_3PO_4 (85%, w/w) and 1 mL of diphenylamine were added. Excess of $K_2Cr_2O_7$ was titrated with a standard solution of $FeSO_4$.

Statistical analysis

Statistical analysis was performed using Statistica 8 software (StatSoft, Tulsa, USA). In order to determine the statistically significant difference, Student's t-test ($p < 0.05$) was used. Multivariate techniques that have been applied were hierarchical cluster analysis (HCA) and principal component analysis (PCA).

Results and Discussion

Metal concentration

The elements present in the soil can be divided into macroelements, whose concentration exceeds 100 mg kg^{-1}, and trace elements, whose concentration is smaller than this value (Sposito, 2008). The macroelements include O, Si, Al, Fe, C, K, Ca, Na, Mg, Ti, N, S, Ba, Mn, and P. Trace elements, especially metals are of importance in terms of environmental chemistry. They play an important role for flora and fauna, but in high concentrations can be toxic to plants, and humans (Jaishankar et al., 2014).

In the analyzed soil samples, the content of macroelements (Fe, Al, Ca, Mg, Na and Ba) and trace elements, including heavy metals (Pb, Sr, Ag, As, Cu, Cr, Hg, and Cd) were determined.

Concentrations of analyzed macroelements were presented in Figure 2.

Min	Sample	0	0.01	0.1	1	10	100	Sample	Max	Mean
3.9	15				Al			1	19.4	11.0
0.10	15			Ba				14	0.18	0.14
n.d.	15			Ca				8	35.8	22.6
6.6	15				Fe			1	25.0	17.8
2.04	15				Mg			8	9.3	4.4
n.d.	6		Na					15	0.34	0.20

Figure 2. Macroelements concentration in soil from the city of Niš (mg g^{-1})

Element with the highest concentration in analyzed samples was Ca. The highest concentration of this element was recorded for sample 8 (35.8 mg g^{-1}). Calcium is an important nutrient, which helps the root and stem in plant growth. This metal was commonly found in lower parts of the soil profile (Pritchett and Fisher, 1987). Interestingly, this metal concentration was below the limit of detection for sample number 15, a sample collected near houses and road with low traffic frequency. However, in this sample, the highest concentration of Na was recorded (0.34 mg g^{-1}). High sodium concentration in soil may contribute to the plant damage. According to Environment Canada (2004), plant damage may occur at 16 mg of Na per kg of soil. The higher concentration of Na and Mg in the soil might be due to the usage of deicing salts, especially in urban areas (Cunningham et al., 2007). Bryson and Barker (2002) analyzed sodium accumulation in soils and plants near the roadside due to the application of deicing salts. The concentrations of Na in roadside soil ranged from 0.1 mg g^{-1} at 1.5 m to 0.02 mg g^{-1} at 9 m from the roadside. Content of Na in the urban area of Niš was higher on some sampling localities than in samples analyzed by Bryson and Barker (2002). Soil samples in this study were collected in the winter season, so a higher concentration of Na might be due to the usage of deicing salts.

Soil structure is the result of the arrangement of elementary soil particles bound to organic matter (OM), iron and aluminum oxides, colloidal silica, or calcium carbonate (Borůvka et al., 2011). Al and Fe concentrations in samples from the city of Niš did not exceed common values in soils (Bech et al., 2008). The concentration of Fe in analyzed soil samples varied between 6.6 (sample 15) to 25.0 mg g^{-1} (sample 1). Similar results were achieved in a study at the Institute of field and vegetable crops, Novi Sad (2006). The maximum value of Al content in this study was 19.4 mg g^{-1} (sample 1). This sample was located near the bus station, so a higher amount of analyzed metals might be due to traffic pollution.

Concentrations of analyzed microelements were presented in Figure 3.

Min	Sample	0	0.001	0.01	0.1	Sample	Max	Mean
0.0033	15		Ag			3	0.0126	0.0070
0.0032	15		As			3	0.0110	0.0059
0.00034	13	Cd				11	0.00081	0.00050
0.028	15			Cu		1	0.086	0.064
0.044	15			Cr		11	0.127	0.068
n.d.	1,10,13	Hg				7	0.00046	0.00012
0.022	15			Pb		11	0.352	0.081
0.019	10			Sr		5	0.205	0.122

Figure 3. Microelements concentration in soil from the city of Niš (mg g^{-1})

Among analyzed microelements, the highest concentration was recorded for Pb (0.352 mg g^{-1}, sample number 11). This sample was collected near the bus station and road with high traffic frequency. According to the Gazette of the Republic of Serbia (Ministry of Environmental Protection, 2010), the limit for Pb concentration in soil is 0.085 mg g^{-1}. Out of 15 analyzed samples, 3 of them (7, 11, and 12) had higher Pb concentration than this value. Natural emission share for lead is less than 15%, so this is a reliable indicator of anthropogenic pollution of the environment (Davies, 1995). Exhaust gases of motor vehicles dominantly emit lead (Hashisho and El-Fadel, 2004). Analyzed samples were collected near the road, so a higher concentration of Pb might be due to vehicles gases. Metals also emitted from vehicles are Cu, Zn, and Cd (Blok, 2005; Guney et al., 2010). Cd is one of the elements with unknown biological functions. The concentration of cadmium in the analyzed samples was in the range of 0.00034 to 0.00081 mg g^{-1}. The only sample collected on locality 11 had a higher concentration than the limit value prescribed by the Gazzete (Ministry of Environmental Protection, 2010). Mercury is also an element without biological function. The Gazzete of the Republic of Serbia (Ministry of

Environmental Protection, 2010) prescribes the limit value for the content of Hg in the soil (0.0003 mg g^{-1}), and only one sample (7) had a higher value of this metal compared to the permitted value.

Soil chemical characteristics

Soil chemical characteristics, such as organic matter content, pH, and conductivity, affect the behavior of metals in soil. pH in water, pH in KCl solution, conductivity, and organic matter content were presented in Table 3.

The pH values of the aqueous solutions of the analyzed soil samples were in the range of 7.26 for sample 15 to 10.94 for sample 14. The pH of the analyzed soils in the KCl solution was lower than those determined in the aqueous solution and ranged from 5.41 for sample 1 to 10.52 for sample 14. According to the USDA classification (1993), most of the analyzed soil samples belong to neutral and weakly alkaline soil types. The soil conductivity ranged from 0.12 mS cm^{-1} (sample 9) to 10.1 mS cm^{-1} (sample 14). Soil conductivity affects the availability of nutrients to the plants, and the higher conductivity is, the availability of minerals from the soil to the plant is larger. Soil organic matter was present in analyzed soil samples within the range of 0.41-6.77%.

Table 3. Soil chemical characteristics in samples from city of Niš

Sample	pH (H_20)	pH (KCl)	Conductivity (mS cm^{-1})	Soil organic matter (%)
1	7.7	5.41	0.32	1.78
2	7.83	7.08	0.31	2.23
3	8.03	7.06	0.19	1.08
4	8.11	7.17	0.23	1.94
5	7.79	7.04	0.23	2.33
6	7.76	7.11	0.17	2.97
7	7.65	7.06	0.32	4.27
8	8.12	7.19	0.88	6.77
9	7.72	7.24	0.12	1.13
10	7.78	7.34	0.14	0.41
11	7.84	7.16	0.34	3.60
12	7.59	7.21	0.67	2.57
13	7.75	7.14	0.14	2.23
14	10.94	10.52	10.1	1.54
15	7.26	6.9	0.67	1.74

Statistical analysis

Multivariate statistical techniques (PCA and cluster analysis) were applied to data obtained by analyzing metal content and soil chemical characteristics in the urban area of Niš. The aim of statistical analysis was to determine the relationships between sampling localities and to understand relations between the analyzed parameters.

The objective of cluster analysis was the grouping of soil samples based on the content of analyzed metals. The cluster analysis was performed using Ward's method. The Euclidean distances are presented as the ratio $(D_{link}/D_{max})\times100$, where D_{link} is the distance between the variables that are grouped and D_{max} is the maximum distance between the variables. Results obtained using cluster analysis, were presented on a dendrogram (Figure 4).

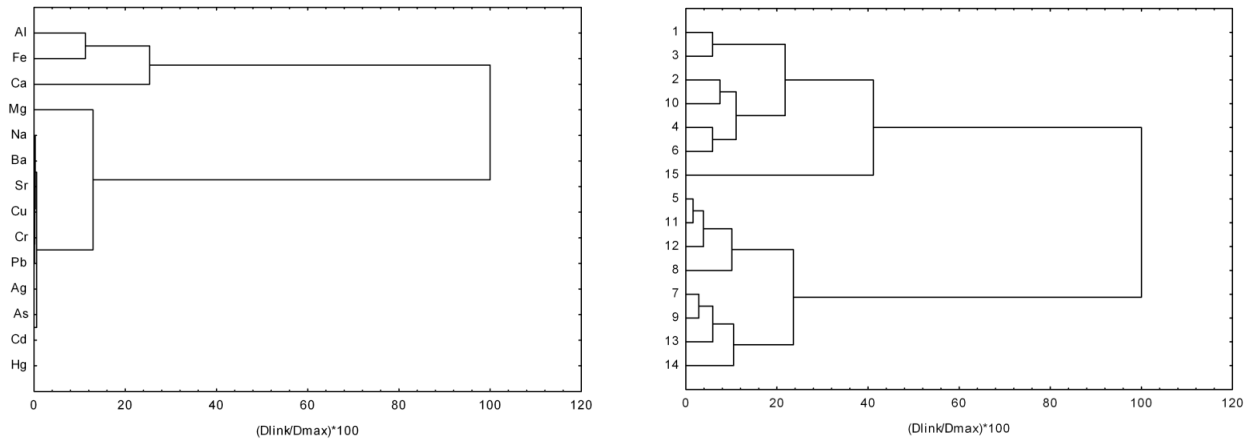

Figure 4. Dendrogram showing grouping of a) analyzed metals b) analyzed soil samples based on metal content

According to hierarchical cluster analysis metals are grouped into two clusters (D_{link}/D_{max}<50). The first cluster was composed of Al, Fe, and Ca. Those metals concentration is higher than other analyzed metals, so this separation was expected. The second cluster was composed of Mg, Na, Ba, Sr, Cu, Cr, Pb, Ag, As, Cd and Hg. Existence of a sub-cluster in this cluster was observed, but also the separation of Mg from other metals. The smallest Euclidean distance (2) was recorded between Cd and Hg, metals without proven function in living organisms and their concentrations in analyzed soil samples were the smallest.

Analyzed soil samples were grouped into two clusters based on the metal content (D_{link}/D_{max} <50). The first cluster was composed of samples 1, 2, 3, 4, 6, 10, and 15, while the other samples were grouped in the second cluster. The minimum Euclidean distance (1298) was recorded between samples 5 and 11, so these two samples can be considered to be the most

similar in terms of metals content. Euclidean distance among samples was high, so in terms of metal content samples collected in the city of Niš are quite different.

The goal of PCA analysis is to reduce the number of data to a smaller number of variables (principal components - PC) that correspond to a linear combination of the original variables. Of the obtained principal components, only those whose sum involves a high percentage of the total variance are usually used in further analysis. According to the criterion set by Kaiser (Kaiser, 1960), significant components are those whose eigenvalue exceeds 1. Variables used for PCA analysis were a concentration of analyzed metals, while supplementary variables were soil chemical characteristics. Of the 14 components obtained by PCA analysis, five of them had an eigenvalue higher than 1, and they account for 86.43% of the total variance. PC1 had the highest contribution to the total variance (32.71%). Out of 5 principal components that had an eigenvalue higher than 1, only PC1 and PC2 were analyzed because they provide the highest contribution to the total variance. Score and loading plots are presented in Figure 5.

PC1 had a negative load for three analyzed metals: Sr (-0.350), Hg (-0.260), and Na (-0.048). Negative loading was also recorded for soil organic matter (-0.09), so it can be concluded that soil organic matter significantly affects the bioavailability of Sr, Hg, and Na. Quenea et al. (2009) showed the influence of organic substances on the availability and behavior of certain metals. The bioavailability of metals such as Cd, Zn, Cu, and Pb has been significantly reduced in the presence of soil organic substances, much more than in the presence of mineral substances.

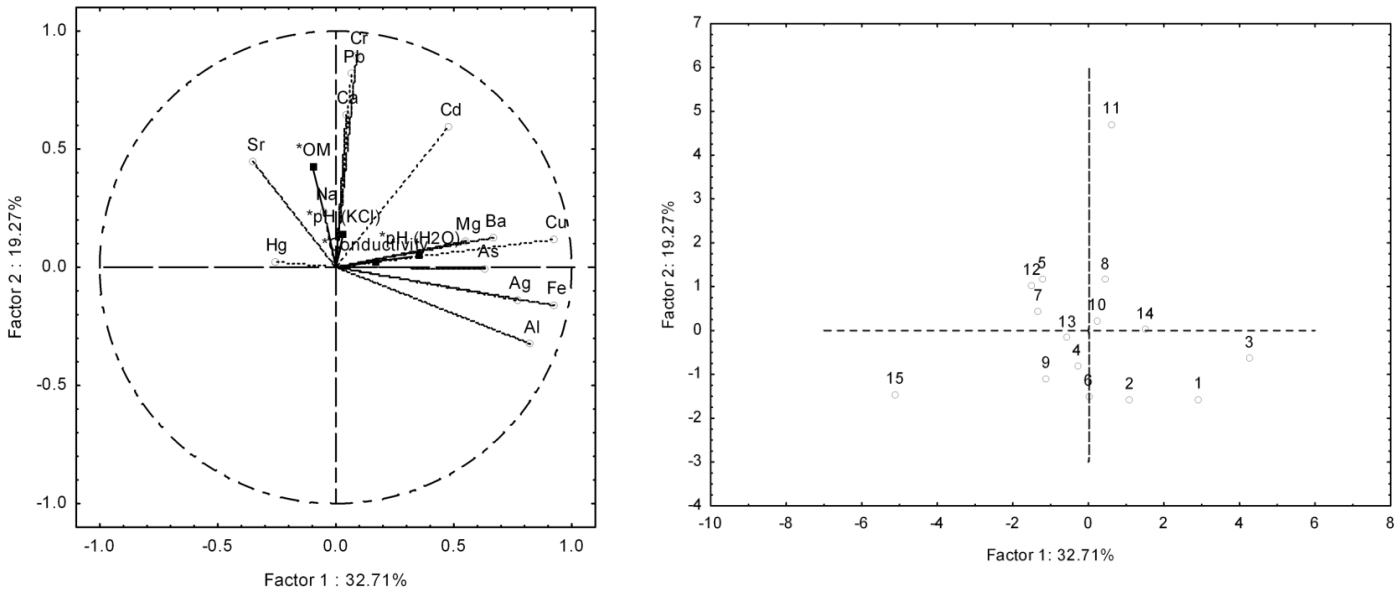

Figure 5. Principal component analysis plots of soil samples from Niš

The remaining metals and soil chemical characteristics have positive loadings on PC1. PC2 explains 19.27% of the total variance. The highest positive loadings on PC2 were recorded for Cr (0.898) and Ca (0.645). Soil pH in KCl solution was grouped with Ca, Pb, Cr, and Cd, which indicates that soil pH affects these metals behavior in soil. According to Ghosh and Singh (2005), soil pH greatly affects the solubility or retention of metal in soils. Conductivity and pH value were grouped with Mg, Ba, and Cu, which indicates that these parameters affect Mg, Ba, and Cu behavior in soil samples from Niš.

Soil samples are grouped based on metal concentration and soil chemical characteristics using PCA analysis. Sample 11 and 15 were separated from other analyzed samples. Sample 15 had the lowest concentration of Al, Ba, Ca, Fe, Mg, Ag, As, Ba, Cu, Cr and Pb, and the highest concentration of Na, so separation of this sample is expected. This sample is located on the opposite side of all metals, which indicates that PCA can be used as a powerful tool to analyze

complex data set. Sample 11 had the maximum concentration of two major soil pollutants (Cd and Pb) and Cr. Sample 11 was in the same quadrant with Cr, Pb, Ca and Ca, metals with high concentrations in this sample. The highest negative contribution to PC1 was recorded for sample 15 (-5.117), while the highest positive loading on PC2 was recorded for sample 11 (4.712).

Conclusion

Content of metals (Al, Ca, Fe, Mg, Na, Ag, As, Ba, Cd, Cu, Cr, Hg, Pb, and Sr) and four soil chemical characteristic was determined in soil samples collected in the urban area of Niš. From the analyzed macroelements, Ca was the element with the highest concentration (mean concentration of 22.64 mg g^{-1}). Among analyzed microelements, Pb had the highest mean concentration (0.081 mg g^{-1}). The concentration of this metal exceeded the permitted value prescribed by Gazzete of the Republic of Serbia on three sampling localities. Analyzed samples were grouped in two statistically significant clusters using cluster analysis, based on metal content. Five principal components were extracted, accounting 86.43% of the total variance. Metals were grouped with chemical characteristics, which indicates that they could affect metal behavior in soil. Used chemometric techniques are a powerful tool for simple analysis of a large data set.

Acknowledgment

The research was supported by the Ministry of Education, Science and Technological Development of the Republic of Serbia [project number OI 172051].

Conflict-of-Interest Statement

No potential conflict of interest was reported by the authors.

References

Bech, J., Tume, P., Longan, L., Reverter, F., Bech, J., Tume, L., & Tempio, M. (2008). Concentration of Cd, Cu, Pb, Zn, Al, and Fe in soils of Manresa, NE Spain. Environmental Monitoring and Assessment, 145, 257–266.

Borůvka, L., Valla, M., Donátová, H., & Němeček, K. (2011). Vulnerability of soil aggregates in relation to soil properties. Plant, Soil and Environment, 48, 329–334.

Bryson, G. M., & Barker, A. V. (2002). Sodium accumulation in soils and plants along Massachusetts roadsides. Communications in Soil Science and Plant Analysis, 33, 67–78.

Cunningham, M. A., Snyder, E, Yonkin, D., Ross, M., & Elsen, T. (2007). Accumulation of deicing salts in soils in an urban environment. Urban Ecosystems, 11, 17–31.

Davies, B.E. (1995). Lead. In B.J. Alloway (Ed.), Heavy Metals in Soils (pp. 206-223). London: Blackie and Son Ltd.

Environment Canada (2004): Code of practice for the environmental management of road salts. Ottawa, Canada.

European commission (EC), (2006). Soil – The story behind the strategy, Luxembourg: Office for Official Publications of the European Communities.

Ghosh, M., & Singh, S.P. (2005). A review on phytoremediation of heavy metals and utilization of its byproducts. Applied Biology and Environmental Research, 3, 1–18.

Guney, M., Onay, T. T, & Copty, N. K. (2010). Impact of overland traffic on heavy metal levels in highway dust and soils of Istanbul, Turkey. Environmental Monitoring and Assessment, 164, 101–110.

Haq, M., Khattak, R. A., Puno, H. K., Saleem Saif, M., Memon, K. S., & Sial, N. B. (2005). Bioaccumulation of Trace Elements by Different Plant Species Grown on Potentially Contaminated Soils of NWFP, Pakistan. Asian Journal of Plant Sciences, 4, 383–387.

Hashisho, Z., El-Fadel, M. (2004). Impacts of traffic-induced lead emissions on air, soil and blood lead levels in Beirut. Environmental Monitoring and Assessment, 93, 185-202.

Blok, J. (2005). Environmental exposure of road borders to zinc. The Science of the Total Environment, 348, 173–190.

He, Z. L., Zdenko Yang, X. E., & Stoffella, P. J. (2005). Trace elements in agroecosystems and impacts on the environment. Journal of Trace Elements in Medicine and Biology, 19, 125-140.

Impellitteri, C. A., Lu, Y., Saxe, J. K., Allen, H. E., & Peijnenburg W. J. G. M. (2002). Correlation of the partitioning of dissolved organic matter fractions with the desorption of Cd, Cu, Ni, Pb and Zn from 18 Dutch soils. Environment International, 28, 401–410.

Impellitteri, C. A., Lu, Y., Saxe, J. K., Allen, H. E., & Peijnenburg, W. J. G. M. (2002). Correlation of the partitioning of dissolved organic matter fractions with the desorption of Cd, Cu, Ni, Pb and Zn from 18 Dutch soils. Environment International, 28, 401–410.

Institute of Field and Vegetable Crops Novi Sad (2006). Environmental quality control on the territory of AP Vojvodina - soil of industrial zones - number: 08-100 / 526 27.02.2006.

Jaishankar, M., Tseten, T., Anbalagan, N., Mathew, B. B., & Beeregowda, K. N. (2014). Toxicity, mechanism and health effects of some heavy metals. Interdisciplinary Toxicology, 7, 60–72.

Kazlauskaitė-Jadzevičė, A., Volungevičius, J., Gregorauskienė, V., & Marcinkonis S. (2014). The Role Of Ph In Heavy Metal Contamination Of Urban Soil. Journal of Environmental Engineering And Landscape Management, 22, 311–318.

Kaiser, H. F. (1960). The Application of Electronic Computers to Factor Analysis. Educational and Psychological Measurement, 20, 141-151.

Kirpichtchikova, T. A., Manceau, A., Spadini, L., Panfili, F., Marcus, M. A., Jacquet, T. (2006). Speciation and solubility of heavy metals in contaminated soil using X-ray microfluorescence, EXAFS spectroscopy, chemical extraction, and thermodynamic modeling. Geochimica et Cosmochimica Acta, 70, 2163–2190.

Ministry of Environmental Protection (2010). Decree on the program for systematic monitoring of land quality, indicators for assessing the risk of land degradation and the methodology for the development of remediation programs, ("Official Gazette of the Republic of Serbia", No. 88/2010).

Pritchett, W. L., & Fisher, R. F. (1987). Properties and management of forest soils. (2nd ed). John Wiley.

Quenea, K., Lamy, I., Winterton, P., Bermond, A., & Dumat, C. (2009). Interactions between metals and soil organic matter in various particle size fractions of soil contaminated with waste water. Geoderma, 149, 217–23.

Schumacher, B. (2002). Methods for the determination of total organic carbon (TOC) in soils and sediments. Las Vegas: US EPA.

Sposito, G. (2008). The Chemistry of Soils. (1st ed). Oxford University Press.

United States Department of Agriculture (USDA) (1993). Soil Survey Division Staff. Soil survey manual. Soil Conservation Service. U.S. Department of Agriculture Handbook.

Wuana, R. A., & Okieimen, F. E. (2011). Heavy Metals in Contaminated Soils: A Review of Sources, Chemistry, Risks and Best Available Strategies for Remediation. ISRN Ecology, 2011 1–20.

Mineralni sastav zemljišta iz urbanih delova Niša-hemometrijski pristup

Jelena S. Nikolić[1*], Violeta D. Mitić[1], Marija V. Dimitrijević[1], Marija D. Ilić[2], Slobodan A. Ćirić[1], Vesna P. Stankov Jovanović[1]

1- Univerzitet u Nišu, Prirodno-matematički fakultet, Departman za hemiju, Višegradska 33, 18000 Niš, Srbija

2- Veterinarski specijalistički institut "Niš", Dimitrija Tucovića 175, Niš, Srbija

SAŽETAK

Cilj istraživanja je bila evaluacija sadržaja makro i mikroelementata u uzorcima zemljišta prikupljenih u urbanim delovima Niša, Srbija, kao i određivanje uticaja hemijskih karakteristika zemljišta na raspoloživost metala u zemljištu. Sadržaj četrnaest metala (Al, Ca, Fe, Mg, Na, Ag, As, Ba, Cd, Cu, Cr, Hg, Pb, i Sr) i četiri hemijske karakateristike zemljišta (pH H_2O, pH KCl, sadržaj organske materije i provodljivost) su određeni u 15 uzoraka zemljišta prikupljenih blizu puteva u urbanim delovima Niša. Element sa najvišom koncentracijom u analiziranim uzorcima je bio kalcijum (35.8 mg g^{-1}). Među analiziranim mikroelementima, Pb je imalo najvišu koncentraciju (0.352 mg g^{-1}). Hijerarhijska klasterska analiza podelila je uzorke na dva statistički značajna klastera. Primena PCA analize je pokazala uticaj hemijskih karakteristika zemljišta na sadržaj metala, kao i to da je dozvoljena separacija sadržaja metala prema hemijskim karakteristikama zemljišta.

Ključne reči: metal, ICP-OES, hemijske karakteristike zemljišta, klaster, PCA (engl.)

Composition minérale des sols de l'agglomération de Niš – approche chimiométrique

Jelena S. Nikolić[1]*, Violeta D. Mitić[1], Marija V. Dimitrijević[1], Marija D. Ilić[2], Slobodan A. Ćirić[1], Vesna P. Stankov Jovanović[1]

1- Université de Niš, Faculté des sciences naturelles et des mathématiques, Département de chimie, Višegradska 33, 18000 Niš, Serbie

2- Institut vétérinaire spécialisé « Niš », Dimitrija Tucovića 175, Niš, Serbie

RÉSUMÉ

L'objectif de l'étude était d'évaluer le contenu en macroéléments et en microéléments des échantillons du sol prélevés dans la zone urbaine de la ville de Niš (Serbie), ainsi que la détermination de l'impact des caractéristiques chimiques du sol sur la disponibilité des métaux dans le sol. Quatorze métaux (Al, Ca, Fe, Mg, Na, Ag, As, Ba, Cd, Cu, Cr, Hg, Pb et Sr) et quatre caractéristiques chimiques du sol (pH H2O, pH KCl, teneur en matière organique et conductivité) ont été déterminés dans 15 échantillons du sol prélevés près des routes dans la zone urbaine de Niš. L'élément de la concentration la plus élevée dans les échantillons analysés était le calcium (Ca 35,8 mg g^{-1}). Parmi les microéléments analysés, le plomb avait la concentration la plus élevée (Ph 0,352 mg g^{-1}). L'analyse hiérarchique de grappe a divisé les échantillons en deux grappes statistiquement significatives. L'application de l'analyse PCA a révélé l'impact des caractéristiques chimiques du sol sur la teneur en métal et a permis la séparation de la teneur en métal basée sur des caractéristiques chimiques du sol.

Mots-clés : métal, ICP-OES, caractéristiques chimiques du sol, grappe, PCA (angl.).

Минеральный состав почвы городской местности Ниша – хемометрический подход

Елена С. Николич[1], Виолета Д. Митич[1], Мария В. Димитриевич[1], Мария Д. Илич[2], Слободан А. Чирич[1], Весна П. Станков Йованович[1]

1- Университет в Нише, Факультет естественных наук и математики, Департамент химии, Вышеградская 33, 18000 Ниш, Республика Сербия

2- Институт ветеринарных специальностей "Ниш", Димитрия Туцовича 175, Ниш, Сербия

АННОТАЦИЯ

Цель исследования – оценка содержания макроэлементов и микроэлементов в пробах почвы, отобранных в городских районах Ниша, Сербия, а также определение влияния химических характеристик почвы на наличие металлов в почве. Содержание четырнадцати металлов (Al, Ca, Fe, Mg, Na, Ag, As, Ba, Cd, Cu, Cr, Hg, Pb и Sr) и четырех химических характеристик почвы (pH, H_2O, pH KCl, содержание органических веществ и проводимости) были определены в 15 образцах почвы, собранных вблизи дороги в городской местности Ниш. Элементом с самой высокой концентрацией в анализируемых образцах был Ca (35,8 мг $г^{-1}$). Среди анализируемых микроэлементов Pb имел самую высокую концентрацию (0,352 мг $г^{-1}$). Иерархический кластерный анализ разделил выборки на два статистически значимых кластера. Применение анализа PCA показало влияние химических характеристик почвы на содержание металлов и позволило разделить содержание металлов на основе химических характеристик почвы.

Ключевые слова: металл, ICP-OES, химические характеристики почвы, кластер, PCA,

Mineralische Bestandteile des Bodens aus den Stadteilen von Niš – chemometrischer Ansatz

Jelena S. Nikolić[1*], Violeta D. Mitić[1], Marija V. Dimitrijević[1], Marija D. Ilić[2], Slobodan A. Ćirić[1], Vesna P. Stankov Jovanović[1]

1- Universität in Niš, Mathematisch-Naturwissenschaftliche Fakultät, Lehrstuhl für Chemie, Višegradska 33, 18000 Niš, Serbien

2- Veterinärmedizinisches Fachinstitut "Niš", Dimitrija Tucovića 175, Niš, Serbien

ABSTRAKT

Die Bewertung des Makro- und Mikroelementgehalts in den Bodenproben, die in den Stadtgebieten von Niš, Serbien, entnommen wurden, war das Ziel dieser Arbeit, sowie die Bestimmung der Auswirkung der chemischen Eigenschaften des Bodens auf die Metallverfügbarkeit im Boden. Der Gehalt an vierzehn Metallen (Al, Ca, Fe, Mg, Na, Ag, As, Ba, Cd, Cu, Cr, Hg, Pb und Sr) und vier Eigenschaften des Bodens (pH H2O, pH KCl, Gehalt an organischer Substanz und Leitfähigkeit) wurden in 15 Bodenproben bestimmt, die in Straßennähe in Stadtgebieten von Niš gesammelt wurden. Das Element mit der höchsten Konzentration in den analysierten Proben war Kalzium (35,8 mg g^{-1}). Unter den analysierten Mikroelementen hatte Pb die höchste Konzentration (0,352 mg g^{-1}). Die hierarchische Clusteranalyse teilte die Proben in zwei statistisch signifikante Cluster. Die Anwendung der PCA-Analyse zeigte die Auswirkung der chemischen Eigenschaften des Bodens auf Metallgehalt und die zulässige Trennung des Metallgehalts aufgrund der chemischen Eigenschaften des Bodens.

Schlüsselwörter: Metall, ICP-OES, chemische Eigenschaften des Bodens, Cluster (engl.), PCA(engl.)

Chemia Naissensis, Vol 2, Issue 1, EXPERT ARTICLE,138-143

Virtual Analytical Chemistry Software

Aleksandra Gošnjić Ignjatović

Gymnasium "9.maj", Jeronimova 18, 18000 Niš, Republic of Serbia

ABSTRACT

Chemistry subjects are in the most cases strongly interconnected with experiments, both on a fundamental level, but also in the process of teaching/learning. Many high schools in Serbia have a problem with lack of laboratory space and chemicals, which significantly complicates teaching/ learning of practical skills. This work aims to present innovation in high school chemistry teaching as an excellent way to overcome these obstacles. Virtual analytical chemistry software was designed in order to help students in learning qualitative analytical chemistry without entering laboratories.

Keywords: Chemistry, Teaching, Virtual analytical chemistry, Software

**Gymnasium "9.maj", Jeronimova 18, 18000 Niš, Republic of Serbia, e-mail: aleksandragosnjic@gmail.com*

Introduction

Chemistry is an essential basis for many sciences but also allows understanding the world around us. If someone wants to know how materials and drugs are made, how cooking affects substances from food or how detergents work, he/she must consult chemistry. As an experimental science, chemistry should encourage the inclination towards research, logical deduction that leads to results and chemical process analyses with the outcome of applying the knowledge and connections to other disciplines. Chemistry, science, and technology are in tight connections to economies of each highly developed industrialized and technologically advanced society (Burmeister et al., 2012).

Traditionally teaching chemistry way may leave the students with a lack of motivation. The results of PISA tests show that Serbia is falling behind in science education comparing to the countries in the EU. The problem, facing chemistry teachers in many schools in Serbia, has been lack of laboratory space and chemicals. From these reasons, chemistry in schools is taught mostly in classrooms, without entering laboratories. Practical experience is an integral part of chemistry science. The availability of laboratory equipment, chemicals and materials, laboratory personnel, working conditions in the laboratory and safety measures, substantially recommended textbooks and certain periods allocated for the teaching of the subjects are necessary (Adefunke, 2008). The conducted research among one thousand students shows that studying chemistry is a repetition of what has been taught. That fact is the apparent sign that the concept of teaching needs change.

To the best of author's knowledge, this paper is the first report on virtual qualitative analytical laboratory, created to bring closer laboratory work to the high school students in Serbia.

Virtual analytical chemistry software

This whole concept aims to introduce the basics of analytical chemistry in a more interactive way to students with no laboratory access. They will be able to use the software in order to learn through virtual simulation and visualization qualitative analytical laboratory.

The base of the software is its engine. The engine used to develop this software is « Unity Engine ».

The language used and combined with the engine is Microsoft Visual C#. The 3D Models used are a combination of different assets that are compatible with the Unity Engine. The 2D designs were custom made to fit the style of the software.

Virtual analytical chemistry is a software which shows chemical reactions of anions (Cl^-, SO_4^{2-}, NO_3^-, CO_3^{2-}, CH_3COO^-) and cations (Ag^+, Pb^{2+}, Hg^{2+}, Cu^{2+},Fe^{3+}, Al^{3+}, Ca^{2+}, Ba^{2+}, Mg^{2+}, NH_4^+) presence with suitable reagents in an interactive way.

For the schools, which do not have well-equipped laboratories, this software can serve as a removable teaching tool. The software is designed for students of Gymnasium, medicinal, and chemistry schools, which learn analytical chemistry. It should help students to visualize chemical reactions that are the basis of qualitative analytical chemistry. Also, it can help teachers and students in preparations for chemistry competitions.

The simulation of chemical processes is conducted in a chemical laboratory with 3D modeled test tubes (equipment) and reagents through the formation of residue and gases.

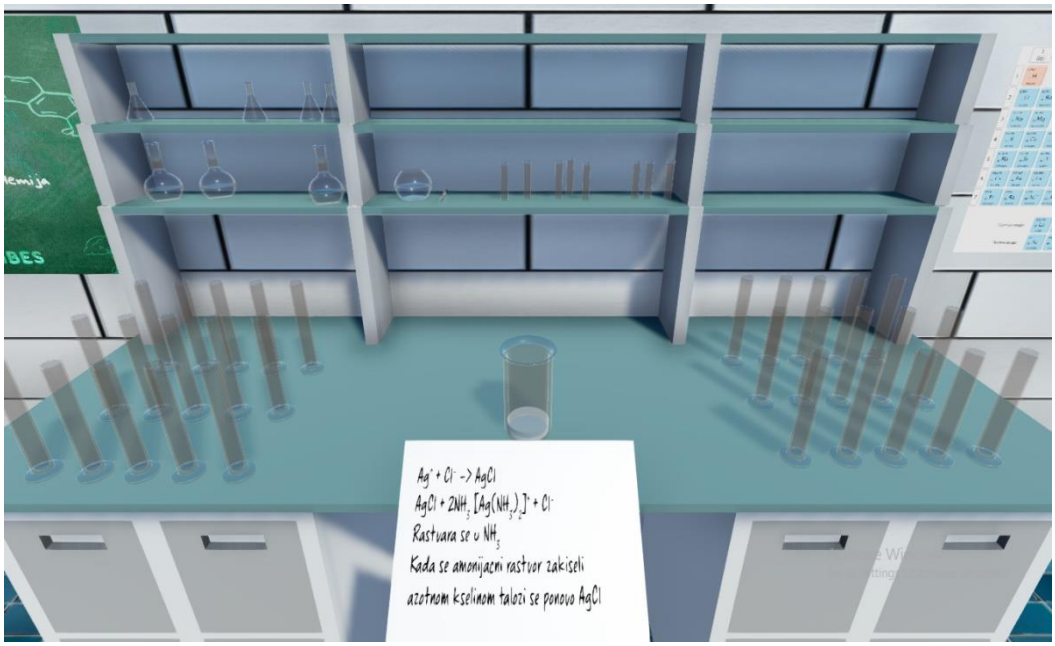

Figure 1. Virtual analytical chemistry software – chloride test reaction

The program consists of two sets of test tubes on the right-hand and left-hand sides. The test tubes are marked with numbers, and the combination of two numbers leads to a specific reaction. When the combination of two numbers does not give the expected reaction, that is, when for a certain anion or cation a wrong reagent is used, a ’virtual explosion’ happens in the virtual laboratory.

Figure 2. Virtual analytical chemistry software – wrong reagent used

There are many advantages of using this software. The virtual chemistry laboratory is always available to students in Serbia. With the combination of the right reagents, we get correct reactions of cations and anions, which makes the process much more economical and functional for use outside a physical laboratory. The students are more motivated to use and implement the software into new chemical situations safely.

The goal is modernizing and increasing the openness in teaching chemistry, increasing the interest of students and improving the education of chemistry.

Conclusion

The software is designed for pupils from Gymnasium, Medical and Chemistry schools in qualitative chemical analysis aimed to serve as a portable teaching tool. It should help students to visualize the chemical reactions that are the basis of qualitative analytical chemistry. The described way of teaching enables students to understand the chemical laws in a modern way, which is in line with the modern world, new technologies, and scientific achievements, without entering the chemical laboratory. We expect that modernization and increasing visualization of chemistry can

increase the interest of students and improve the level of knowledge in chemistry. It can also help teachers and students to prepare for chemistry competitions.

It is necessary to inspect the influence of the software on student interests for chemistry and in the level of knowledge in this area using the parallel group method. In case the results are positive, there is a possibility that similar software is made for different topics in chemistry and other sciences.

Conflict-of-Interest Statement

Author declares no conflict of interest.

References

Adefunke, T. O. (2008). Quality assurance in the upper basic education through effective curriculum implementation. Nigerian Journal of Curriculum Studies, 15, 23-33.

Burmeister, M., Rauch, F., & Eilks, I. (2012). Education for Sustainable Development (ESD) and chemistry education. Chemical Education Research and Practice, 13(2), 59-68

Softver za virtualnu analitičku hemiju

Aleksandra Gošnjić Ignjatović

Gimnazija "9.maj", Jeronimova 18, 18000 Niš, Republika Srbija

SAŽETAK

Hemijski predmeti su u većini slučajeva jako povezani sa eksperimentima, kako na fundamentalnom nivou, tako i u procesu predavanja/učenja. Mnoge srednje škole u Srbiji imaju problem sa nedostakom laboratorijskog prostora i hemikalija, što značajno komplikuje predavanje/učenje praktičnih veština. Ovaj rad ima za cilj da predstavi inovaciju u predavanju hemije u srednjoj školi kao odličan način za prevazilaženje ovih prepreka. Softver za virtualnu analitičku hemiju je dizajniran da bi pomogao studentima u izučavanju kvalitativne analitičke hemije bez ulaska u laboratorije.

Ključne reči: Hemija, predavanje, virtualni, softver

Chemia Naissensis, Vol 2, Issue 1, EXPERT ARTICLE, 145

Logiciel de chimie analytique virtuelle

Aleksandra Gošnjić Ignjatović

Lycée « 9. maj », Jeronimova 18, 18000 Niš, Serbie

RÉSUMÉ

Les matières de la chimie sont, dans la plupart des cas, fortement liées aux expériences chimiques tant au niveau fondamental que lors du processus d'enseignement/apprentissage. En Serbie, de nombreuses écoles secondaires souffrent d'un manque d'espace de laboratoire et de produits chimiques, ce qui complique considérablement l'acquisition des compétences pratiques. Ce travail vise à présenter une innovation dans l'enseignement de la chimie au lycée en tant qu'excellent moyen de surmonter les obstacles mentionnés. Un logiciel de chimie analytique virtuelle a été conçu en vue d'aider les étudiants à examiner la chimie analytique qualitative sans entrer dans les laboratoires.

Mots-clés : chimie, enseignement, virtuel, logiciel.

Программное обеспечение для виртуальной аналитической химии

Александра Гошнич Игнятьович

Гимназия «9. Мая», Еронимова 18, 18000 Ниш, Республика Сербия.

АННОТАЦИЯ

Предметы химии в большинстве случаев тесно связаны с экспериментами, как на фундаментальном уровне, так и в процессе преподавания / обучения. Многие средние школы в Сербии встречаются с проблемой отсутствия лабораторного пространства и химикатов, что значительно усложняет преподавание / изучение практических навыков. Цель этой работы – представить инновации в преподавании химии в старших классах как отличный способ преодолеть эти препятствия. Программное обеспечение виртуальной аналитической химии было разработано с целью помочь студентам в качественном изучении аналитической химии, без присутствия в лаборатории.

Ключевые слова: химия, преподавание, виртуальная аналитическая химия, программное обеспечение

Chemia Naissensis, Vol 2, Issue 1, EXPERT ARTICLE, 147

Software für virtuelle analytische Chemie

Aleksandra Gošnjić Ignjatović

Gymnasium "9. maj", Jeronimova 18, 18000 Niš, Serbien

ABSTRAKT

Chemiefächer sind in den meisten Fällen stark mit Experimenten verbunden, sowohl auf der grundlegenden Ebene als auch im Lehr- und Lernprozess. Viele Mittelschulen in Serbien haben Probleme mit dem Mangel an Laborräumen und Chemikalien, was das Lehren und Lernen von praktischen Fertigkeiten erheblich erschwert. Diese Arbeit zielt darauf ab, eine Innovation im Chemieunterricht an Mittelschulen als hervorragende Möglichkeit zur Überwindung dieser Hindernisse vorzustellen. Die Software für virtuelle analytische Chemie wurde entwickelt, um Studenten das Erlernen der qualitativen analytischen Chemie zu erleichtern, ohne Labore betreten zu müssen.

Schlüsselwörter: Chemie, Unterricht, virtuell, Software

Chemia Naissensis (ISSN 2620-1895)

Published only in electronic form

Volume 2, Number 1, July 2019

Publisher:

Faculty of Sciences and Mathematics, University of Niš

Editor-in-Chief:

Deputy Editor:

Editors:

Inorganic Chemistry

Dr Dragan Đorđević, Department of Chemistry, Faculty of Sciences and Mathematics, University of Niš, Republic of Serbia

Chemical Engineering

Dr Marjan Ranđelović, Department of Chemistry, Faculty of Sciences and Mathematics, University of Niš, Republic of Serbia

Chemical Education

Dr Vesna Stankov-Jovanović, Department of Chemistry, Faculty of Sciences and Mathematics, University of Niš, Republic of Serbia

Members of the Editorial Board:

Language Editors:

3. **Dr Velimir Ilić**, Department for Russian, Faculty of Philosophy, University of Niš, Republic of Serbia (Russian)
4. **Dr Nenad Blagojević,** Department for Russian, Faculty of Philosophy, University of Niš, Republic of Serbia (Russian)
5. **Nikoleta Momčilović**, Department of German, Faculty of Philosophy, University of Niš, Republic of Serbia (German)
6. **Katarina Stamenković**, Department of German, Faculty of Philosophy, University of Niš, Republic of Serbia (German)

PR Manager:

Lazar Kulašević, Department of Chemistry, Faculty of Sciences and Mathematics, University of Niš, Republic of Serbia

IT Support:

Predrag Nikolić, Team Lead
Petar Petković, Web Developer

Chemia Naissensis
ISSN 2620-1895
July 2019 Volume 2, Issue 1
www.pmf.ni.ac.rs/chemianaissensis

Cover Designer
Jovana Janković